INVESTIGATION OF LONG-ACTING ANTIRETROVIRAL NANOFORMULATION PHARMACOKINETICS USING EXPERIMENTAL AND COMPUTATIONAL METHODS

Thesis submitted in accordance with requirements of the University of Liverpool for the degree of Doctor of Philosophy

by

Rajith Kumar Reddy Rajoli

January 2017

This thesis is the results of my own work. The material contained within the thesis has not been presented, either wholly or in part, for any other degree or qualification.

Rajith Kumar Reddy Rajoli

This research was carried out in the

Liverpool HIV Pharmacology Group

Department of Molecular and Clinical Pharmacology

University of Liverpool, UK

TABLE OF CONTENTS

ACKNOWLEDGEMENTS

The presented studies in this thesis were carried out in the Department of Molecular and Clinical Pharmacology, University of Liverpool. The funding was provided by the University of Liverpool for which I am grateful.

PhD necessitates wide interdisciplinary knowledge for which I would like to express my sincere gratitude to those who have supported me and contributed in successful completion of the studies. Firstly I would like to thank my supervisors Dr Marco Siccardi and Professor Andrew Owen for providing me with the opportunity of pursuing a PhD at the University of Liverpool. Dr Siccardi has directed me throughout my PhD by providing invaluable inputs, supervised every aspect of my work leading to outstanding research and has been extremely patient during our brainstorming sessions for which I am extremely thankful. I would like to thank Prof Owen for his 'out of box thinking' ideas which widened my scientific thinking and also for providing financial support to address the hardships of an international student. Prof David Back has been an occasional mentor who has given valuable inputs to address important HIV pharmacological issues for which I am grateful. I would like to thank Dr Catia Marzolini, Dr Jose Moltó, Dr Adeniyi Olagunju, Dr Paul Curley and Dr Darren Moss for extensively testing my developed mathematical models and assisted me in expanding the developed models to evaluate various clinical scenarios. I would also like to thank my colleagues in the PhD and postdoc office – Christopher David, Dr James Hobson, Dr Beth Williams, Dr Lee Tatham, Dr Neill Liptrott, Dr Owain Roberts, Christina Chan, Louise Tidbury, Rohan Gurjar, Megan Neary, Ana Jimenez-Valverde, Hannah Kinvig for putting up with me with their invaluable time and support during scientific and social discussions.

I would also like to thank my friends Dr Abhishek Srivastava without which I would not have heard about this PhD position, Dr Dinesh Kumar, Dr Jyothibasu Selvaraj, Dr Sudhanva Kashyap, Dr Nitesh Kumar, Jithin Sasi and Yogeswaran Sundaramurthi for their social, financial and intellectual support without which I would not have successfully completed my PhD.

Lastly, but most importantly I would like to thank my mom, dad, sister and my cousins for their constant love, support and patience throughout my PhD even though we are five thousand miles apart from one another.

ABBREVIATIONS

AbCYP3A	Abundance of CYP3A
ADME	Absorption, Distribution, Metabolism and Elimination
AIDS	Acquired immunodeficiency syndrome
API	Active pharmaceutical ingredient
ART	Antiretroviral treatment
ARV	Antiretroviral
AUC	Area under the curve
BSA	Body Surface Area
CDC	Centers for Disease Control and Prevention
CL	Systemic clearance
CL/F	Apparent oral clearance
Cl_{app}	Total apparent clearance
C_{av}	Average plasma concentration
Cl_{gut}	Gut clearance
Cl_{int}	Intrinsic clearance
C_{max}	Maximum plasma concentration
CNS	Central Nervous System
$C_{ss,avg}$	Steady state average plasma concentration
C_{trough}	Trough plasma concentration
DNA	Deoxyribose Nucleic Acid
EMA	European Medicines Agency
F	Oral bioavailability
FBS	Fetal Bovine Serum
FDA	Food and Drug Administration
F_g	Intestinal bioavailability
F_h	Hepatic bioavailability
FTC-TP	Emtricitabine triphosphate
f_u	Fraction unbound in plasma
$f_{u,gut}$	Fraction unbound in gut
HAART	Highly Active Antiretroviral Therapy
HBD	Hydrogen Bond Donor
HERVs	Human Endogenous Retroviruses

HIV	Human Immunodeficiency virus
HPLC	High Performance Liquid Chromatography
IC90	90% inhibitory concentration
IIs	Integrase inhibitors
IM	Intramuscular
Ind_{50}	50% induction
Ind_{max}	Maximum induction
IPA	Isopropyl alcohol
IVIVE	*In vitro - in vivo* extrapolation
k_a	Absorption rate
k_m	Maximum velocity of anabolism
LAI	Long-Acting Injectable
MEC	Minimum Effective Concentration
MPPGL	Microsomal protein per gram of liver
MSC	Maximum Safe Concentration
NNRTI	Non-Nucleotide Reverse Transcriptase Inhibitor
NPs	Nanoparticles
NRTI	Nucleoside Reverse Transcriptase Inhibitor
$PAIC_{95}$	Protein binding adjusted IC95
P_{app}	Apparent permeability
PBPK	Physiologically Based Pharmacokinetic
PBS	Phosphate Buffer Saline
PI	Protease Inhibitor
PrEP	Pre-exposure prophylaxis
PSA	Polar Surface Area
Q_{gut}	Blood flow rate through gut in L/h
Q_{hv}	Blood flow rate through the liver in L/h
R	Blood-to-plasma ratio
RED	Rapid Equilibrium Dialysis
RNA	Ribonucleic acid
RT	Reverse Transcriptase
S.D.	Standard deviation
SC	Subcutaneous

SDNs	Solid Drug Nanoparticles
SIF	Simulated Interstitial Fluid
SIV	Simian Immunodeficiency Virus
TCL_{int}	Total intrinsic clearance of an enzyme
TFV-DP	Tenofovir diphosphate
UNAIDS	Joint United Nations Programme on HIV/AIDS
USP	United States Pharmacopeia
V_d	Volume of distribution
V_{max}	Maximum uptake velocity
WHO	World Health Organization

PUBLICATIONS

Moss DM, Marzolini C, **Rajoli RK**, Siccardi M. Applications of physiologically based pharmacokinetic modeling for the optimization of anti-infective therapies. Expert Opin Drug Metab Toxicol. 2015: 11(8):1203-17

Rajoli RK, Back DJ, Rannard S, Freel Meyers CL, Flexner C, Owen A, Siccardi M. Physiologically Based Pharmacokinetic Modelling to Inform Development of Intramuscular Long-Acting Nanoformulations for HIV. Clin Pharmacokinet. 2015 Jun: 54(6):639-50

Siccardi M, **Rajoli RK**, Curley P, Olagunju A, Moss D, Owen A. Physiologically based pharmacokinetic models for the optimization of antiretroviral therapy: recent progress and future perspective. Future Virology. 2013: 8(9):871-890

Rajoli RK, Back DJ, Rannard S, Meyers CF, Flexner C, Owen A, Siccardi M. In Silico Dose Prediction for Long-Acting Rilpivirine and Cabotegravir Administration to Children and Adolescents. Clin Pharmacokinet. 2017:1-12.

COMMUNICATIONS

Oral Presentations

Rajoli RK, Back D, Rannard S, Owen A, Siccardi M. Predicting Utility of Long-Acting Injectables in Paediatric Patients With PBPK Models. British Society of Nanomedicine Early Career Research Meeting, Swansea, UK, August 2016.

Rajoli RK, Back D, Rannard S, Owen A, Siccardi M. Optimisation of Intramuscular Sustained Release Nano-Formulations Using *In Silico* Modelling. Early Career Research Meeting, British Society of Nanomedicine Young Researchers Meeting, Liverpool, UK, August 2015.

Themed Discussion

Rajoli RK, Back D, Rannard S, Owen A, Siccardi M. Predicting Utility of Long-Acting Injectables in Paediatric Patients With PBPK Models. 23st Conference on Retroviruses and Opportunistic Infections, Boston, Massachusetts, USA, March 2016.

Poster Presentations

Rajoli RK, Back D, Rannard S, Owen A, Siccardi M. Predicting Utility of Long-Acting Injectables in Paediatric Patients With PBPK Models. 23st Conference on Retroviruses and Opportunistic Infections, Boston, Massachusetts, USA, March 2016.

Rajoli RK, Back D, Rannard S, Owen A, Siccardi M. Optimisation of Intramuscular Sustained Release Nano-Formulations Using *In Silico* Modelling. 21st Conference on Retroviruses and Opportunistic Infections, Boston, Massachusetts, USA, March 2014.

ABSTRACT

Antiretrovirals (ARVs) can find clinical application for both treatment and prevention of HIV infection. Pre-exposure prophylaxis (PrEP) strategies have been recently introduced to protect individuals who are at high risk of acquiring HIV infection. The majority of existing ARVs are oral formulations which necessitate lifelong daily dosing and suboptimal adherence to this dosing regimen could result in development of viral resistance against treatment. Long-acting injectable (LAI) nanoformulations administered either intramuscularly or subcutaneously could be a valuable pharmacological option. LAIs could potentially simplify dosing regimen, reducing the total amount of drug consumed thus reducing the oral cost of treatment/PrEP and most importantly addressing the problem of suboptimal adherence. The development of novel LAI therapies is complicated by several pharmacological factors including ARV pharmacokinetics and compatibility with existing formulation strategies. The overall aim of this thesis was to investigate and simulate the pharmacokinetics of LAI formulations in order to provide effective tools to inform the future development of formulations.

A number of different strategies to investigate the pharmacokinetics of LAI formulations were developed in this thesis. Physiologically based pharmacokinetic (PBPK) modelling represents the mathematical description of anatomical, physiological and molecular processes that define pharmacokinetics in humans. In the recent past, PBPK models have been developed for several disease areas to simulate pharmacokinetics in humans, which currently play an active role in the design of clinical trials and regulatory approvals. In Chapter 2, human adult PBPK models have been developed and validated against clinically available pharmacokinetic data of oral formulations for eight ARVs. These validated models were then used to identify theoretical optimal dose and release rates of LAI formulations for weekly and monthly administration. Clinical studies in paediatric patients encounters ethical issues and possesses concerns during dose optimization. In Chapter 3 and 4, PBPK models have been developed and validated for children and adolescents for existing LAI formulations of cabotegravir and rilpivirine. Doses were optimised for monthly administration such that the plasma concentrations stay over the assumed target concentrations, for paediatric population according to different weight groups recommended by World Health Organisation. In Chapter 5, experimental methods (static release dialysis, sample-and-separate method and dynamic release dialysis) to evaluate the drug release rate from the site of injection were developed. The *in vitro* release rates were correlated with clinical release rates to obtain a mathematical equation describing the *in vitro in vivo* extrapolation (IVIVE) in Chapter 6.

Novel computational and experimental methods to support the development and optimisation of LAI formulations are required. These findings represent valuable applications of novel methods to simulate and characterise the pharmacology of LAI formulations. The reported findings could help simplify ARV dosing strategies by providing an initial dosing guideline for clinical trials in humans. This approach could improve therapy thus addressing the problem of suboptimal adherence and reduce cost of overall treatment. PBPK models and IVIVE could be an innovative strategy to evaluate drug pharmacokinetics in humans and optimise dose and release rates of novel formulations for LAI HIV therapy.

CHAPTER 1

General Introduction

Contents

1.1. Human immunodeficiency virus

Human immunodeficiency virus (HIV) is a retrovirus and since its discovery in 1983, it has infected an estimated total of 75 million people globally [1, 2]. Among them 36.9 million people are currently living with HIV and 2 million people were infected in 2014, a 35 % decrease in the number of new infections compared to the year 2000 indicating that there is a remarkable progress in controlling the spread of this infection [3]. In 1996, UNAIDS was formed to limit virus diffusion by identifying preventive and therapeutic strategies, with the target of providing treatment access to every HIV infected individual by 2030 [3, 4].

Although HIV was discovered more than 30 years ago, treatment and prevention strategies can be characterised by suboptimal efficacy and side effects [5]. This is mainly due to lack of understanding of the pathophysiological mechanisms of infection and optimal pharmacological tools to inhibit viral replications [6]. The progress in HIV research has almost doubled with the number of articles reaching up to 16,317 in the year 2015 compared to 9,991 in 2000 [7]. Efforts are currently in progress to design vaccines that could prevent the virus from infecting HIV-negative individuals [8-10].

1.2. HIV Life Cycle

HIV is a lentivirus which belongs to the family Retroviridae, known for causing various neuro- and immunological conditions in humans [11]. This particular class of virus requires long incubation times in the host and the infection progresses to acquired immunodeficiency syndrome (AIDS) in less than a decade without medication [12]. The primary receptor for HIV is CD4 antigen, which is expressed on CD4+ T

lymphocytes and macrophages – cells of the immune system [13]. HIV has the capability to transfer its ribose nucleic acid (RNA) strands through an intact nuclear membrane in an infected cell thus gaining an advantage of replication in terminally differentiated cells, a unique ability among its family of viruses [12, 14].

The outer membrane of HIV is a bilayer consisting of important components that assist in gaining access to the host cell [15]. Trimers of glycoprotein gp120 and gp41 are expressed on the surface of the viral membrane [13]. The inner portion of the bilayer is lined with the gag protein which constitutes a 7 nm thick matrix [16]. Moreover the internal core of the virus contains a conical shaped shell, called the capsid with several copies of key enzymes and proteins such as the integrase, reverse transcriptase (RT), nucleocapsid, viral protein and two copies of RNA strands [16].

HIV does not have the capability to reproduce by itself and therefore needs a suitable host cell i.e. humans [14]. The primary step after the successful transmission of HIV is binding of the virus to the cell membrane receptors of the target cells with the help of protein gp120 and the viral envelope protein present on its surface [17]. During the process of entry into the cell, the virus loses its outer membrane and only the core enters into the cytoplasm of the cell [12]. Once in the cytoplasm, the core undergoes readjustments and releases the viral contents into the cytoplasm [11]. The RNA contents form a deoxyribose nucleic acid (DNA) complex in the cytoplasm with the assistance of reverse transcription complex [18]. The viral proteins send false signals to the nucleus of the infected cell to allow the newly formed DNA complex and other viral proteins through the nuclear membrane [19]. Utilising the help of integrase enzyme, the viral DNA is integrated with the cellular genome [20]. This process allows the production of viral proteins and RNA which are packed in the viral shell with the

help of protease enzymes to produce a mature virion thereby successfully constructing the replication of HIV virions through an infected cell. [11, 14, 17].

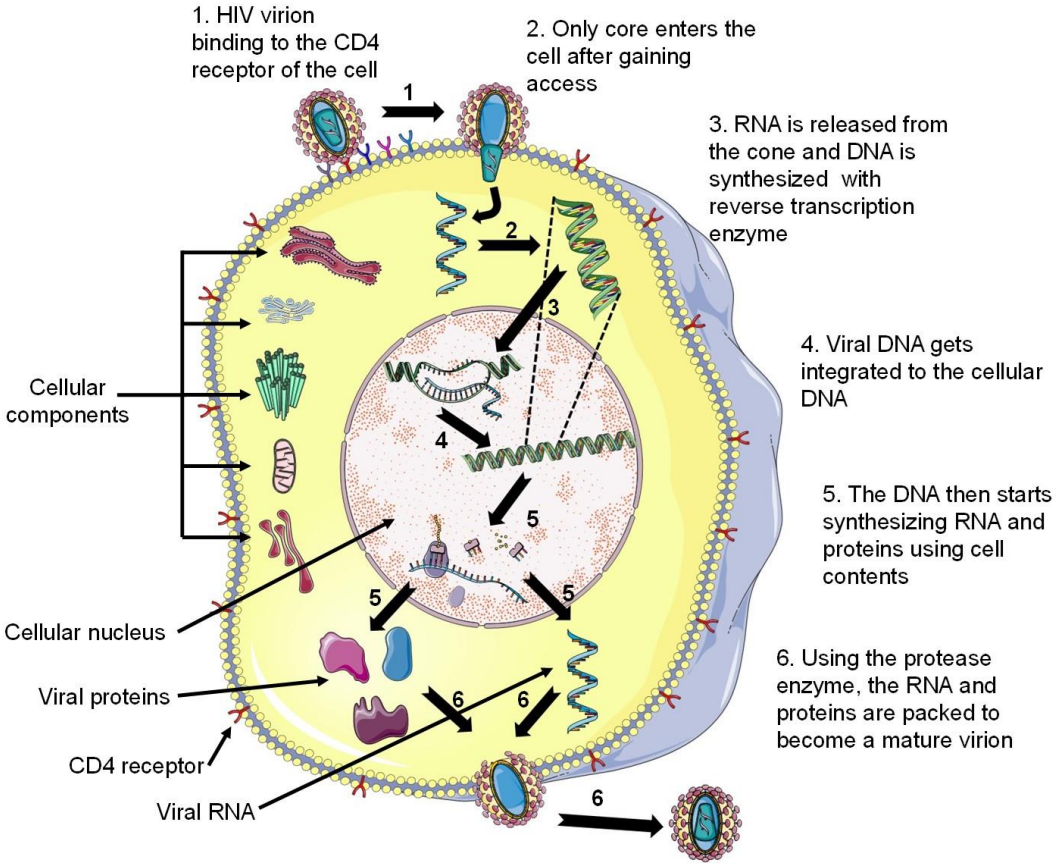

Figure 1.1 HIV life cycle in the cellular membrane of an infected cell [17]

1.3. Antiretroviral therapy

Antiretroviral (ARV) therapy can effectively control HIV replication rate and support the maintenance of low viral load in plasma and tissues [21]. This can also reduce the risk of viral transmission to other individuals. Extensive research through the years in the field of HIV facilitated the discovery of drugs that improve the survival rate of infected individuals similar to that of a healthy individual [22]. ARV therapy is based on the combination of three different ARVs from two of the five existing classes of ARVs, inhibiting the viral replication at different stages.

1.3.1. Entry inhibitors

As previously described in section 1.2, HIV gains access to the T cells through the interaction of gp120 protein onto the CD4 receptor and the co-receptors CCR5 or CXCR4 [23]. The gp120 protein undergoes conformational changes when it interacts with CD4 receptor to expose the co-receptors. HIV gains access to the cytoplasm of the T cell using gp41 protein [24]. Entry inhibitors can effectively block the interaction of viral proteins with CD4 receptor, inhibiting HIV entry into the host cell.

Maraviroc is the first and only available entry inhibitor that blocks CCR5, but there is a possibility for HIV to access the CXCR4 co-receptor through other mechanisms [25]. An alternative entry inhibitor - enfuvirtide, is a peptide which acts by forming a six-helix bundle with gp41 of the virus thus preventing any interaction with host cell [26].

1.3.2. Nucleoside reverse transcriptase inhibitors (NRTIs)

NRTIs target the reverse transcription process of HIV virus. Viral replication involves the transcription of its RNA to DNA mediated by viral reverse transcriptase. Viral reverse transcriptase is typically not present in host cells, making it an ideal target for ARV therapy [27].

NRTIs are competitive inhibitors of the viral RT and can successfully inhibit the synthesis of the viral DNA. NRTIs are prodrugs which convert to their active form – the di- or triphosphate analogues by host kinases to compete with the nucleotides in order to be used in this process [28]. Zidovudine was the first clinically available NRTI and later several others such as abacavir, lamuvidine, tenofovir and emtricitabine have followed. Currently, tenofovir and emtricitabine are used widely as first-line therapy drugs against HIV [29].

1.3.3. Non-nucleoside reverse transcriptase inhibitors (NNRTIs)

NNRTIs inhibit the reverse transcription process. Unlike NRTIs, NNRTIs inhibit RT non-competitively without the need of converting into its triphosphate form [30]. These are small molecules typically hydrophobic in nature and interfere with the viral transcription process by binding to a single position on the p66 subunit of the viral RT protein. This hinders the ability to handle endogenous nucleosides and nucleotides during reverse transcription, thereby affecting the replication cycle [31].

Classification of NNRTIs is divided into two categories – 1st and 2nd generation. The drugs in the 1st generation consist of nevirapine and efavirenz; and the 2nd generation include doravirine, etravirine and rilpivirine [29, 32].

1.3.4. Protease inhibitors (PIs)

PIs inhibit maturation of the immature virions. Post transcription, the immature viral RNA and viral proteins migrate to the cytoplasm of the host cell from the endoplasmic reticulum. Viral protein shell is synthesized using the infected cellular components. Detachment of the viral components from the host cell is defined as the maturation stage. Protease enzymes cleave peptides to specific chain lengths that are crucial viral components. PIs target these enzymes thus preventing the packing of essential peptides during the viral replication. The main precursor proteins such as *gag* and RT are targeted in this process [34].

Amprenavir, fosamprenavir, indinavir, lopinavir, nelfinavir, ritonavir and saquinavir are the first generation PIs; atazanavir and darunavir are the 2nd generation PIs, which are highly potent against HIV [29].

1.3.5. Integrase inhibitors

Integrase inhibitors target the integration process of the viral DNA post reverse transcription. Viral integrase enzyme plays a key role in DNA integration with the host DNA. Integrase inhibitors bind to the viral enzyme inhibiting its function and interrupting viral replication [28].

Raltegravir was the first integrase inhibitor approved for clinical use [35]. Later dolutegravir, elvitegravir and cabotegravir followed[29, 36].

1.4. Highly Active Antiretroviral Therapy (HAART)

HAART is a strategy designed to address the problem of viral resistance to ARVs. During HIV replication, the virus undergoes various mutations due to its inability to proofread the enzymes produced in the host cell. This leads to various mutated HIV strains and although most of them are inferior to the parent HIV and not harmful, few may develop resistance to antiretroviral therapy (ART) thus making the treatment ineffective [37]. Combinational therapy with drugs from different classes are given to patients to address this problem.

HAART generally consists of a combination of three drugs having synergistic effect to successfully suppress viral replication. Factors influencing drug combinations include total viral load, CD4 T cell count, survivability and occurrence of other opportunistic infections [38]. HAART reduces the probability of spontaneous mutation strains thereby lowering chances of the virus gaining resistance. Currently HAART is available as a single tablet consisting of multiple drugs. A few combinations are shown in Table 1.1.

Table 1.1. Various combinations of fixed dose combinations approved in the past 12 years for use in ART [29]

Brand Name	Combination	Approval date
Epzicom	Abacavir and lamivudine	August 2, 2004
Truvada	Emtricitabine and tenofovir disoproxil fumarate	August 2, 2004
Atripla	Efavirenz, emtricitabine, and tenofovir disoproxil fumarate	July 12, 2006
Complera	Emtricitabine, rilpivirine, and tenofovir disoproxil fumarate	August 10, 2011
Stribild	Elvitegravir, cobicistat, emtricitabine, and tenofovir disoproxil fumarate	August 27, 2012
Triumeq	Abacavir, dolutegravir, and lamivudine	August 22, 2014
Evotaz	Atazanavir and cobicistat	January 29, 2015
Prezcobix	Darunavir and cobicistat	January 29, 2015
Genvoya	Elvitegravir, cobicistat, emtricitabine, and tenofovir alafenamide fumarate	November 5, 2015

Prevention strategies are also being implemented in addition to treatment. Pre-exposure prophylaxis (PrEP) focuses on HIV-negative or uninfected individuals who are at high risk of acquiring HIV. Recently, Truvada® has been accepted for PrEP in addition to its use in ART [39]. It reduces the risk of HIV in healthy individuals up to 92 % [40]. Other ARVs - rilpivirine and cabotegravir are currently being evaluated for PrEP in clinical trials [41, 42].

1.5. Antiretroviral pharmacokinetics

Pharmacokinetics is the study of what the body does to the administered drug through the description of drug distribution in tissues and organs. Plasma is the most frequently used biological matrix due to its ease of access and abundance, and plasma concentration represents an essential marker to describe drug exposure in the body [43]. The pharmacokinetic parameters that are commonly used to describe drug exposure are: C_{max} - the maximum concentration attained by the drug in plasma during a single dosing interval, C_{trough} - the minimum concentration attained just before the following dose and AUC – the total area under the curve when the drug concentration is plotted against time (Figure 1.2).

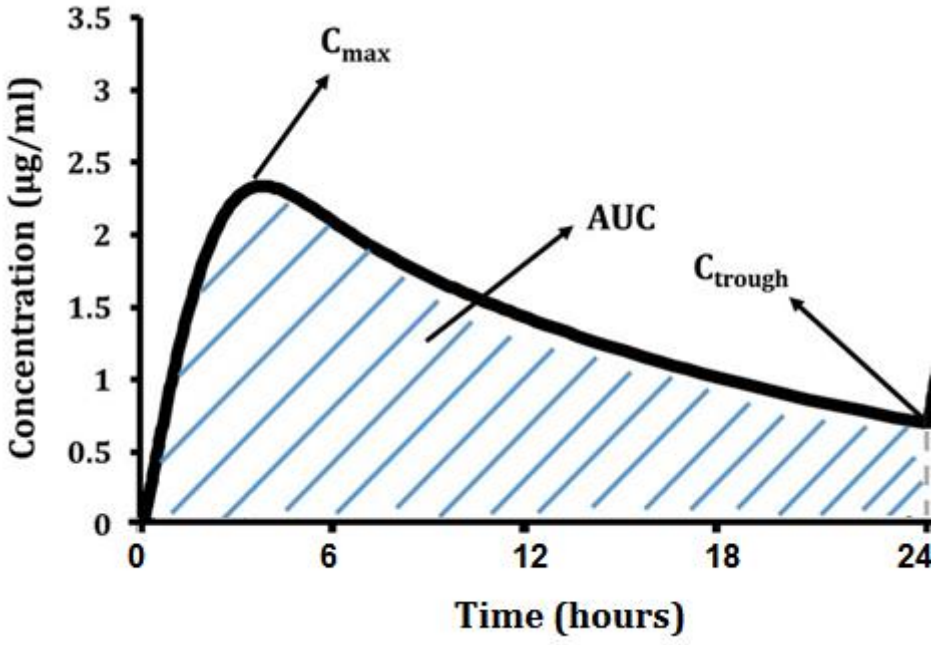

Figure 1.2 An example of a pharmacokinetic curve with time in hours on x-axis and concentration on y-axis. The arrows represent the key pharmacokinetic parameters – maximum concentration (C_{max}), trough concentration (C_{trough}) and area under the curve (AUC) shaded in blue.

The majority of the clinically available ARVs are administered orally with the exception of enfuvirtide which is administered as a subcutaneous (SC) injection twice daily thus restricting long-term usage [26].

Drug pharmacokinetics is mediated by absorption, distribution, metabolism and elimination (ADME) processes in various organs and tissues. Some of the common pharmacokinetic terms used include bioavailability, drug clearance and induction and inhibition effects of drugs. Absolute bioavailability is the total fraction of drug reaching the systemic circulation after administration. Poor bioavailability can lead to drug plasma concentrations not reaching the therapeutic range, rendering the medications unsuitable. Few causes include low solubility and low permeability leading to decreased oral absorption; extensive first-pass metabolism and high clearance rate [44]. Rapid metabolism and fast clearance are influenced by drug physiochemical properties such as low protein binding in plasma and low blood-to-plasma partition ratio [45]. Administering a drug metabolised by the same enzyme that competes for its degradation could address the problem of fast clearance. Ritonavir is a potent inhibitor of CYP3A4 - the most abundant enzyme in the body. PIs – atazanavir, darunavir and lopinavir are co-administered with ritonavir which boosts the absolute bioavailability of these drugs [46]. Tenofovir and emtricitabine are the most commonly used NRTIs - are hydrophilic in nature, have good absorption through the small intestine and also have longer mean plasma and intracellular half-lives to give a prolonged effect [47, 48]. NRTIs are prodrugs which undergo phosphorylation after cell penetration to convert into their active form for therapeutic outcome [49]. Cell penetration is the key requirement to interfere with the HIV life cycle and restrict the replication since most of the ARVs (except entry inhibitors) interfere with the replication process undergone inside the infected cell. Sanctuary sites are the places in the body where the drug

cannot penetrate but the virus can [50]. These represent a major challenge to completely eradicate viral replication. They are divided into two types depending on the sites – anatomical and cellular sanctuary sites. The anatomical sites include the central nervous system (CNS), genital tract, lymphatic circulation, spleen and lung. Dendritic cells, infected CD4+ cells and macrophages represent the cellular sanctuary sites [50, 51].

Low drug absorption and high clearance leads to the requirement for higher dosing amounts thereby increasing the risk of side effects and cost of overall treatment [52]. Maintenance of drug concentrations in the therapeutic range is essential to suppress viral load and prevent viral resistance against therapy [53]. Raltegravir has high inter- and intra-patient variability where two efficacy studies failed therapy in 18 % and 33 % patients with no evidence of HIV mutations, indicating raltegravir exposure and/or adherence could be the cause for treatment failure [54]. Combinational therapy may utilise small amounts of multiple drugs having synergistic effect, thus lowering the extent of side effects. Darunavir undergoes extensive intestinal and first-pass metabolism by CYP3A4 due to which it is administered along with ritonavir. Ritonavir boosts plasma concentrations of darunavir almost 11-fold by inhibiting its metabolism by CYP3A4 enzyme [55].

Drug physiochemical properties play a vital role in reflecting their pharmacokinetic profiles. Lipinski's "rule of 5" provides a summary of the ideal features a drug should possess to have a satisfactory ADME pattern. Intestinal absorption is highly dependent on drug permeability through the gut in addition to molecular properties such as log P, polar surface area and hydrogen bond donors. The extent of drug distribution is governed by protein binding, pKa and logP of the drug. Clearance of the

drug is affected by blood-to-plasma ratio, protein binding, volume of distribution and the drug's ability to either induce or inhibit the metabolism in liver [56-58].

Drug formulation research for safe administration is a challenging process. Day by day, drug delivery is facing more and more challenges, due to continuous growth in the number of water-insoluble drugs [60]. Type of drug delivery depends on factors such as onset time, drug targeting issues and drug characteristics such as stability and solubility [61]. Almost 40 % of the new molecules which are capable candidates for treatment are hydrophobic in nature, implying the necessity of an appropriate vehicle to transport the molecule passively or actively into the systemic circulation [62]. Reaching therapeutic concentrations without major side-effects at the site of action represents a key barrier in the pharmaceutical sector [63]. Absence of appropriate delivery agents that could deliver the drugs to their respective site of action drastically decreases the therapeutic potential of the active ingredient *in vivo* [64].

Drug formulation includes excipients which assist the active pharmaceutical ingredient (API) in a number of ways. Examples of them include solubility enhancers, longer shelf-life, prevention of degradation in the stomach and specific tissue targeting agents [65]. Design of appropriate formulation is dependent on the therapeutic requirement, ease of dosing and the route of administration. Broadly, routes of administration are categorised into three types – enteral, parenteral and topical. Tablets, capsules, oral solutions, oral suspensions, oral emulsions, suppositories, sustained or delayed release tablets or capsules etc. are considered as enteral formulations as they are administered through the gastrointestinal tract. Intravenous, intramuscular (IM), intradermal, SC and intra-arterial are a few commonly used parenteral routes. Inhalations, ophthalmic, ear and locally administered drugs on the skin (e.g. patches) are considered as topical routes. Numerous drug delivery templates have been designed

such as micro- or nanoparticles, micelles, dendrimers, polydendrons, liposomes etc. Each route of administration employs a drug delivery type that suits its purpose, for example – pulmonary administration of a vasodilator, 5(6)-carboxyfluorescein solution encapsulated as nanoparticles had prolonged action and targeted delivery than the free drug in an isolated rabbit lung model [66-69]. In a separate study, enhanced gene delivery of plasmid DNA was observed in bone-marrow derived mesenchymal stem cells of rat using multivalent-functionalised generation 5 poly(amidoamine) dendrimers [70]. Elastic liposomes made from Epikuron 200 loaded with a potent analgesic, ketorolac tromethamine, a hydrophilic drug showed increased penetration through the transdermal route [71].

Oral administration is the most widely used route of delivery due to its ease of administration [72]. Bioavailability was found to be low in conventional ARV formulations [73] and efforts are in progress to improve the oral bioavailability of ARVs. Recently, solid drug nanoparticles (SDNs) were designed by freeze-drying emulsions with high drug loading and long-term stability [74]. These SDNs improved the apparent permeability of efavirenz in caco-2 cells thereby potentially increasing the oral bioavailability close to four-fold (as predicted by the computational model). In rats, increased concentrations were observed with efavirenz SDNs compared with the existing formulation when dosed with the same amount of the drug [74]. In another study, atazanavir was prepared as a self-emulsifying system. *In vitro* studies indicate that the novel emulsion has three times higher dissolution rate compared to pure drug and *in vivo* studies in wistar rats show a two-fold increase in C_{max} and AUC when compared to the pure drug [75].

1.6. Long-acting formulations

Each route of administration has its own advantages and disadvantages. Long-acting (LA) formulations address the essential problem of nonadherence in HIV patients. The two most commonly used routes of administration for LA formulations are IM and SC routes. Implants and osmotic pumps could also be an alternative option but these require personnel who are surgically experienced. This limits their use due to the cost, risk and time spent on a single patient and also shortage of healthcare personnel in remote areas leads to further complications [76, 77].

Drugs administered in-between the muscle are considered IM formulations and injections just below the subcutis, the area under the dermis and epidermis are SC formulations. Major difference between these two routes is the contact environment. Intramuscular, as the name suggests are mainly muscle cells surrounding the drug depot whereas adipose cells are the neighbours for drugs administered subcutaneously. Drug diffusion into the surrounding blood capillaries and lymph nodes is dependent on the nature of the formulation – aqueous or non-aqueous. Drug diffusion in aqueous formulations is either solubility limited or restricted by polymers forming the micro- or nanoparticles. Oil, a common vehicle for non-aqueous formulations, could be an additional barrier for drug dissipation into systemic circulation to control its pharmacokinetic profile [78]. Toxicity profile for the drugs and excipients included in these formulations have to be evaluated extensively to ensure no adverse reactions and side-effects occur.

IM and SC routes could be ideal resolutions for addressing issues such as ease of administration and cost of treatment. They provide alternative routes for drugs that

are insoluble or have low solubility due to their low absorption in the gut; and intravenous administration may have limited use as it does not provide sustained drug release and not suitable for insoluble drugs. Maintenance of drug concentrations for a long-period of time via IM or SC routes at therapeutic exposure utilises less drug in total as absorption through the gut and first pass metabolism are avoided thus making the overall treatment cost cheaper. Additionally, high exposure through oral formulations could be avoided, reducing adverse effects seen with chronic daily-dosing [79, 80].

Existing ARVs necessitate life-long daily dosing and adherence to this dosing regimen is essential to treat HIV. Suboptimal adherence places the patient at high risk of treatment failure or low protection rates in the case of PrEP strategies [81]. Nonadherence to HIV therapy has been observed in an estimated 50 % to 70 % of patients who were prescribed multiple medications [82]. Currently ARV treatment has reduced to a mere one pill a day. Only 60-85 % patients adhered to the recommended dosing regimen due to forgetfulness, being busy or some other reason. There is difficulty in finding the perfect solution, although steps are taken to remind patients to administer the doses at regular intervals [83-85]. Use of LA formulations lasting multiple weeks or months, opens up the possibility of simplifying dosing regimens, increase adherence, reduce the amount of drug consumed thus decreasing the overall cost and effectiveness of treatment and PrEP [86].

The pharmacokinetics of a conventional oral formulation varies widely in a single dosing interval with plasma concentrations fluctuating from minimum effective concentration (MEC) to maximum safe concentration (MSC) (Figure 1.3). Suboptimal adherence to the prescribed dosing regimen can lead to HIV developing resistance against ART. A single dose of a LA formulation could result in sustained plasma

exposure solving the problem of suboptimal adherence observed with oral formulations (Figure 1.4).

Efforts are currently in progress to design LA formulations for HIV patients. Rilpivirine long-acting injectable (LAI) nanoformulation was developed in 2009 and the pharmacokinetic profile of IM and SC routes of administration in beagle dogs were compared. A similar pharmacokinetic profile after 12 weeks from the injection was described with a relatively lower C_{max} and sustained release for SC compared to IM, however higher lymph concentrations in adjacent lymph nodes were observed with IM administration and were better tolerated compared to SC administration [86]. The same formulation was later tested in humans showed only 10-20 ng/ml decrement from the C_{max} in drug plasma concentration between 3-6 months indicating potential in LA administration of ARVs [87]. Recently cabotegravir, an analogue of dolutegravir with a longer half-life, low metabolic clearance, low solubility and low daily dose was discovered that is capable of providing therapeutic drug exposure over a period of three months with an 800 mg formulation administered IM [36].

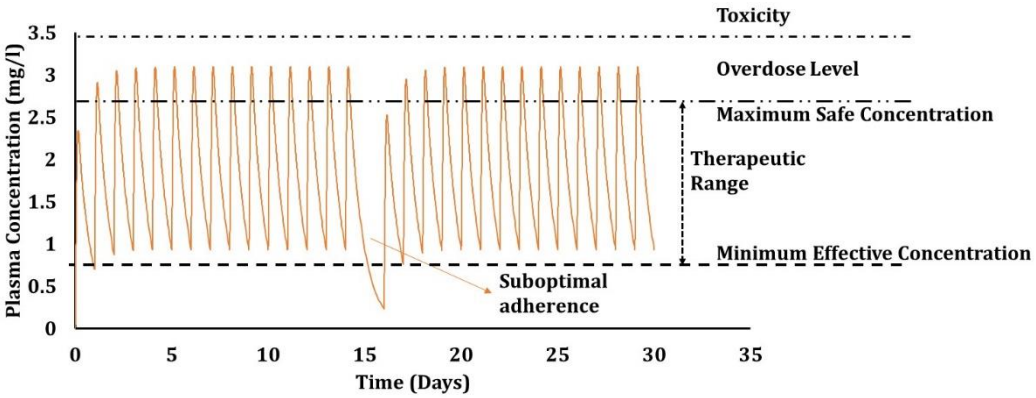

Figure 1.3 Representative pharmacokinetics of a conventional oral formulation and suboptimal adherence are shown.

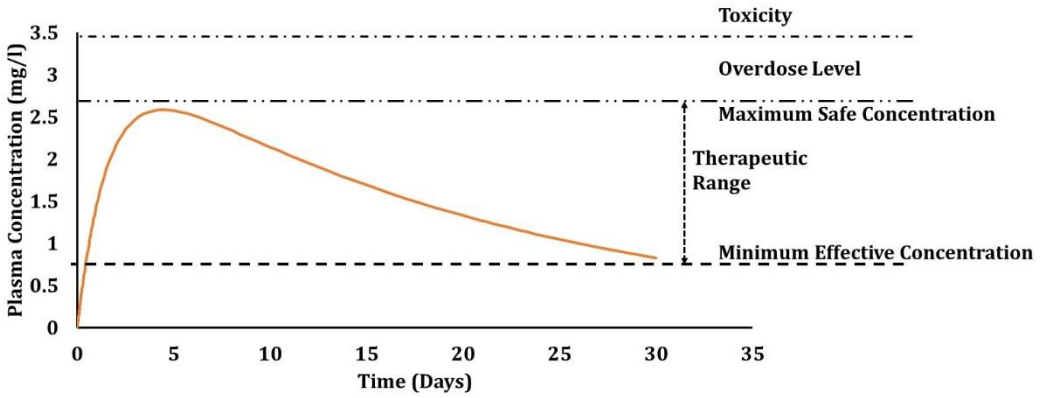

Figure 1.4 Representative pharmacokinetics of an ideal long-acting release formulation.

1.7. Pharmacokinetics of LAI formulations

Depot formulations avoid three major processes undergone by oral formulations. These are drug dissolution, drug absorption through the gastrointestinal tract and first-pass metabolism. These processes can significantly limit the drug absorption thus increasing the overall amount administered [88]. Drug dissolution is a relevant step in drug delivery making it an influential aspect in discovery of any drug, particularly in the absorption phase for oral formulations. It also has importance in LA formulations as the major factor controlling the release of the drug from the depot. Evidence shows that only dissolved drug leaves the depot through the connective tissue for systemic distribution [79]. Drug absorption is dependent on the physicochemical properties of the drug and the excipients used in its formulation. Solubility and intestinal permeability are the two important factors regulating the absorption process [65]. Also excipients such as solubility enhancers, membrane permeability enhancers used in the formulation could improve the net drug absorbed [89]. Absorption process also includes intestinal metabolism by CYP450 enzyme which further reduces the oral bioavailability of drugs metabolised by this enzyme. These processes are avoided as the drug directly diffuses into the surrounding blood or lymph capillaries from the depot, thus escaping this process. First-pass metabolism eliminates a substantial amount of

drug at the entry point to the circulatory system. Subsequent to absorption, drug traverses through the portal vein from the small intestine to the liver. Liver hepatocytes metabolise the drug and only a fraction passes through the heart for systemic distribution [90]. In few cases, depending on the drug properties, chronic usage of oral formulations can lead to hepatotoxicity in the long-term due to extensive usage of hepatocytes in the metabolic process. This step is also eluded in these two routes which further reduces the quantity of drug utilised [91, 92].

There is no ideal route for drug delivery as each have their advantages and disadvantages. Discontinuation of therapy could be complicated as the depot has to be removed surgically which require experienced personnel. Drug absorption from the depot could be hampered if the area is poorly accessible for blood capillaries [93]. Local pain and swelling was observed initially at the site of injection which can cause discomfort and irritation in patients [94]. In some cases, there is a possibility of potential muscle damage at the site. Individuals having fear of injections would not be compliant with this route of delivery. Special populations such as neonates, infants and individuals with abnormally low muscle or adipose tissues pose a risk which can hinder the treatment. Although these routes have disadvantages, they make it an interesting and attractive way to deliver drugs cost effectively with reduced side-effects compared to oral administration [95].

LAI formulations represent an innovative strategy to improve the administration of ARVs. Although they could provide an effective alternative to the problems encountered with current oral therapy, the design of novel formulations is challenging. These formulations have to ensure that the therapeutic efficacy is maintained during the dose interval otherwise HIV might attain resistance against the therapy. Release rate is one of the key parameters in designing LA formulations. Rate of release could

be affected by numerous factors and a few major influencing factors include dissolution rate of drug, protein binding, particle size, dosage and hepatic clearance.

1.7.1. Clearance

Extent of drug clearance is associated with the concentration of drug present in blood plasma. More drug in plasma increases the amount of drug cleared which can be perceived with oral formulations where the plasma concentration increases to C_{max} and decreases to C_{trough} in a short span of time. A similar situation occurs with LA formulations - the higher the release rate the greater the clearance. Dose and release rate optimisation should be essential so that therapeutic exposure is achieved for the desired time period [58].

1.7.2. Dissolution rate

Dissolution is an essential part of any formulation. Undissolvable drug is of no use for medical purpose. Rate of dissolution should be higher in the case of oral compared to LA formulations as there is limited time in the small intestine for absorption. The designed formulations should disintegrate and dissolve rapidly for effective absorption. Excipients play an important role in improving the disintegration and dissolution rate of the formulation (e.g. disintegrating agents, solubility enhancers). Controlled release rate is desirable in LA formulations, as the drug is expected to diffuse at a slower pace just enough to maintain therapeutic concentrations for an extended time. Excipients also influence the release rate - with hydrophilic or lipophilic polymers, the release rates of the active ingredients from the formulation could be increased or decreased [96]. The drug to excipient ratio had a significant effect on the release of atenolol from hydroxypropylmethylcellulose (HPMC) polymeric matrices [97] and also the release of paclitaxel from nanoparticles formulated with varying

ratios of hydrophilic/lipophilic polymers and surfactants indicate the importance of excipients in controlling drug dissolution [98].

1.7.3. Dose

Dosage plays an important role in maintaining therapeutic exposure of a drug. The amount administered into the muscle or SC area should be tolerable. Literature shows that the maximum dose that has been injected and well tolerated in an individual is 1.5 g of cefuroxime formulation [99]. Larger doses attract higher amounts of immune cells to the depot site, leading to the formation of a granuloma, which could be beneficial in further controlling the drug release rate and might facilitate the drug to the lymphatic system [79]. Utilisation of optimal doses is essential for use in therapy to reduce potential occurrence of toxicological and adverse events.

1.7.4. Particle size

Particles can be prepared either using bottom-up approach (e.g. self-assembly) or top-down approach (e.g. milling). Spherical particles undergo relatively faster and uniform dissolution than irregularly shaped particles. Particle size influences the surface area exposed to the surrounding body fluid at the site of depot. Increase in surface area leads to more contact with blood or lymph at the depot, facilitating the dissolution process of the active ingredient, thereby increasing drug exposure in plasma [100].

1.7.5. Protein binding

Drug release rate is influenced by protein binding in a number of ways. High protein affinity of the drug can increase the release rate at the site of depot and in plasma, the available free drug decreases, which in turn reduces metabolic clearance. This leads to an increase in half-life thus prolonging therapeutic exposure. Protein binding

also influences the extent of drug distribution and the steady-state volume of distribution [101]. There is evidence of nanoparticle binding to proteins which can further change the drug biodistribution profile and alter the immunogenicity due to the formation of a protein corona [102].

1.8. Physiologically Based Pharmacokinetic (PBPK) Modelling

Discovery of novel drugs and developing them into potential formulations typically consumes a substantial amount of time. Balance between physiochemical properties and ADME underpins the safety aspects during treatment. Essential components include safety and efficacy profile, low systemic toxicity and no or mild long-term adverse effects [56]. Only 18 % of the drugs in infectious diseases category tend to get accepted for clinical trials out of which less than 15 % percent reach the market [59]. The drug discovery phase is commonly followed by preclinical and clinical trials before reaching larger populations. These steps necessitate drug companies to invest largely in a single drug to reach the pharmaceutical market and intermittent failure during clinical studies leads to significant loss of time and money. Mathematical models were designed to tackle some of these key situations, which provide a rough estimate of the pharmacodynamics or pharmacokinetics of medications in humans prior to preclinical and clinical studies [103]. Various models have been used ever since that can identify the potential factors influencing the pharmacokinetic-pharmacodynamic profiles of novel drugs. Although there are quite a few models which use clinical data to compute ADME parameters, PBPK models have a unique feature which use only *in vitro* data to extrapolate the pharmacokinetics in humans [104]. However, the quality of the end result from the PBPK model depends on the quality of the *in vitro* data used in these models, suggesting the importance of the standardisation of *in vitro* assays. The concept of PBPK modelling dates back to the year 1937, but

complexities associated with computations due to the lack of workstations limited the use of these models until now [105]. The use of PBPK modelling is on the rise, with 33 Federal Drug Administration (FDA) applications having simulated data between 2008 – 2013 [106].

In vitro – in vivo extrapolation is a bottom-up method which combines various data types such as anatomical and physiological parameters of a population, drug parameters (e.g. protein binding, lipophilicity, solubility and absorption rate) to evaluate the four crucial factors - ADME with mathematical equations, commonly termed as PBPK modelling [50]. *In vitro* studies such as apparent permeability, intrinsic clearance using baculosomes, octanol-to-water partition coefficient are performed for the desired drug and then extrapolated to human data using mathematical equations. These *in vitro* data help in computing parameters such as net absorption rate from the apical to basolateral side of the small intestine, total hepatic clearance, volume of distribution, induction and inhibition activity of CYP450 metabolising enzymes etc. [57, 107, 108]. All these parameters assist in precisely determining the pharmacokinetic profiles of drugs in different tissues of the human body. PBPK models have the ability to simulate the pharmacokinetics of drugs administered through different routes including oral, intravenous, transdermal etc. There are different versions of the models, broadly divided into open and closed sourced. Users having freedom to construct and customise their own models with the help of an application are termed as open sourced, for e.g. Berkeley Madonna™, MATLAB®, python™, NONMEM®. But the user needs appropriate training in order to use these applications where are models are built from scratch and are usually time consuming. Readily available models provide simple and user friendly interface and are also less time consuming which

however are expensive and are marketed by companies such as Simcyp®, GastroPlus™, and PKSIM® which restrict the usage in terms of flexibility and charge the user for the provided service [50, 109].

PBPK models utilise the concept of compartments to denote the organs and tissues of the human body. These are connected to each other by means of predetermined mathematical equations representing the kinetics between the two compartments. Basic PBPK model can be represented with three compartments: one representing the blood plasma concentrations, the second one representing the metabolism processes occurring in liver and the final one representing the tissues of the body which is in equilibrium with the first compartment (Figure 1.5). Once the drug reaches the plasma compartment after the initial absorption process, simultaneous distribution to tissue reservoirs and metabolism in liver kick in to eliminate a fraction of the drug [110]. This process advances in a continuous cycle until all of the drug is either metabolised or excreted and eliminated by the body. Dosing schedules can also be accommodated to simulate fixed or variable dose therapies in virtual individuals. Researchers are currently expanding this basic model into a whole-body PBPK model where a single tissue represents a single compartment (Figure 1.7). This way, identification of pharmacokinetics for each and every tissue is possible and a comprehensive report is obtained [111].

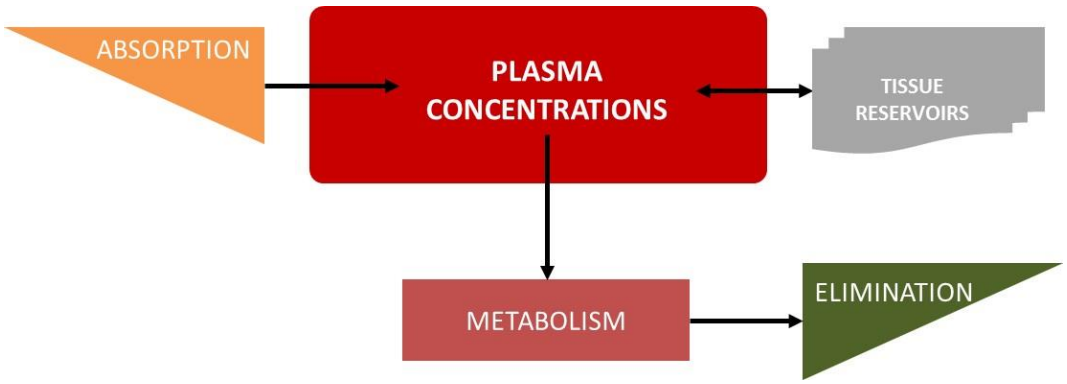

Figure 1.5 Example of a simple PBPK model consisting three compartments to measure the pharmacokinetics of a drug in plasma.

Key details could be identified such as affinity of the drug to a particular tissue(s), extent of drug penetration into various layers of a tissue, influence of gastrointestinal transit times in adults vs. children, effect of variable clearance rates among different alleles, drug-drug interactions, different routes of administration and various types of formulations (Figure 1.6). Safety and efficacy of drug exposure-response in a particular tissue could be quantified and evaluated along with identification of intracellular concentrations. Tissue penetration could identify potential drugs that pass through inaccessible sites such as brain, spinal cord, testes, lymphatic system and also analyse their respective concentrations, which could be difficult to observe *in vivo*. This feature could be helpful in identifying the reach of ARVs across both anatomical and cellular sanctuary sites [112]. Lack of information on various drug-drug interactions could be investigated using PBPK modelling and the doses could be optimised accordingly. Dose adjustments were suggested for artemether which requires 160 mg more of the antimalarial drug to induce a similar effect when administered in combination with efavirenz [113, 114]. Genetic variations affecting the clearance of the drug could result in toxicity or under exposure which can be addressed with modelling to inform optimal doses needed for appropriate therapy. Xu et al. have used clinical data

to validate PBPK models at different clearance rates of efavirenz observed for different CYP2B6 alleles [115]. Pharmacokinetics of clopidogrel and its active metabolite were predicted and compared in populations with CYP2C19 genetic polymorphisms having slow, intermediate, rapid and ultrafast clearance rates [116]. Different age groups can be segregated and an optimum dose could be informed in special population, decreasing the toxicity profile of drugs and adverse effects in chronic dosing. Potential routes of administration could be compared and the optimal dose to reach therapeutic efficacy could be informed along with the study of the interaction between formulation and human environment [111].

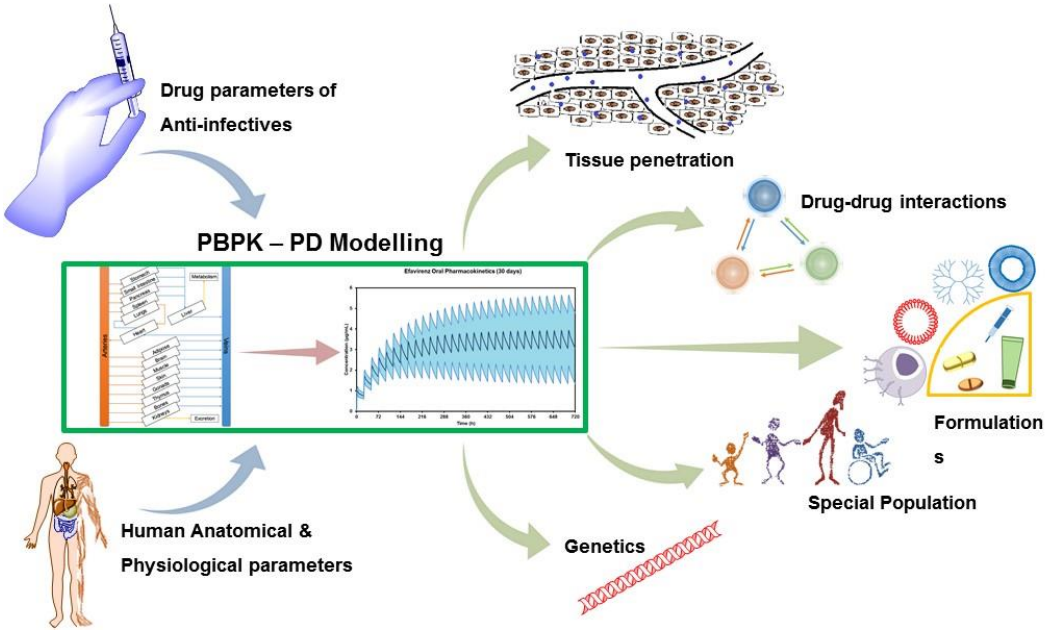

Figure 1.6 A flow chart representing the summary of various factors that can be evaluated with a PBPK model using physiochemical parameters of the drug, anatomical and physiological parameters of an individual. (Adapted from Moss et al. 2015 [111])

PBPK models can predict a virtual population if variability is introduced into the parameters of the model. It would be possible to examine the effect of one constraint on the drug pharmacokinetics by performing sensitivity analysis to identify the influencing physicochemical parameter during drug discovery process [117]. In addition,

the pharmacodynamic profile could be scrutinized when PBPK models are combined with *in vivo* parameters to identify non-toxic drug levels required for therapeutic exposure [111].

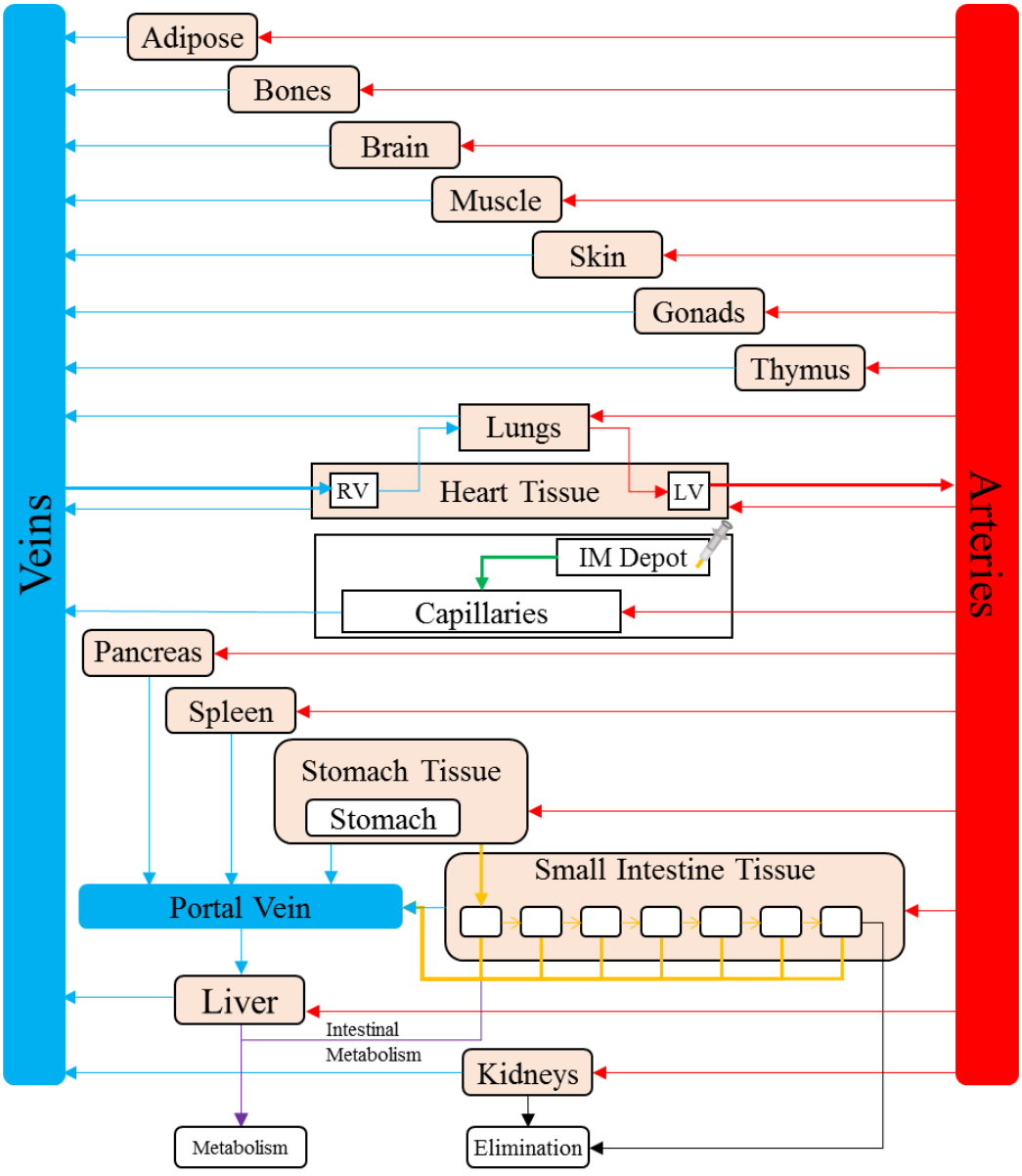

Figure 1.7 A whole-body PBPK model representing various tissues and organs in compartments. Small intestine was divided into seven compartments for effective absorption. Each line in the figure represents a first-order kinetic equation which computes the distribution of drug through the tissues. [118-120]

1.9. Aims

The overall aim of the thesis was to generate innovative computational and experimental methods to support the rational design of LAI formulations. The clinical success of LA administration strategies can be deeply influenced by multiple factors including pharmacokinetics and formulation characteristics. Consequently, a comprehensive understanding of ARV pharmacology, suitable experimental methods for the characterisation of formulation properties and predictive pharmacokinetic models for the simulation of clinical scenarios can represent valuable tools to inform the design of novel LA strategies. Novel PBPK models for virtual adult and paediatric populations were developed to identify the optimal dose and release rates for ARVs. Additionally, the release rate of existing LAI formulations was determined using *in vitro* methods in order to extrapolate the values to human parameters through *in vitro-in vivo* extrapolation (IVIVE).

The main objective of Chapter 2 was to design and construct a novel PBPK model for the simulation of the pharmacokinetics of most commonly used ARVs to hypothesise the potential use of LAI IM formulations in adults. Optimal dose and release rates were identified for eight different ARVs. The following study in Chapter 3 was to design and validate a PBPK model for paediatric patients aged 3-18 years, providing a comprehensive mathematical evaluation of physiological and anatomical characteristics of children and adolescents. Further to the validation, in Chapter 4, simulations were performed to inform the dose of cabotegravir and rilpivirine LAI formulations in children and adolescents. Informed dose in paediatric individuals was simulated for standard weight categories according to World Health Organization (WHO) guidelines.

Drug release from three *in vitro* methods for LAI formulations were evaluated in Chapter 5. I*n vitro* experiments were performed with four different clinically available LAI formulations to identify the release rate from formulations. PBPK models for the four formulations were constructed and the predicted release rates were compared against *in vitro* release rates to inform IVIVE in Chapter 6, in order to develop an integrated approach for the prediction of the pharmacokinetics of future LAI formulations.

CHAPTER 2

Optimisation of intramuscular dose and release rate for long-acting nanoformulations using PBPK modelling in adults

Contents

2.1. Introduction

LAI formulations of ARVs rilpivirine and S/GSK1265744/cabotegravir have been developed with the potential for once monthly dosing, or less frequently [121]. The development of the first LAI ARV formulations has led to considerable interest amongst patients; a recent study found that 84 % of surveyed patients would definitely or probably try a once-monthly LAI ARV [122]. The LAI formulations are based on nanoparticulate suspensions milled with an average particle size of 200 nm for both these drugs [86, 123] which release the drug from the depot over a protracted period of time. The optimisation of nano-formulations for LA administration is complicated by several pharmacokinetic factors and has to take into account - the optimal dose and drug release into the circulation to achieve therapeutic or prophylactic plasma concentrations for the entire dosing interval.

The pharmacokinetics of a drug are determined by processes that can be simulated through PBPK models. Specifically, PBPK can be used to predict pharmacokinetics as a function of formulation and route of administration [124]. These predictions can then inform the design of LAI formulations, identifying optimal characteristics in terms of dose and depot release rate. For ARVs, this modelling approach has been applied to identify factors influencing the pharmacokinetics of novel formulations[74], the effect of genetics on drug distribution [125], pharmacokinetics in special populations [126] and drug-drug interactions [127].

The aim of this study was to simulate the pharmacokinetics of ARVs after administration of virtual IM LAI formulations using PBPK modelling. An open sourced software Matlab was used to design and develop PBPK models due to its ease of use with a minimal knowledge of programming languages. The PBPK models were first

validated against clinical data for oral counterparts, to assess the accuracy of the simulation. Theoretical target dose and release rate combinations for once weekly and once monthly IM administration were then identified.

2.2. Methods

Virtual patients between the ages of 18 to 60 years were generated. All organs and tissues were represented as individual compartments. The model was based on the assumptions: 1) well-stirred compartments with instant distribution of the drug; 2) no oral drug absorption from the colon; and 3) the model is blood-flow limited. The PBPK model was designed using Simbiology v.4.3.1, a product of Matlab v.8.2 (MathWorks, Natick, MA, USA 2013). The PBPK approach has been developed for key ARVs (two NRTIs, tenofovir and emtricitabine; three NNRTIs, efavirenz, rilpivirine and etravirine; two integrase inhibitors (IIs), raltegravir and dolutegravir and an unboosted protease inhibitor (PI), atazanavir.

2.2.1. Anatomy

The age, body mass index (BMI), and weight of the individual were initially defined. Using allometric equations, the body surface area [128] and height are derived as follows:

$$Height\ (in\ m) = \frac{Weight\ (in\ kg)}{BMI\ (in\ m^2/kg)}$$

$$Body\ surface\ area\ (in\ m^2) = Weight\ (in\ kg)^{0.425} \times Height\ (in\ cm)^{0.725} \times 0.007184$$

These initial values were used for the calculation of organ and tissue volumes through allometric equations shown in Table 2.1a [129]. The blood circulation was represented by considering the cardiac output and regional blood flows as shown in Table 2.1b [130].

Table 2.1a Allometric equations to compute the weights of each tissue and organ represented in kg [129]

Adipose = ((((1.20*BMI)+(0.23*Age)-16.2)*Weight)/100) ± 0.041
Blood = 3.33*BSA-0.81 ± 0.1
Bones = exp(0.0689+2.67*log(Height)) ± 0.166
Brain = 0.405*exp(-Age/629)*(3.68-2.68*exp(-Age/0.89)) ± 0.084
Gonads = (3.3+53*(1-(exp((-Age/17.5)^5.4)))/1000 ± 0.049
Heart = exp(-2.502+2.13*log(Height)) ± 0.069
Intestines = exp(-1.351+2.47*log(Height)) ± 0.049
Kidneys = exp(-2.306+1.93*log(Height)) ± 0.14
Liver = exp(-0.6786+1.98*log(Height)) ± 0.028
Lungs = exp(-2.092+2.1*log(Height)) ± 0.195
Muscle = 0.93*Weight-Total weight
Pancreas = exp(-3.431+2.43*log(Height)) ± 0.245
Remaining = exp(-0.072+1.95*log(Height) ± 0.049
Skin = exp(1.64*BSA-1.93) ± 0.049
Spleen = exp(-3.123+2.16*log(Height)) ± 0.156
Stomach = exp(-3.266+2.45*log(Height)) ± 0.0965
Thymus= 14*((7.1-6.1*exp(-Age/11.9))*((0.14+0.86*exp(-Age/10.3))))/1000 ± 0.049
Total weight = Lungs+Heart+Bones+Kidneys+Stomach+Intestines+Spleen+Pancreas+ Liver+Remaining+Brain+Skin+Blood+Adipose+Thymus+Gonads

Age is in years, BMI is in kg/m^2, BSA is in m^2, height is in m, and weight is in kg

Table 2.1b Cardiac output and the blood flow reaching each organ and tissue represented as fraction of the cardiac output in L/h [130]

Cardiac Output (in L/h)	15*(Weight^0.75)
Adipose tissue	0.052
Bones	0.042
Brain	0.11
Gonads	0.01
Gut	0.05
Hepatic artery	0.12
Hepatic vein	0.32
Kidneys	0.175
Lungs	0.025
Muscle	0.19
Pancreas	0.05
Portal vein	0.20
Remaining tissues	0.01
Skin	0.06
Spleen	0.05
Stomach	0.05

Weight is in kg

2.2.2. Intestinal Absorption

A compartmental absorption and transit model has been integrated to simulate for oral drugs as previously described [118]. Absorption rate was evaluated using the apparent permeability obtained from caco-2 cells or the polar surface area (PSA) and hydrogen bond donor (HBD) values as previously described [131]. The IVIVE correlation was obtained using 25 compounds with a standard protocol in order to evaluate the apparent permeability from caco-2 monolayers and comparing against *in vivo* values [57, 132]. The integrity of the monolayers was evaluated using transepithelial

electrical resistance (TEER) value (mean ~ 260 Ω cm^2) and lucifer yellow as a non-radioactive alternative [132].

2.2.3. Intestinal Metabolism

The clearance of drugs in the gut (CL_{gut}) was calculated considering the *in vitro* intrinsic clearance (CL_{int}) and as an example, the abundance of cytochrome P450 family 3, subfamily A (CYP3A) in the intestinal tissue (Ab_{CYP3A}) is given as follows [57, 131]:

$$CL_{gut}\ (L/h) = \frac{CL_{int} \times Ab_{CYP3A} \times 1000 \times 60}{1000000}$$

The fraction of the drug transiting to the liver after metabolism in the gut (F_g) was computed using the following equation:

$$F_g = \frac{Q_{gut}}{Q_{gut} + f_{u,gut} \times CL_{gut}}$$

where Q_{gut} represents the blood flow to the gut and $f_{u,gut}$ is the fraction unbound in the gut.

2.2.4. First pass metabolism

The total intrinsic clearance (TCL_{int}) of an enzyme was calculated as:

$$TCL_{int} = \frac{CL_{int} \times \text{Abundance} \times \text{Liver weight} \times \text{MPPGL} \times 1000 \times 60}{1000000}$$

where Abundance is the amount of enzyme present in a milligram of microsomal protein and MPPGL is amount of microsomal protein per gram of liver [107]:

$$\text{MPPGL} = 10^{1.407 + 0.0158 \times \text{Age} - 0.00038 \times \text{Age}^2 + 0.0000024 \times \text{Age}^3} \pm 4$$

Then the sum of intrinsic clearances of all the enzymes that are metabolising the drug in the liver gives the total apparent clearance (CL_{app}):

$$CL_{app} = \sum_{n=1}^{n} TCL_{int}$$

The systemic clearance (CL) is calculated from the blood and not the liver and is given by the equation:

$$CL = \frac{Q_{hv} \times f_u \times CL_{app}}{Q_{hv} + CL_{app} \times f_u} \quad (6)$$

where Q_{hv} is the hepatic flow rate and f_u is the fraction unbound in plasma.

The fraction of the active drug that is available after first pass hepatic metabolism (F_h) is given as:

$$F_h = 1 - CL/Q_{hv} \quad (7)$$

2.2.5. Systemic Distribution

The volume of distribution and systemic circulation was calculated using previously published equations [119, 133].

2.2.6. Intramuscular depot compartment

A compartment was created to virtually represent the depot with a maximum volume of 6 mL, since it is the maximum volume of injection that has been previously used for IM administration, although lower volumes are usually needed for optimal tolerability. The blood flow to this area was calculated accordingly [99]. The release of the drug from the depot to the blood capillaries present in the muscle was given as [124]:

$$\frac{d}{dt}A = k \times A \quad (8)$$

where A is the amount of drug released from the depot and k is the first-order release rate. A variability of ± 10 % for the release rate values was considered as it would be difficult to design nanoparticles with the exact release rate.

2.2.7. Model validation

The physicochemical properties of ARVs used to build the PBPK models are represented in Table 2.2. The models were primarily validated against clinical data at steady state for oral formulations of the ARVs (Table 2.3a, b). The model was also verified against an existing LAI formulation of rilpivirine [87]. The PBPK models were assumed to be qualified if the mean simulated value is ± 50 % from the mean clinically reported value.

2.2.8. Prediction of pharmacokinetics following IM injection

In the prediction of IM pharmacokinetics, the dose of the ARV and release rate were optimised such that the mean C_{trough} was above the 90/95 % inhibitory concentration ($IC_{90,}$ IC_{95}) for wild type HIV virus or protein-binding adjusted inhibitory concentration ($PAIC_{95}$) after 7- or 30-days after injection. A dose cut-off of 1500 mg was considered for IM administration.

2.2.9. Prediction of Intracellular concentrations

The active phosphate metabolite of tenofovir, tenofovir diphosphate (TFV-DP) intracellular concentrations were simulated as previously described [49]. The first order elimination rate of emtricitabine triphosphate (FTC-TP) from the cellular compartment was calculated considering the half-life of FTC-TP [48]. The maximum uptake velocity (V_{max}) and maximum velocity of anabolism (k_m) were fitted to obtain a zero-order dose input rate (k_{in}) such that the mean intracellular concentration of the

active metabolite at steady state ($C_{ss,avg}$) was in accordance to available clinical data following this equation:

$$k_{in} = (V_{max} \times C)/(k_m + C) \quad (9)$$

where C is the concentration in the plasma.

Values of 0.9 ± 0.18 ng.h/ml and 18 ± 3.6 ng/ml for V_{max} and k_m were suitable to obtain $C_{ss,avg}$ values comparable to previously published data for oral administration [48]. The optimisation of the dose and release rates for emtricitabine and tenofovir considered not only plasma concentrations but also the intracellular FTC-TP and TFV-DP over the reported *in vitro* IC_{50} values of 142 fmol/10^6 cells and 150 fmol/10^6 cells [134].

2.2.10. Sensitivity analysis

Differential sensitivity analysis was performed to identify the key parameters that impact the pharmacokinetic profiles of LAI formulations [135]. The sensitivity coefficient (ϕ_i) indicates the change of plasma concentration values (Y) with respect to a unit change in a parameter (X) as shown in equation 1 [135].

$$\emptyset_i = \frac{\%\Delta Y}{\%\Delta X} \quad (1)$$

Analysis was performed with the first monthly IM dose for all the 8 ARVs in adults. Sensitivity was analysed using the provided inbuilt feature of Simbiology at user-defined values without normalisation in the computation. Six parameters – blood-to-plasma ratio, cardiac output, clearance, weight, protein binding, and release rate were analysed against plasma concentration of the drug. Each parameter was varied 20 % from its mean value and 100 simulations were run while keeping the rest of

the parameters constant and the analysis was performed. Sensitivity greater than 0.1 was considered to have a substantial effect on the drug exposure over time.

Table 2.2 Physicochemical properties, *in vitro* and population pharmacokinetic data of ARVs

Drug Properties								
	Atazanavir	**Dolutegravir**	**Efavirenz**	**Emtricitabine**	**Etravirine**	**Raltegravir**	**Rilpivirine**	**Tenofovir**
Molecular weight	704	419	316	247	435	444	366	287
log $P_{o:w}$	3.17	2.20	4.60	-0.43	5.20	0.58	4.32	1.25
Protein binding	86.0 %	99.3 %	99.0 %	4.0 %	99.9 %	83.0 %	99.7 %	0.7 %
pK_a	7.4	8.3	10.2	2.65	3.75	6.67	3.26	3.75
R	0.75 [127]	0.535 [136]	0.74 [114]	1.0 [137]	0.7 [138]	0.6 [54]	0.67 [139]	[b]1
PSA ($Å^2$)	-	-	38.33	-	120.64	-	-	-
HBD	-	-	1	-	3	-	-	-
P_{app} (10^{-6} cm/s)	-	-	2.5 [114]	-	-	6.6 [54]	12 [139]	-
k_a (h^{-1})	1.5 [127]	1.63 ± 1.03 [140]	-	1.0 [141]	-	-	-	1.03 [47]
F	68 %	-	-	93 %	-	-	-	20 %
V_d (L/kg)	1.2 [127]	-	3.6	1.4 ± 0.3	[a]6.03	0.6	-	0.813 [142]

Metabolism								
	Atazanavir	**Dolutegravir**	**Efavirenz**	**Emtricitabine**	**Etravirine**	**Raltegravir**	**Rilpivirine**	**Tenofovir**
CL/F (L/h)	[a]12.6(10.5-15.4) [143]	1 (15 %) [144]	-	-	-	4.62 [58]	-	-
Renal Clearance (L/h)	-	-	-	12.80 ± 5.34 [137]	-	3.6 [54]	-	11.3 ± 6.2 [145]
CYP2A6 CL_{int}	-	-	0.08 [114]	-	-	-	-	-
CYP2B6 CL_{int}	-	-	0.55 [114]	-	-	-	-	-
CYP1A2 CL_{int}	-	-	0.07 [114]	-	-	-	-	-
CYP3A4 CL_{int}	-	[†]3.0 [146]	0.007 [114]	-	0.012 [147]	-	2.04 [139]	-
M2 CYP3A4 CL_{int}	-	-	-	-	0.00091 [147]	-	-	-
CYP3A5 CL_{int}	-	-	0.03 [114]	-	-	-	-	-
CYP2C19 CL_{int}	-	-	-	-	0.75 [147]	-	-	-
UGT1A1 CL_{int}	-	[†]3.2 [146]	-	-	-	[‡]12.4 [54]	-	-

CYPs induction								
	Atazanavir	**Dolutegravir**	**Efavirenz**	**Emtricitabine**	**Etravirine**	**Raltegravir**	**Rilpivirine**	**Tenofovir**
CYP3A4 Ind_{max}	-	-	6.5 [114]	-	2.5 [147]	-	-	-
CYP2B6 Ind_{max}	-	-	5.7 [114]	-	-	-	-	-
CYP3A4 Ind_{50}	-	-	3.9 [114]	-	-	-	-	-
CYP2B6 Ind_{50}	-	-	0.8 [114]	-	-	-	-	-

[a] An average adult body weight of 70 kg was assumed, [b] Value was an assumption (as the drug is similar to emtricitabine and tenofovir value was not available in the literature), † The units are in µl/min/mg, ‡ The units are in µl/min/10^6 hepatocytes; log $P_{o:w}$ – Partition coefficient between octanol and water; pKa – logarithmic value of the dissociation constant; R – blood-to-plasma drug ratio; PSA – polar surface area; HBD – number of hydrogen bond donors; P_{app} – drug permeability from apical to basolateral in caco-2 cell monolayer;; K_a – absorption coefficient; F – absolute bioavailability; V_d – volume of distribution; CL/F – Apparent oral clearance; Cl_{int} – intrinsic clearance (µL/min/pmol); CYP – cytochrome P450; UGT - uridine diphosphate glucuronosyltransferase; M2 – Second metabolite; Ind_{max} – induction maximum; Ind_{50} – 50 % induction; '-' – data not available/ not applicable

Table 2.3a Validation of antiretrovirals at steady state: Clinical vs. Predicted AUC, C_{max} and C_{trough}

Drug	Dose (mg)	AUC (ng×h/ml)		C_{max} (ng/ml)		C_{trough} (ng/ml)	
		Clinical	[a]Predicted	Clinical	[a]Predicted	Clinical	[a]Predicted
Efavirenz	600 OD	[a]57,150 ± 27,300 [148]	65,006 ± 16,383	4,000 ± 1,710 [148]	3,193 ± 699.7	2,380 ± 1,140 [148]	2,298 ± 671.0
Etravirine	200 BD	[a]3,713 ± 2,069 [149]	3,939 ± 1,249	451.3 ± 232.3 [149]	375.0 ± 106.1	235.9 ± 163.1 [149]	285.4 ± 100.5
Rilpivirine	25 OD	[a]2,589 ± 868.8 [139]	3,590 ± 1,256	203.8 ± 75.81 [139]	214.1 ± 53.9	89.85 ± 38.07 [139]	95.7 ± 49.5
Raltegravir	400 BD	[a]7,076 ± 4,071 [150]	9,584 ± 2,160	2,519 ± 1,930 [150]	2,002 ± 378.9	71 ± 50 [150]	54.6 ± 52.1
Atazanavir	400 OD	[a]29,303 ± 8,263 [151]	24,354 ± 4,307	5,358 ± 1,371 [151]	2,718 ± 392.2	218 ± 191 [151]	326.9 ± 150.0
Tenofovir	300 OD	[b]3,324 (41.2 %) [142]	4,707 ± 1,004	326 (36.6 %) [142]	580.2 ± 80.6	64.4 (39.4 %) [142]	20.7 ± 17.7
Emtricitabine	200 OD	[b]10,100 (18 %) [48]	9747 ± 2326	1,720 (16 %) [48]	1,136 ± 236.3	73 (28 %) [48]	52.5 ± 32.2
Dolutegravir	50 OD	[b]53,600 (27 %) [144]	63,615 ± 8,802	3,670 (20 %) [144]	3,474 ± 519.6	1,110 (46 %) [144]	1,867 ± 309.0

[a] Arithmetic Mean ± S.D., [b] Geometric Mean (% CV – coefficient of variation expressed as a percentage), AUC – area under the concentration-time curve, C_{max} – maximum plasma concentration, C_{trough} – trough plasma concentration, OD – once daily, BD – twice daily.

Table 2.3b Validation of antiretrovirals at steady state: Percentage difference between clinical vs. predicted AUC, C_{max} and C_{trough}

Drug	AUC	C_{max}	C_{trough}
Efavirenz	13.7%	-20.2%	-3.4%
Etravirine	6.1%	-16.9%	21.0%
Rilpivirine	38.7%	5.1%	6.5%
Raltegravir	35.4%	-20.5%	-23.1%
Atazanavir	-16.9%	-49.3%	50.0%
Tenofovir	41.6%	78.0%	-67.9%
Emtricitabine	-3.5%	-34.0%	-28.1%
Dolutegravir	18.7%	-5.3%	68.2%

2.3. Results

The validation was conducted by comparing the mean simulated $C_{trough,}$ C_{max} and AUC with the available clinical data for oral administration and also for an existing LA IM formulation of rilpivirine (600 mg; 100 mg/ml) (shown in Figure 2.1). For emtricitabine and tenofovir, the $C_{ss,avg}$ of FTC-TP and TFV-DP were compared with clinical data [48]. Although the commonly agreeable limits of variability for validation is 2-fold from the mean value, we used a more stringent value of 0.5-fold to enhance the accuracy of the predictions [152].

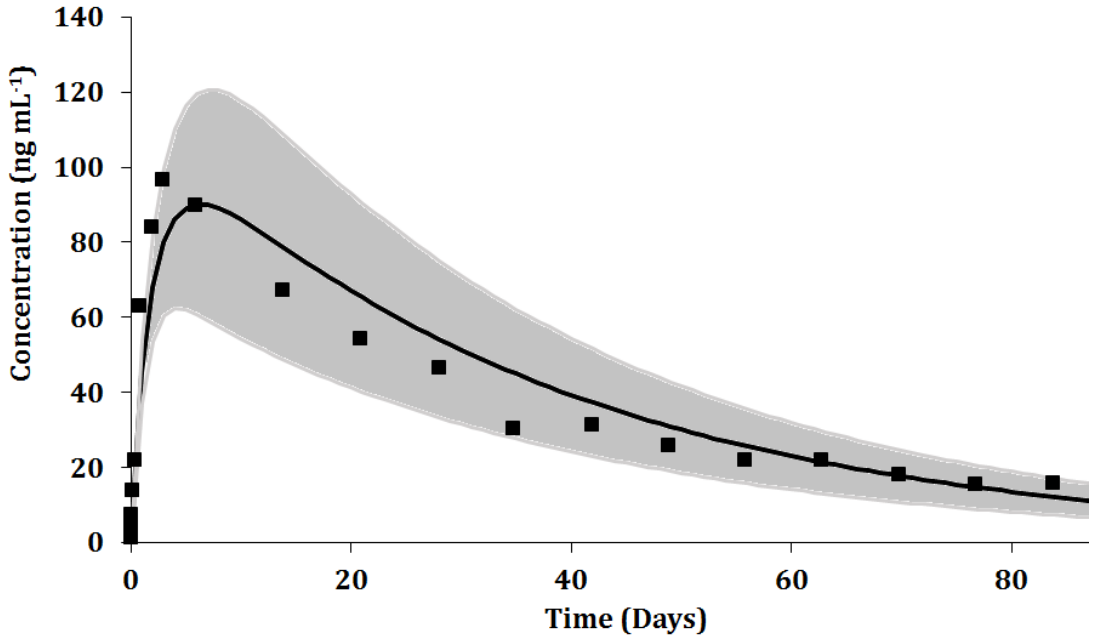

Figure 2.1 Validation of the physiologically based pharmacokinetic strategy against clinical data for an existing rilpivirine long-acting nanoformulation (600 mg; 100 mg/ml) [87]

For IM formulations, multiple dose and release rate combinations were simulated to obtain mean predicted C_{trough} greater than the defined cut-off. For tenofovir and emtricitabine, the dose and release rates for IM injection were optimised such that the plasma concentrations were over the IC_{90} value and also the $C_{ss,avg}$ were over the intracellular IC_{50}.

A summary of the predicted AUC, C_{max} and C_{trough} for eight ARVs following optimal IM injection is shown in Table 2.4.

2.3.1. Rilpivirine

The validation of the PBPK model for rilpivirine was done using available oral clinical data. The simulated mean AUC, C_{max} and C_{trough} values deviated +38.7 %, +5.1 % and +6.7 %, respectively from the clinical data [139]. The PBPK model was additionally validated against an existing LA IM formulation of rilpivirine (600 mg; 100 mg/mL) [87]. The release rate from the IM depot was predicted after matching the model to the clinical pharmacokinetic data. The drug release followed dose-dependent first-order kinetics and the release rate was predicted to be between 0.0009 and 0.0012 h^{-1} (Figure 2.1). The mean values for AUC were 84.0 ng×h/ml vs. 83.38 ± 33.34 ng×h/ml, C_{max} 96.7 ng/ml vs. 86.73 ± 30.51 ng/ml and C_{trough} 15.7 vs. 11.81 ± 6.3 ng/ml for clinical versus simulated data. After the validation step with both oral and LA IM formulations, the optimal dose and release rates of both weekly and monthly injection regimens of rilpivirine were identified such that the plasma concentration is over the $PAIC_{95}$ value of 20.3 ng/ml [153]. A weekly dose of 60 mg with a release rate of 0.02 h^{-1} and a monthly dose of 250 mg with a release rate of 0.002 h^{-1} were predicted to maintain the plasma concentrations above the target cut-off.

2.3.2. Atazanavir

The validation at steady-state for the oral administration of unboosted atazanavir resulted in mean predicted AUC, C_{max} and C_{trough} values which were -16.9 %, -49.3 % and +50.0 % of those observed clinically [151]. An IM dose of 1500 mg atazanavir was predicted to result in plasma concentrations after 30 days below the $PAIC_{95}$ (60 ng/ml) and was therefore deemed unsuitable for monthly injection. An IM weekly

dose of 400 mg however was predicted to achieve mean concentrations in excess of the $PAIC_{95}$ with a release rate of 0.009 h^{-1} [154].

2.3.3. Dolutegravir

The predicted variation from the clinical values for mean AUC, C_{max} and C_{trough} in the validation of oral administration of dolutegravir were +18.7 %, -5.3 % and +68.2 %, respectively [144]. Considering the $PAIC_{95}$ value of 64 ng/ml as the target concentration, the simulated IM administration requires an estimated weekly dose of 20 mg with a release rate of 0.006 h^{-1} and a monthly dose of 105 mg with a release rate of 0.002 h^{-1} [155].

2.3.4. Emtricitabine

The predicted variation from the clinical values in mean AUC, C_{max} and C_{trough} for oral emtricitabine were -3.5 %, -34.0 % and -28.1 %, respectively [137] and the simulated mean $C_{ss,avg}$ of intracellular FTC-TP has a deviation of +10.9 % from the clinical value (Table 2.5). The IC_{90} value of 50.2 ng/ml and intracellular IC_{50} of 127 fmol/10^6 cells were considered as target concentrations [48, 156]. The simulated IM injection required a dose of 375 mg with a release rate of 0.009 h^{-1} for a weekly administration and 1500 mg with a release rate of 0.0015 h^{-1} for a monthly administration [48].

2.3.5. Efavirenz

The validated PBPK model yielded AUC, C_{max} and C_{trough} values, which were +13.7 %, -20.2 % and -3.4 % compared to the clinical values [148]. In order to obtain plasma concentrations above the $PAIC_{95}$ value of 126 ng/ml, a weekly IM dose of 200

mg (release rate - 0.015 h^{-1}) and monthly dose of 800 mg (release rate - 0.007 h^{-1}) were required [154].

2.3.6. Etravirine

The validated PBPK model with oral administration of etravirine resulted in mean AUC, C_{max} and C_{trough} values which were +6.1 %, -16.9 % and +21.0 % compared to the clinical values [149]. The IM predictions indicate that etravirine may be suitable for weekly administration with a dose of 700 mg and release rate of 0.015 h^{-1} but not for monthly administration as the drug concentrations fall below the $PAIC_{95}$ value even for an IM dose of 1500 mg [154].

2.3.7. Raltegravir

The predicted mean AUC, C_{max} and C_{trough} of orally administered raltegravir were +35.4 %, -25.0 % and -30.3 % compared to the clinical values, respectively [150]. To maintain the plasma concentrations above the IC_{95} value (15 ng/ml), the prediction suggested a dose of 200 mg (release rate – 0.005 h^{-1}) and 800 mg (release rate – 0.002 h^{-1}) may enable weekly and monthly IM administration of raltegravir, respectively [157].

2.3.8. Tenofovir disoproxil fumarate (TDF)

The validated PBPK model for TDF predicted mean AUC, C_{max} and C_{trough} which were +41.6 %, +78.0 %, -67.9 % compared to the clinical data, respectively [142]. The deviation of the intracellular $C_{ss,avg}$ was +4.2 % compared to the clinical value (Table 2.5). 200 mg TDF with a release rate of 0.008 h^{-1} was predicted to provide a sufficient exposure following weekly IM injection and 1300 mg with a release rate of

0.002 h^{-1} was an adequate dose for a monthly IM administration, maintaining mean plasma concentrations above the IC_{90} and intracellular TFV-DP above the IC_{50} [134].

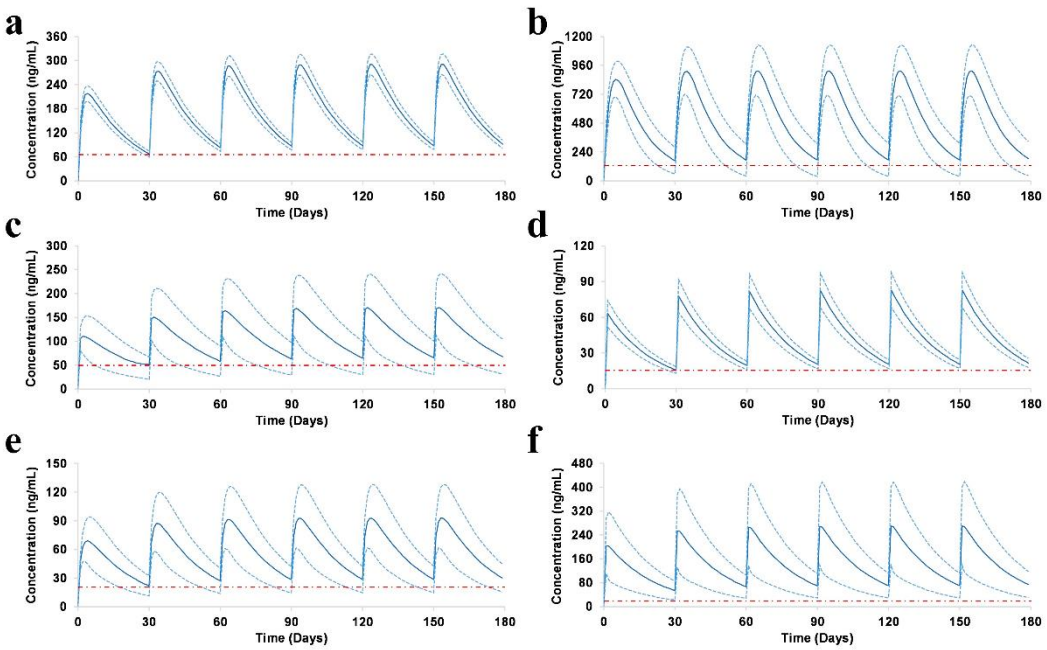

Figure 2.2 Pharmacokinetics of monthly administration of antiretrovirals over a period of 6 months. a) Dolutegravir, b) Efavirenz, c) Emtricitabine, d) Raltegravir, e) Rilpivirine and f) Tenofovir. Mean, Mean ± S.D., $PAIC_{95}/IC_{95}$

Table 2.4 Prediction of the dose and release rate of single intramuscular injection of antiretrovirals (Mean ± S.D.)

Drug	Intramuscular Dose (mg)	Release rate (h^{-1})	Weekly/ Monthly	AUC (µg.h/ml) (Mean ± SD)†	C_{max} (ng/ml) (Mean ± SD)†	C_{trough} (ng/ml) (Mean ± SD)†	Target concentration (ng/ml)
Nucleoside Reverse Transcriptase Inhibitors (NRTIs)							
Emtricitabine	1,500	0.0015	Monthly	43.1 ± 15.4	94.2 ± 32.5	51.2 ± 41.3	50.2 [48] (IC_{90})
	375	0.009	Weekly	20.5 ± 8.9	199.4 ± 76.1	55.6 ± 26.4	
Tenofovir	1,300	0.002	Monthly	52.2 ± 15.4	99.2 ± 28.6	43.8 ± 17.2	18 [158] (IC_{90})
	200	0.008	Weekly	16.6 ± 7.1	155.6 ± 58.5	49.1 ±23.0	
Non-Nucleoside Reverse Transcriptase Inhibitors (NNRTIs)							
Efavirenz	800	0.007	Monthly	333.9 ± 99.3	850.4 ± 194.6	140.0 ± 50.8	126 [154] ($PAIC_{95}$)
	200	0.015	Weekly	73.2 ± 22.1	546.5 ± 139.5	273.3 ± 81.8	
Etravirine	700	0.015	Weekly	43.4 ± 12.3	359.3 ± 80.7	126.1 ± 60.7	116 [154] ($PAIC_{95}$)
Rilpivirine*	250	0.002	Monthly	32.9 ± 14.7	75.4 ± 30.1	22.6 ± 8.2	20.3[153] ($PAIC_{95}$)
	60	0.015	Weekly	10.8 ± 4.8	97.4 ± 33.3	26.1 ± 18.7	

Integrase Inhibitors (IIs)							
Dolutegravir	105	0.002	Monthly	95.6 ± 8.5	212.1 ± 18.1	65.7 ± 7.1	64 [155] ($PAIC_{95}$)
	20	0.006	Weekly	24.2 ± 2.8	169.5 ± 18.1	101.7 ± 14.8	
Raltegravir	800	0.002	Monthly	26.1 ± 5.2	66.9 ± 13.1	15.7 ± 2.8	15 [157] (IC_{95})
	200	0.005	Weekly	8.23 ± 1.47	69.4 ± 12.1	30.1 ± 5.4	
Protease Inhibitors (PIs)							
Atazanavir	400	0.009	Weekly	38.9 ± 8.3	334.3 ± 70.7	114.8 ± 25.4	60 [154] ($PAIC_{95}$)

* Note that this dose is not for the existing rilpivirine formulation; †Arithmetic Mean and standard deviation; AUC – area under the concentration-time curve, C_{max} – maximum plasma concentration, C_{trough} – trough plasma concentration, IC_{90} – 90 % inhibitory concentration, $PAIC_{95}$ – 95 % protein binding adjusted inhibitory concentration

Table 2.5 Validation and prediction of intracellular concentration of emtricitabine triphosphate and tenofovir diphosphate

Active Drug	Intracellular $C_{ss,avg}$ (fmol/10^6 cells)		Weekly/	Intramuscular Prediction (fmol/10^6 cells)		*In vitro* IC_{50}
	Clinical	Simulated	Monthly	Intracellular C_{trough}	Intracellular C_{max}	(fmol/10^6 cells)
Emtricitabine triphosphate	1124.4 ± 592.1 [48]	1,154 ± 456	Monthly	163.0 ± 124.6	228.2 ± 106.1	127 [156]
			Weekly	270.0 ± 130.0	431.8 ± 198.4	
Tenofovir di-phosphate	150.7 ± 92.9 [49]	156.5 ± 59.5	Monthly	154.2 ± 46.5	164.6 ± 49.3	150 [134]
			Weekly	163.0 ± 59.0	174.9 ± 62.8	

$C_{ss,avg}$ – Average steady state concentration, C_{trough} - trough concentration at the end of the duration, C_{max} – maximum concentration, IC_{50} - 50 % inhibitory concentration

2.3.9. Sensitivity analysis

The mean differential sensitivity analyses of 100 runs performed for the eight ARVs is presented in Figure 2.3. Atazanavir and dolutegravir consist of two charts each as shown in Figure 2.3a due to high sensitivity observed for two parameters.

Atazanavir was highly sensitive to the weight of the individual compared to unbound fraction (f_u), blood-to-plasma ratio (R), IM release rate (K_{im}) and cardiac output (CO) and not sensitive to systemic clearance (CL). Weight, f_u and CO showed a positive relationship against plasma concentration in the initial days indicating an increase in plasma concentration with increase in these parameters than in the subsequent days with a negative correlation. A delayed pattern with lower sensitivity could be observed for R, however K_{im} showed a negative correlation throughout imposing a negative effect on the plasma concentration as this parameter increases.

Dolutegravir plasma concentration is highly sensitive to K_{im} with a positive correlation. Change in f_u does not have any effect on the plasma concentration. The rest of the parameters have a low sensitivity negative relationship with a decrease in plasma concentration if there is an increase in these parameters.

Efavirenz drug specific parameters f_u, K_{im}, R and weight of the individual were observed to have a negative correlation against plasma concentration throughout the analysis indicating a decrease in the exposure as these parameters increase. However, systemic clearance and cardiac output doesn't seem to have any effect on the plasma concentration.

Emtricitabine pharmacokinetic curve has a negative correlation with all the six parameters. However the sensitivity is below 0.1 for all the parameters, which implies that they do not have any substantial effect on the plasma concentration curve.

Weight of the individual is highly sensitive and has a negative correlation against plasma concentration of etravirine. Rest of the parameters lie between ± 0.03, indicating a minimal effect. Clearance was observed to have an initial positive correlation and changes to a negative correlation as time progresses, but the rest of the parameters show a negative correlation.

Raltegravir, rilpivirine and tenofovir have a minimal effect on their respective plasma concentrations with a change in these six parameters since the sensitivity against this parameters lies within a mere ± 0.004 throughout the dosing interval.

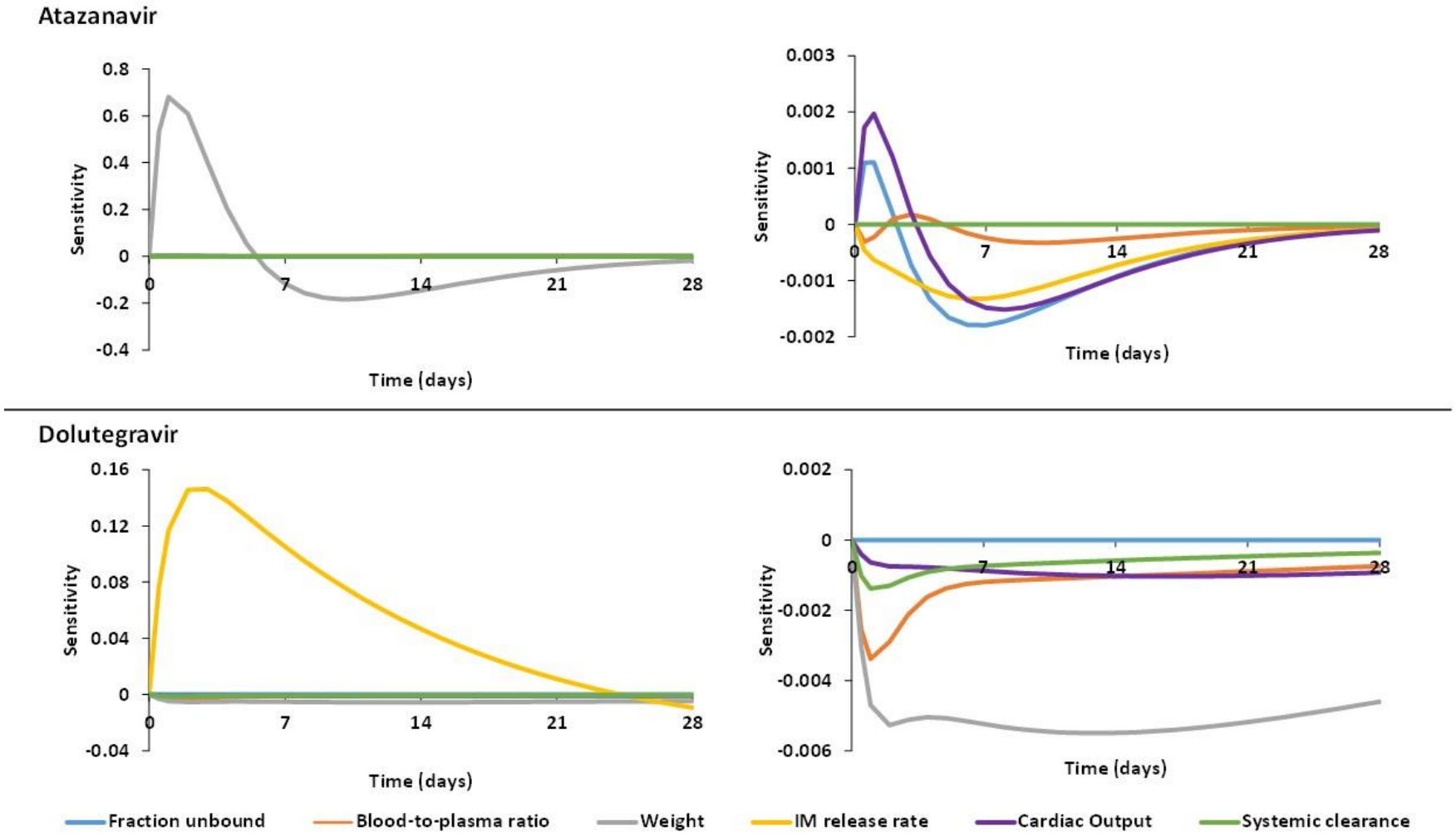

Figure 2.3a Sensitivity analysis of six different parameters against plasma concentration for a single IM dose of dolutegravir and atazanavir

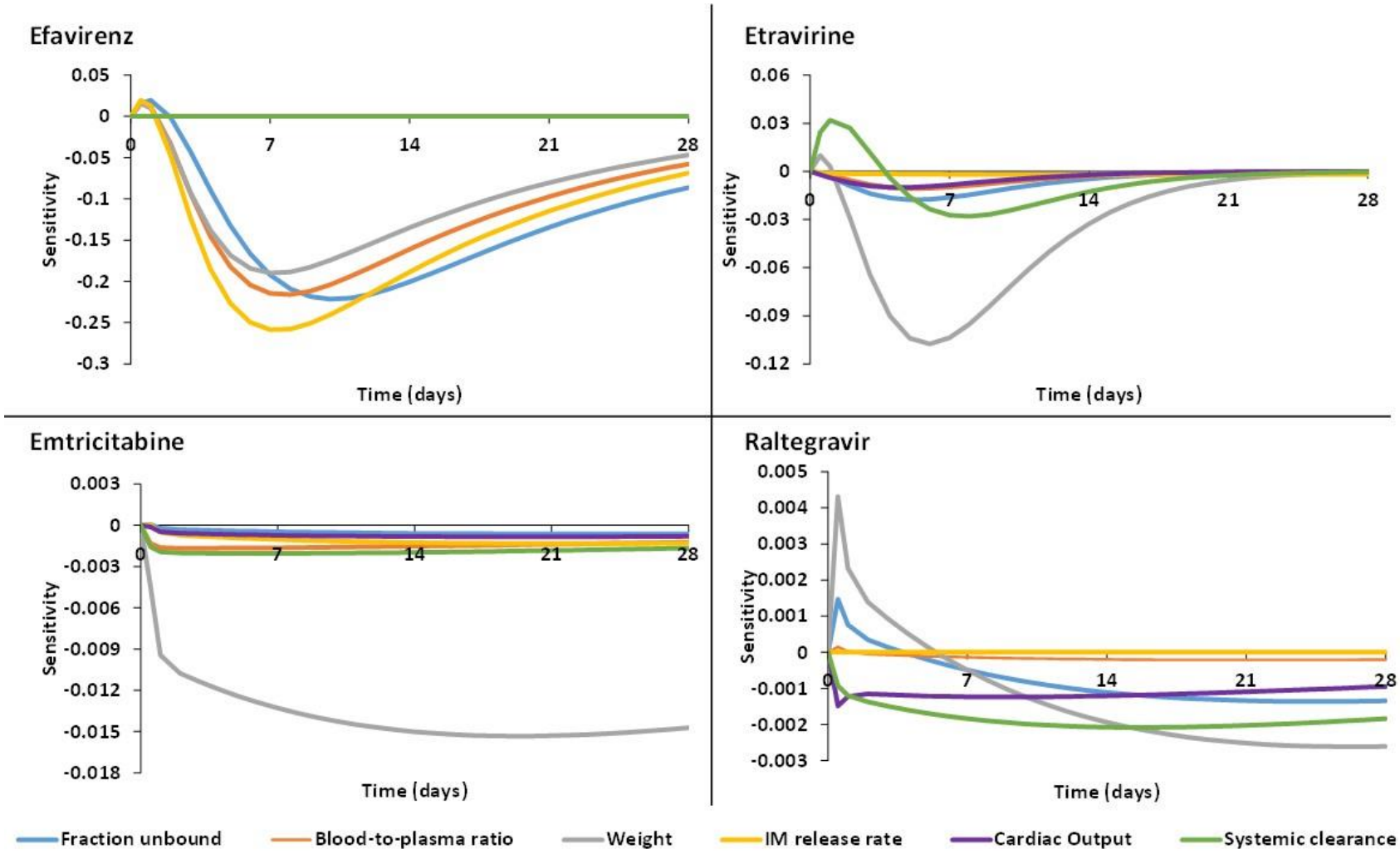

Figure 2.3b Sensitivity analysis of six different parameters against plasma concentration for a single IM dose of efavirenz, etravirine, emtricitabine and raltegravir

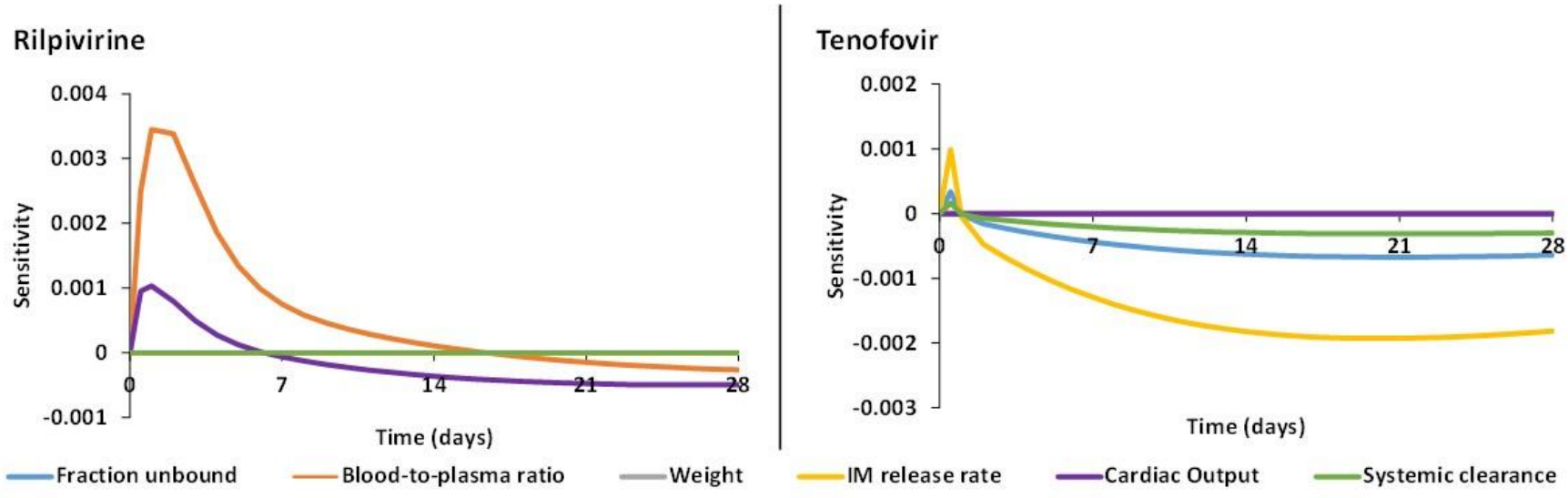

Figure 2.3c Sensitivity analysis of six different parameters against plasma concentration for a single IM dose of rilpivirine and tenofovir

2.4. Discussion

Imperfect adherence to daily oral ARV formulations continues to hinder the efficacy of HIV therapy and PrEP. Alternative administration strategies are beginning to emerge that provide opportunities for once monthly or even less frequent administration. A greater understanding of formulation characteristics is required to predict dose and release rates that provide adequate pharmacokinetic exposure relative to potency. This information will facilitate development of newer LAI ARV formulations.

In this study, PBPK modelling was used to predict the pharmacokinetics of ARVs following IM injection. The PBPK models were initially validated for eight orally administered ARVs against available clinical data for oral formulations. Subsequently, IM administration was simulated by adding an additional compartment to the model to represent the IM depot. For this, a first-order kinetics constant was applied to represent the diffusion of ARVs from the depot to the surrounding blood capillaries (as shown in Chapter 1 Figure 1.7). This approach was validated comparing simulated pharmacokinetics of rilpivirine following IM injection versus available clinical data for the LAI formulation. The primary objective of this study was to identify whether drug-specific doses and release rates from the depot predicted compatibility for IM administration. To obtain the suppression of the viral replication, ARV C_{trough} should reach and be maintained at concentrations above the susceptibility of the virus to that drug. Where possible, dose and release rate were optimised such that the ARV C_{trough} remained above previously identified target values. Target concentrations were identified as equal to $PAIC_{95}$ which represent the ARV concentration that can inhibit 95 % of the virus replication *in vitro*. Since emtricitabine and tenofovir are characterised by very low protein binding (< 4 % and < 0.7 % respectively) IC_{90} values were considered (IC_{95} data not available). The intracellular concentrations of FTC-TP and

TFV-DP were also used as target concentrations in the optimisation of IM dose and release rates for emtricitabine and tenofovir. Although the $PAIC_{95}$ represents a rational pharmacodynamic cut-off and has been discussed extensively elsewhere, some ARVs do not exert a good relationship between trough concentrations and virologic efficacy [154]. In certain cases clinical studies have suggested that the minimum effective concentrations for therapy might be higher than the *in vitro* IC_{95}.

The validation of PBPK models is essential to identify the correct parameters for an accurate simulation of each ARV. Since evidence suggests that dissolved molecule rather than nanoparticle predominates systemically after IM administration of SDNs [79], the volume of distribution, metabolism and elimination were fixed irrespective of the route of administration. As such, it should be noted that the presented data are only applicable when this is assumed to be the case, and these models cannot be applied to technologies that change these parameters (e.g. nanocarrier systems such as nanoemulsions or polymeric nanoparticles). In these cases, part of the formulation should be considered as intravenous administration, if the carrier systems reach the blood stream intact. Depending on the carrier stability in the aqueous environment, the nanoparticles can either provide instant or prolonged release thus changing the drug distribution kinetics. Additionally, particles less than 5 nm are eliminated by kidneys, altering the elimination pattern [159]. Each model prediction was carried out at steady-state to better represent the long-term ARV pharmacokinetics and relevant clinical scenarios. The model was considered validated if the mean AUC of the simulation for each ARV was within ± 50 % compared to clinically reported values. The simulated values from all the included PBPK models were in agreement with available clinical data and were therefore used for prediction of pharmacokinetics after IM

administration. The simulations were carried out for weekly and monthly administration and the maximum injectable dose was set to 1.5 g since doses above this have not previously been practical for IM formulations [99]. Table 2.4 illustrates that the release rate was inversely proportional to the dosage, and a slower release rate was required for monthly administration.

Our PBPK models predicted that two NRTIs, emtricitabine and tenofovir, may be suitable for weekly or monthly administration. Importantly, emtricitabine and tenofovir are widely used in HIV treatment and prevention, and LAI formulations of these agents would make possible multi-drug regimens that match current clinical paradigms for therapy. These agents also represent good candidates for monthly PrEP due to their excellent safety and efficacy profiles. Tenofovir alone, or tenofovir combined with emtricitabine, have already been shown to provide good protection against HIV infection in individuals at high risk of infection [160].

Considering NNRTIs, efavirenz and rilpivirine were both predicted to be suitable for monthly administration. Both have long half-lives, which are favourable for development of LAI agents. The high systemic clearance of etravirine limits the possibility of a monthly administration format when a dose limit of 1.5 mg is applied. Conversely, both integrase inhibitors, dolutegravir and raltegravir, were predicted to be suitable for monthly administration. A low dose of 105 mg was predicted to be sufficient for monthly administration of dolutegravir if a formulation with optimised release rate can be developed. It should be noted that cabotegravir is chemically closely related to dolutegravir, and development of a dolutegravir LAI formulation may therefore not be warranted. Our simulation indicated that raltegravir could potentially be developed as a monthly IM injection with a dose of 800 mg. The optimised dose and release rate for unboosted atazanavir predicted feasibility of an injectable

weekly option at 600 mg, but doses higher than 1500 mg would be required for monthly administration.

The optimisation of LAI strategies should be based on a rational analysis of several pharmacokinetic factors. For many agents, it is likely that the pharmacokinetic variability after IM administration will be reduced compared to oral formulations, due to the lower complexity of the absorption process and avoidance of intestinal transporters and first-pass metabolism. However, additional complexities with the accumulation of macrophages, formation of granuloma at the injection site could arise which should be investigated further [79]. Therapeutic plasma concentrations were predicted to be achieved in approximately eight hours for emtricitabine and tenofovir, and ~24 h for the remaining ARVs after a single IM injection (as shown in Figure 2.2). Since a day is needed to achieve therapeutic plasma concentrations for the other ARVs, a loading oral dose equivalent to the daily regimen may be necessary. This could represent a minor risk for the development of drug resistance and therapeutic failure, but PBPK modelling may help to inform the ongoing debate regarding some aspects of the need for an oral lead-in with the same drugs. The co-administration of multiple injectable ARVs is possible, but a rational selection of concomitant agents is needed to avoid drug-drug interactions. Studies to validate the utility of co-administration of the two existing LAI drugs, rilpivirine and cabotegravir, are underway [161].

The PBPK approach is characterised by some intrinsic limitations due to existing knowledge gaps and the complexity of biological processes underpinning drug distribution. For example, muscle tissues are well connected to the lymphatic circulation, and drugs with high lipophilicity tend to diffuse through lymphatics rather than blood vessels [124]. Consequently, higher accumulation of ARVs in lymph nodes might be

possible, but there is a paucity of clinical data in this area for available LAI formulations. Similarly, efflux and influx transporters are of clear importance to intestinal absorption, distribution and clearance of drugs, but there is currently very little data on the activity of the transporters (or metabolic enzymes) that are expressed at the depot sites. Gender has been correlated with changes in plasma exposure in a recent clinical study of rilpivirine LAI. [162]. Although it has been suggested that several factors can define this, the physiological and anatomical mechanisms characterising the differences between genders have not been fully elucidated and consequently have not been included in our simulations.

Although the doses and release rates identified through these simulations set targets for optimal nanoparticle design, it is important to underscore that the technological challenges in achieving these formulation characteristics are not addressed in this work. Long-term stability of the ARVs in the interstitial fluid present at the depot site is another important consideration. Since SDN strategies do not involve the use of a carrier with stable size and dissolution rates over time, the nanoparticle properties are likely to change over the dosing interval. Since this will alter the surface to mass ratio, an effect on ARV release kinetics with downstream effect on the overall pharmacokinetics cannot be ruled out. It may also be important to consider other SDN components, such as polymers and surfactants, which will also be gradually released over time [163]. The use of LAI ARVs might determine specific complications at the site of injection as described for other treatments; additionally given the prolonged systemic exposition of LAI ARV and the inability to interrupt the drug in the event of side effects, a period of oral induction might be considered before initiating LAI. For patients discontinuing the LAI ARV therapy, an oral administration strategy should

be hypothesised in order to prevent resistance development due to the diminishing plasma concentrations [121].

CHAPTER 3

PBPK model development and validation for paediatrics

Contents

3.1. Introduction

The dose adjustments for paediatric patients is commonly derived by scaling down adult dosing. Scarcity in volunteer enrolment and associated ethical issues can represent a barrier for clinical studies in paediatric patients as well as other special population of patients [164]. Studies have shown that dose adjustments in paediatric patients can lead to inadequate or excessive exposure resulting in sub-optimal therapeutic effect and increased adverse effects [165, 166]. Currently, the majority of the dosing strategies for children are based on empirical scaling from adult doses based on weight or body surface area (BSA).

Dose optimisation is particularly critical in the paediatric population because the patient physiological and anatomical characteristics and the maturation of relevant enzymes are characterised by non-linear changes over time. Chloramphenicol, an antibiotic used in the 1950s for various infections increased mortality rate especially in neonates and infants who were prescribed a dose by scaling down adult dose by weight [167]. This study along with the investigation of cytochrome P450 ontogeny [168] and growth charts by CDC [169] indicated that child growth is not linear and could put the paediatric patients at risk of receiving sub-therapeutic or too high doses during chronic drug usage [170].

Pharmacokinetic modelling has been increasingly used to support the optimisation of dosing in special populations [171]. Recent regulatory changes in U.S. and Europe are supporting the integration of clinical studies for paediatric patients to rationalise the selection of suitable dosing strategies [164, 172]. Unfortunately, ethical constraints hamper the clinical investigations, consequently the integration of predictive

computational tools can support a more rational identification of therapeutic doses for paediatric patients.

Traditional allometric scaling from adults to paediatrics using age and body surface area does not take into account the organ growth and protein expression changes which can have a major effect on ADME processes and pharmacokinetics. PBPK modelling may be successfully used to predict pharmacokinetics in paediatric patients [172]. This modelling technique can integrate the current knowledge of the physiological and anatomical changes in different age groups in a mathematical mechanistic description of ADME [172, 173]. PBPK modelling could be used to inform the optimal doses without clinical intervention, informing a rational design of prospective clinical studies.

The aim of this chapter was to validate the anatomy and physiology of the paediatric model for different age groups between 2-18 years. To improve the confidence of the model, it has also been validated against available clinical data in paediatric population aged between 3-18 years for intravenous lorazepam and an intramuscular administration of ceforanide.

3.2. Methods

Anatomy and physiology of children between the ages 2-7 and 7-18 years were validated. The assumptions of the PBPK model were mentioned in section 2.2. The PBPK model was constructed using Simbiology v.4.3.1, a product of Matlab v.8.2 (MathWorks, Natick, MA, USA 2013). The simulated pharmacokinetics were validated against published clinical data for lorazepam, an anti-anxiety agent and cefoperazone, an anti-bacterial agent as model drugs [174, 175].

3.2.1. Anatomy

The weight and body mass index of the individuals were defined using Centers for Disease Control and Prevention (CDC) growth charts. The charts were digitalised using Plot Digitizer Tool (plotdigitizer.sourceforge.net) and polynomial trend line feature in Microsoft Excel was used to obtain the relation between age and other parameters [176]. Using these defined parameters as reference, height and body surface area [177] were calculated using allometric equations from the literature (Table 3.1).

3.2.2. Tissue and organ weights

The tissue and organ weights were computed using allometric equations. All the organ weights were validated against published data for both male and female populations at different age groups [178]. Summary of the equations used and their references are shown in Table 3.2a, b.

3.2.3. Blood flow

The cardiac output for different age groups was obtained from literature sources. The blood flow rates of various organs and tissues were adjusted as the percentage of cardiac output such that they match the clinical values [179]. The sum of blood flow

passing through the gut, pancreas, spleen and stomach was considered as the portal vein blood flow rate for PBPK models. The percentage of blood flow passing through each organ or tissue was adjusted according to the data in the literature (Table 3.3) [179].

3.2.4. Validation of anatomy and physiology

Validation was performed for ages 2, 5, 10 and 15 years of children and adolescents. The paediatric characteristics, individual tissue and organ weights and blood flows were validated against available literature data [178, 179]. Simulations were performed for a population (100 individuals) by including standard deviation from the literature or ± 20 % was assumed in each age group if data was not available and the mean value was validated against literature data for both male and female groups.

3.2.5. Pharmacokinetic validation

To improve the confidence of the constructed models, it was also validated against *in vivo* pharmacokinetic data for lorazepam, an anti-anxiety drug and an anti-bacterial agent, ceforanide [174, 175]. These drug was chosen due to the availability of physicochemical and pharmacokinetic data in paediatric individuals required for the construction and validation of the PBPK model. Dose of 0.05 mg/kg to a maximum of 2 mg was administered intravenously for lorazepam and a single intramuscular 20 mg/kg dose of ceforanide were simulated for 500 male individuals in each age group (3-7 and 7-18 years). Maximum concentration (C_{max}), area under the curve (AUC) and volume of distribution (V_d) were compared against clinical data [174].

3.2.6. ADME characteristics

The equations describing the ADME processes defining PK were derived from previously published PBPK models (see Chapter 2, section 2) [119, 120]. The physicochemical and intrinsic clearance values of lorazepam were obtained from Maharaj et al. [180], plasma clearance of ceforanide from Dajani et al. [175] and the extrapolation to systemic clearance and the distribution of drug to different organs and tissues was computed using previously published equations [120, 133].

Table 3.1 Equations describing the anatomical characteristic features for paediatrics (2-18 years)

	Sex	2-7 years	7-18 years
BMI (kg/m^2)	**Male**	(-2E-06*(Age*12)^3+0.0009*(Age*12)^2-0.096*(Age*12)+18.41) ± (4E-09*(Age*12)^4-3E-06*(Age*12)^3+0.0006*(Age*12)^2-0.0421*(Age*12)+1.9366) [176]	(0.004*Age^2+0.5348*Age+10.92) ± 3 [176]
	Female	(-2E-06*Age^3 + 0.0011*Age^2 - 0.1058*Age + 18.249)±(7E-09*Age^4 - 4E-06*Age^3 + 0.0009*Age^2 - 0.0579*Age + 2.2788) [176]	(-0.0204*Age^2 + 1.1067*Age + 7.7386) ± 3 [176]
Weight (kg)	**Male**	(-1E-07*(Age*12)^4+4E-05*(Age*12)^3-0.0052*(Age*12)^2+0.4118*(Age*12)+4.6681) ± (3E-10*(Age*12)^5-2E-07*(Age*12)^4+5E-05*(Age*12)^3-0.0051*(Age*12)^2+0.2379*(Age*12)-2.3971) [176]	(-0.0419*Age^3+1.684*Age^2-17.334*Age+78.678) ± 4.5 [176]
	Female	(-9E-09Age^4 - 6E-06Age^3 + 0.003Age^2 - 0.1028Age + 13.926) ± (4E-10Age5 - 3E-07Age4 + 5E-05Age3 - 0.0045Age2 + 0.1886Age - 1.4623) [176]	(-0.239x^2 + 9.6465x - 39.288) ± 4.5 [176]
BSA (m^2)	**Both**	0.0235*((Height*100)^0.42246)*(Weight^0.51456) [177]	
Height (m)	**Both**	sqrt(Weight/BMI)	

Table 3.2 a) Allometric equations describing organ and tissue weights (kg) for male children between 2-18 years

	2-7 years	7-18 years
Adipose	0.534*Weight-1.59*Age+3.03 [181]	(1.51*BMI-0.7*Age-3.6+1.4)*Weight/100 ± 0.041 [129]
Blood	(-0.0623*(Age^5)+2.4425*(Age^4)-31.37*(Age^3) +149.98*(Age^2) +31.305*Age+393.7)/1000 ± 0.15 [182]	(3.33*BSA-0.81) ± 0.1 [129]
Bones	(-0.0306*(Age^5)+0.5222*(Age^4)+9.7109*(Age^3)-197.97*(Age^2)+1089.7*Age+546.6)/1000 ± 0.15 [182]	exp(0.0689+2.67*log(Height)) ± 0.166 [181]
Brain	(0.405*exp(-Age/629)*(3.68-2.68*exp(-Age/0.89)) ± 0.084 [181]	
Glands	(0.001*(Age^5)-0.0483*(Age^4)+0.8335*(Age^3)-6.6516*(Age^2)+27.512*Age+13.9 ± 0.015)/1000 [182]	
Gonads	(3.3+53*(1-abs(exp((-Age/17.5)^5.4)))/1000 ± exp(0.049) [129]	
Heart	(41.70+0.022*Age*365 ± 25)/1000 [183]	
Intestines	(-4.7817e-2*(Age^4)+1.925*(Age^3)-22.382*(Age^2)+107.09*Age+51.125)/1000 ± 0.05 [182]	
Kidneys	(35.29+0.015*Age*365+34.14+0.015*Age*365)/1000 ± 2.5 [183]	
Liver	(271.58+0.163*Age*365 ± 25)/1000 [183]	
Lungs	(41.31+0.039*Age*365+36.92+0.037*Age*365 ± 5)/1000 [183]	
Muscle	0.93*Weight-(Sum of organ weights) [129]	
Remaining	exp(-0.072+1.95*log(Height) ± 0.049) [129]	
Skin	exp(1.64*BSA-1.93) ± 0.049 [129]	(-0.0992*(Age^4)+4.2762*(Age^3)-62.165*(Age^2)+437.78*Age+203.2)/1000 ± 0.2*(-0.0992*(Age^4)+4.2762*(Age^3)-62.165*(Age^2)+437.78*Age+203.2)/1000 [184]
Spleen	(18.42+0.018*Age*365 ± 2.5)/1000 [183]	
Stomach	exp(-3.266+2.45*log(Height) ± 0.0965) [129]	
Thymus	(14*((7.1-6.1*exp(-Age/11.9))*((0.14+0.86*exp(-Age/10.3))))/1000 ± 0.049 [129]	

b) Allometric equations describing organ and tissue weights (kg) for female children between 2-18 years

	2-7 years	7-18 years
Adipose	0.642*Weight-0.12*Height-0.606*Age+8.98 [181]	(1.51*BMI-0.7*Age+1.4)*Weight/100 ± 0.041 [129]
Blood	(0.0018*(Age^5)+0.0959*(Age^4)-4.4055*(Age^3)+ 44.442*(Age^2)+82.808*Age+292.26)/1000 ± 0.15 [182]	(2.66*BSA-0.46) ± 0.1 [129]
Bones	(-2.831e-3*(Age^5)-0.18184*(Age^4)+10.685*(Age^3)- 142.88*(Age^2)+782.05*Age+609.64)/1000 ± 0.15 [182]	exp(0.0689+2.67*log(Height)) ± 0.166 [181]
Brain	(0.373*exp(-Age/629)*(3.68-2.68*exp(-Age/0.89)) ± 0.084 [181]	
Glands	(0.001*(Age^5)-0.0483*(Age^4)+0.8335*(Age^3)-6.6516*(Age^2)+27.512*Age+13.9 ± 0.015)/1000 [182]	
Gonads	(3.3+90*(1-abs(exp((-Age/16.8)^6.7)))/1000 ± exp(0.049) [129]	
Heart	(41.70+0.022*Age*365 ± 25)/1000 [183]	
Intestines	(-0.0513*(Age^4)+2.0352*(Age^3)-23.478*(Age^2)+110.61*Age+49.229)/1000 ± 0.05 [182]	
Kidneys	(35.29+0.015*Age*365+34.14+0.015*Age*365)/1000 ± 2.5 [183]	
Liver	(271.58+0.163*Age*365 ± 25)/1000 [183]	
Lungs	(41.31+0.039*Age*365+36.92+0.037*Age*365 ± 5)/1000 [183]	
Muscle	0.93*Weight-(Sum of organ weights) [129]	
Remaining	exp(-0.072+1.95*log(Height) ± 0.049) [129]	
Skin	exp(1.64*BSA-1.93) ± 0.049 [129]	(0.00476622*(Age^5)-0.27924*(Age^4)+6.3444*(Age^3)- 70.113*(Age^2)+429.85*Age+252.06)/1000 ± 0.20*(0.00476622*(Age^5)- 0.27924*(Age^4)+6.3444*(Age^3)-70.113*(Age^2)+429.85*Age+252.06)/1000 [184]
Spleen	(18.42+0.018*Age*365 ± 2.5)/1000 [183]	
Stomach	exp(-3.266+2.45*log(Height) ± 0.0965) [129]	
Thymus	(14*((7.1-6.1*exp(-Age/11.9))*((0.14+0.86*exp(-Age/10.3))))/1000 ± 0.049 [129]	

Table 3.3 Equations for cardiac output and percentages of blood flow rate (L/h) to each organ from the cardiac output adjusted according to literature data [179].

	2-7 years		7-18 years	
Cardiac output	60*(10^(0.8914*$\log_{10}$(Weight)-0.654)) [185]		(3.107+(0.012*Weight^1.369))*60 [186]	
Gender → Organ/Tissue ↓	**Male**	**Female**	**Male**	**Female**
Adipose	0.04	0.05	0.04	0.06
Bone	0.02	0.02	0.04	0.04
Brain	0.38	0.38	0.24	0.24
Gut (Q_{gu})	0.12	0.13	0.14	0.15
Hepatic artery	0.08	0.08	0.06	0.07
Kidneys	0.13	0.11	0.17	0.13
Lungs	0.02	0.02	0.02	0.02
Muscle	0.05	0.06	0.12	0.11
Portal vein (Q_{pv})	$Q_{gu}+Q_{st}+Q_{sp}$			
Remaining	0.07	0.06	0.08	0.08
Skin	0.03	0.03	0.04	0.04
Spleen + Pancreas (Q_{sp})	0.05	0.05	0.04	0.04
Stomach (Q_{st})	0.01	0.01	0.01	0.01

Table 3.4 Physicochemical properties, *in vitro* and population pharmacokinetic data of lorazepam and ceforanide

	Lorazepam	**Ceforanide**
Molecular weight	321	519
log $P_{o:w}$	2.39 [180]	-3.7 [188]
Protein binding (%)	0.93 [187]	80.6 [188]
pK_a	1.3 (base), 11.5 (acid) [180]	2.55 (acid), 9.14 (base) [188]
R	0.642 [180]	†0.1173
UGT2B7 CL_{int}	0.439 [180]	-
Renal clearance	0.01 [180]	-
Plasma clearance	-	72 ± 21 [175]

log $P_{o:w}$ – Partition coefficient between octanol and water; pKa – logarithmic value of the dissociation constant; R – blood-to-plasma drug ratio; CL_{int} – intrinsic clearance; UGT - uridine diphosphate glucuronosyltransferase (ml/min/g of liver), renal clearance is in ml/min/kg, † the value was computed from the correlation provided by Paixão et al. [189]

3.3. Results

The mean simulated values of the anatomy and blood flow rates of children and adolescents were compared against literature values [178, 179]. The simulated paediatric characteristic values for BSA, height and weight are in agreement with literature data as shown in Table 3.5. Allometric equations from various literature sources describing the organ and tissues weights and blood flow rates of children and adolescents are in agreement with the published data, shown in Table 3.6 and Table 3.7. A separate 'remaining' compartment was created to accommodate the unaccounted weight (data not shown) and its corresponding blood flow rate in order to improve the model prediction. Since there was no data for age groups other than 2, 5, 10 and 15 years, anthropometric equations for 2 and 5 years were considered to predict anatomy and physiology between the ages 2 and 7 with relative accuracy and precision. Observed growth pattern was slightly different from 7 years onwards therefore different equations were used for allometric scaling [176]. Due to large variation in anatomical and physiological characteristics among children and adolescents, broader validation range i.e. ± 100 % was assumed (less than the conventional two-fold range [152]). The mean values from the chosen anthropometric equations were between the assumed ranges from the reported literature values [179] except for the lung weight of a 10-year-old child (101.2 %). The mean simulated blood flow rates were ± 50 % from the literature value for all the age groups (Table 3.7).

Simulated lorazepam pharmacokinetics were compared against clinical data as shown in Table 3.8. The pharmacokinetics were predicted across all age groups from 3-17 years and the mean value was compared with clinical data. The C_{max}, AUC and V_d were +37.5 %, +22.2 % and -14.6 % from clinical values [174]. The simulated C_{max} (+37.5 %) and AUC (+22.2 %) values are slightly high compared to the mean

clinical values (Figure 3.1). Validation of intramuscular ceforanide against clinical data had a deviation of +7.4 %, +16.6 % and -8.1 % for C_{max}, AUC and V_d respectively [175]. In both these cases, the simulated C_{max} and AUC values are slightly high which can be explained by the low volume of distribution observed (Figure 3.1). . Due to unavailability of data, the blood-to-plasma ratio, fraction unbound, intrinsic and renal clearance were not altered across age groups.

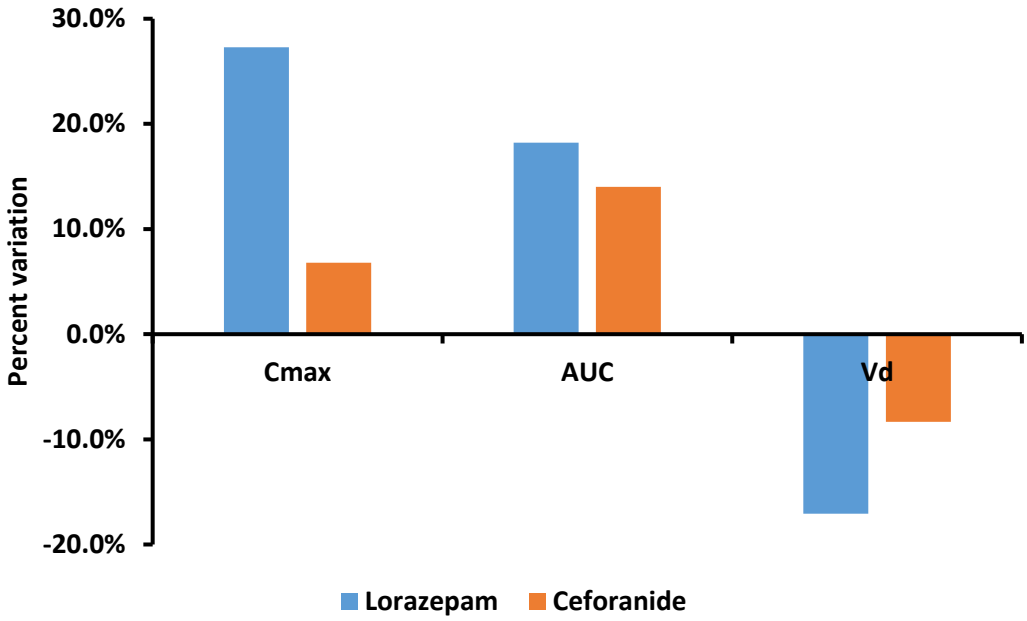

Figure 3.1 Percentage variation of the mean simulated value against mean clinical value of lorazepam and ceforanide

Table 3.5 Validation of characteristic features against literature data for different ages (data represented as Male/Female) [178, 179]

Years →	2		5		10		15	
Characteristic ↓	Simulated	Reference	Simulated	Reference	Simulated	Reference	Simulated	Reference
BSA (m^2)	0.76/0.74	NA	0.91/0.91	0.78/0.78	1.20/1.14	1.12/1.12	1.67/1.49	1.62/1.55
Height (m)	0.87/0.87	NA	1.09/1.09	1.09/1.09	1.39/1.37	1.38/1.38	1.80/1.53	1.67/1.61
Weight (kg)	12.7/12.1	12.6/11.9	18.0/17.2	18.7/17.7	31.0/34.0	31.4/32.6	56.0/52.0	56.7/53.7

Table 3.6a Validation of organ weights (kg) against literature data for different ages (Data represented as Male/Female) [178, 179]

Years →	2		5		10		15	
Organs ↓	Simulated	Reference	Simulated	Reference	Simulated	Reference	Simulated	Reference
Adipose	3.17/2.91	3.76/3.72	4.68/4.26	5.50/5.50	7.45/9.28	8.60/8.60	11.6/14.2	12.0/18.7
Bones	0.74/0.74	0.85/0.82	2.49/2.49	2.43/2.43	4.6/4.47	4.50/4.50	8.32/8.32	7.18/7.18
Brain	1.50/1.50	1.12/1.03	1.48/1.36	1.31/1.31	1.47/1.48	1.40/1.40	1.46/1.34	1.30/1.30
Glands	0.02/0.02	0/0	0.06/0.06	0.04/0.04	0.07/0.07	0.06/0.06	0.06/0.06	0.10/0.10
Heart	0.07/0.06	0.07/0.06	0.08/0.08	0.09/0.09	0.12/0.12	0.14/0.14	0.16/0.16	0.22/0.22
Intestines	0.20/0.19	0.19/0.19	0.24/0.24	0.34/0.34	0.33/0.33	0.58/0.58	0.70/0.69	0.82/0.82
Kidneys	0.10/0.10	0.09/0.08	0.12/0.12	0.11/0.11	0.18/0.18	0.18/0.18	0.23/0.23	0.24/0.24
Liver	0.46/0.45	0.48/0.46	0.57/0.57	0.57/0.57	0.87/0.87	0.83/0.83	1.16/1.16	1.30/1.30
Lungs	0.18/0.18	0.24/0.24	0.22/0.22	0.13/0.13	0.38/0.38	0.21/0.21	0.52/0.52	0.29/0.29
Muscle	3.37/2.92	2.83/2.83	5.23/4.67	5.60/5.60	7.90/10.42	11.0/11.01	17.5/14.6	17.0/17.0
Skin	0.52/0.49	0.41/0.39	0.64/0.62	0.57/0.57	1.65/1.65	0.82/0.82	2.19/2.19	1.70/1.70
Spleen	0.04/0.04	0.07/0.07	0.05/0.05	0.05/0.05	0.08/0.08	0.08/0.08	0.12/0.12	0.13/0.13
Stomach	0.03/0.03	0.03/0.03	0.05/0.05	0.05/0.05	0.09/0.09	0.09/0.09	0.16/0.11	0.12/0.12
Thymus	0.02/0.02	NA	0.03/0.03	0.03/0.03	0.03/0.03	0.04/0.04	0.03/0.03	0.03/0.03

Table 3.6b Percentage difference in mean organ weights against literature data for different ages and genders [178, 179]

Years →	2		5		10		15	
Organs ↓	**Male**	**Female**	**Male**	**Female**	**Male**	**Female**	**Male**	**Female**
Adipose	-15.7	-21.8	-14.9	-22.5	-13.4	7.9	-3.3	-24.1
Bones	-12.9	-9.8	2.5	2.5	2.2	-0.7	15.9	15.9
Brain	33.9	45.6	13.0	3.8	5.0	5.7	12.3	3.1
Glands	0.0	0.0	50.0	50.0	16.7	16.7	-40.0	-40.0
Heart	0.0	0.0	-11.1	-11.1	-14.3	-14.3	-27.3	-27.3
Intestines	5.3	0.0	-29.4	-29.4	-43.1	-43.1	-14.6	-15.9
Kidneys	11.1	25.0	9.1	9.1	0.0	0.0	-4.2	-4.2
Liver	-4.2	-2.2	0.0	0.0	4.8	4.8	-10.8	-10.8
Lungs	-25.0	-25.0	69.2	69.2	81.0	81.0	79.3	79.3
Muscle	19.1	3.2	-6.6	-16.6	-28.2	-5.4	2.9	-14.1
Skin	26.8	25.6	12.3	8.8	101.2	101.2	28.8	28.8
Spleen	-42.9	-42.9	0.0	0.0	0.0	0.0	-7.7	-7.7
Stomach	0.0	0.0	0.0	0.0	0.0	0.0	33.3	-8.3
Thymus	-	-	0.0	0.0	-25.0	-25.0	0.0	0.0

Table 3.7a Validation of organ blood flows (L/h) for different ages against literature values (Data represented as Male/Female) [179]

Years →	2		5		10		15	
Organs ↓	**Simulated**	**Reference**	**Simulated**	**Reference**	**Simulated**	**Reference**	**Simulated**	**Reference**
Cardiac Output	129/122	124/114	176.5/132.7	172.8/157.8	269.5/272.5	234/224.4	363.9/347.2	346.2/309
Adipose	5.1/4.8	5.4/5.8	7.1/8	7.2/7.8	10.8/16.4	10.8/14	14.5/20.8	13.7/25
Brain	41.0/38.7	54.4/50.1	63.2/32	62.7/57.8	65.6/65.8	55.5/51	46.6/42.6	45/39.9
Gut	11.3/10.7	13.1/12.4	24.7/19.9	23.5/22.2	37.7/40.9	35.5/35.5	50.9/52	49.7/47.7
Hepatic Artery	32.1/31.0	43.2/40.8	10.6/9.3	11.3/10.6	16.2/19.1	14.6/15	21.8/24.3	22.7/21.5
Kidney	11.9/11.3	18.5/13.3	30/17.2	22.6/16.7	45.8/35.5	42.6/30	61.8/45.1	63.2/46.8
Lungs	8.4/8.0	9.2/8.28	3.5/2.7	3.3/3.1	5.4/5.5	4.1/4.8	7.3/6.9	8.6/7.2
Muscle	1.6/1.5	2.3/2.3	13.5/14.5	13.1/13.1	31.4/29.8	25.7/25.7	57/45.8	56.2/39.8
Remaining	5.1/4.8	4.9/4.9	14.1/10.6	11/7.3	21.6/21.8	17.7/18.4	29.1/27.7	37/35
Skin	3.4/3.2	3.9/3.7	7.1/5.3	5.3/5.1	10.8/10.9	7.7/7.8	14.5/13.9	14.5/12
Spleen	2.6/2.4	5.0/4.6	7.1/5.3	6.4/6	10.8/10.9	8.9/9.5	14.5/13.9	15.4/13.8
Stomach	1.2/1.1	1.2/1.1	1.8/1.3	2/1.8	2.7/2.7	3.2/3	3.6/3.5	5/4.5

Table 3.7b Percentage difference of mean organ blood flows for different ages against literature values [179]

Years →	2		5		10		15	
Organs ↓	**Male**	**Female**	**Male**	**Female**	**Male**	**Female**	**Male**	**Female**
Cardiac Output	4.0	7.0	2.1	-15.9	15.2	21.4	5.1	12.4
Adipose	-5.6	-17.2	-1.4	2.6	0.0	17.1	5.8	-16.8
Brain	-24.6	-22.8	0.8	-44.6	18.2	29.0	3.6	6.8
Gut	0.0	0.0	5.1	-10.4	6.2	15.2	2.4	9.0
Hepatic Artery	-25.7	-24.0	-6.2	-12.3	11.0	27.3	-4.0	13.0
Kidney	-35.7	-15.0	32.7	3.0	7.5	18.3	-2.2	-3.6
Lungs	-8.7	-3.4	6.1	-12.9	31.7	14.6	-15.1	-4.2
Muscle	-30.4	-34.8	3.1	10.7	22.2	16.0	1.4	15.1
Remaining	4.1	-2.0	28.2	45.2	22.0	18.5	-21.4	-20.9
Skin	-12.8	-13.5	34.0	3.9	40.3	39.7	0.0	15.8
Spleen	-48.0	-47.8	10.9	-11.7	21.3	14.7	-5.8	0.7
Stomach	0.0	0.0	-10.0	-27.8	-15.6	-10.0	-28.0	-22.2

Table 3.8 Validation of lorazepam [174] and ceforanide [175] paediatric model against clinical data

Lorazepam			
	C_{max} (ng/ml)	**AUC** (ng.h/ml)	**V_d** (L/kg)
Simulated	77.14 ± 15.82	1005.62 ± 268.48	1.64 ± 0.13
Clinical	56.1 ± 44.9	822.5 ± 706.1	1.92 ± 0.84
Ceforanide			
	C_{max} (µg/ml)	**AUC** (µg.h/ml)	**V_d** (L/kg)
Simulated	60.4 ± 14.4	250 ± 74.0	0.24 ± 0.16
Clinical	56.3 ± 14.0	215 ± 61.0	0.26 ± 0.67

3.4. Discussion

The validation of the mathematical structure and input parameters of anatomy and physiology of children is a pivotal step to support a reliable PBPK modelling approach. The validation described in this chapter focuses on the anatomical and physiological factors for paediatric and adolescent patients. The anatomy and physiology of the paediatric model was validated at different age groups against available data. Appropriate allometric equations were selected from available literature sources and the mean value of each parameter obtained from the simulation of 100 virtual individuals was compared against clinical data [129, 178, 179, 181, 183, 185, 186]. For major organs/ tissues and blood flow rates, the predicted values were comparable (< 100 % from the mean value) to available data and a difference of >100 % from the mean value was observed for skin weight of 10 year olds in both males and females.

To further evaluate the reliability of this modelling approach, the pharmacokinetics of an IV administered lorazepam and IM administered ceforanide was also validated against available clinical data [174]. Lorazepam and ceforanide were selected as the validation drugs due to data availability in paediatric patients of the desired age group (3-17 years) [174]. The reported IV lorazepam study was conducted in 63 paediatric patients indicating reliability in the presented data and hence was considered to evaluate the drug pharmacokinetics in a PBPK model describing children and adolescents. Ceforanide IM simulations provide confidence in simulating the IM compartment of the PBPK model. The model was considered validated if the mean pharmacokinetic parameters (C_{max}, C_{trough} and AUC) were ± 50 % compared to the clinical data and to verify that the PBPK model has the potential of simulating pharmacokinetics appropriately. Comparison between simulated and clinical lorazepam and ceforanide pharmacokinetics indicate that the PBPK model validation was successful,

suggesting that ADME processes can be implemented in the current mathematical framework. Several routes of administration could be potentially implemented in the PBPK modelling approach, but for the current chapter, the intravenous and intramuscular routes were selected as the primary focus of the thesis is IM LAI Studies have shown variable drug clearance and water content that can alter the volume of distribution, protein binding and blood-to-plasma ratio in ageing children [179, 190, 191]. . Age dependent differences in fraction unbound and blood-to-plasma ratio could not be considered due to unavailability of data and was assumed to be the same across all age groups.

A similar approach was included in previous PBPK applications for paediatric patients where the reliability of the predictions was compared against available clinical data [179, 180, 192, 193]. The validated methods have been used to provide quantitative prediction of potential dose optimisation strategies for paediatric patients across different disease areas. Maharaj et al. simulated the pharmacokinetics of 0.05 mg/kg intravenous lorazepam in various age groups of paediatric patients ranging from 0-18 years [194] and Edginton et al. developed a PBPK model for five compounds - acetaminophen, alfentanil, morphine, theophylline and levofloxacin in paediatric patients ranging from birth to 18 years by scaling down adult clearance values at variable doses across age groups [192]. Bjorkman utilised *in silico* models to simulate the distribution of theophylline (4 mg/kg, intravenous infusion over 5 min) and midazolam (0.2 mg/kg, intravenous infusion over 5 min) in paediatric patients aged from 0-18 years as model drugs [179].

PBPK modelling is a mathematical representation of pharmacokinetics and therefore is based on conceptual and pharmacological assumptions to support a computational simulation of ADME. The current PBPK model was assumed to have well

stirred compartments with instant uniform drug distribution across each tissue and organ. The blood circulation was simulated representing local blood flow to major tissues and organs as described in section 3.2.3. Although lymphatic circulation might mediate drug diffusion for some highly lipophilic compounds, this was not included in the current model due to the lack of available data [124]. Also transporters are also not considered in the model, which can influence the drug absorption, distribution and clearance. Due to unavailability of the data related to the rapid changes in anatomy and physiology of neonates and infants, the PBPK model could not be designed for these age groups.

Clinical scenarios characterised by ethical and logistical barriers represent ideal areas for applications of the PBPK approach, allowing a more rational design of future research. Validated paediatric PBPK models could be used for studying the influence of drugs over a wide range of therapeutic areas in patients with comorbidities, organ dysfunction, under- and overweight etc. In some cases, paediatric patients are receiving multiple treatments in several clinical scenarios, therefore the current model could find potential in the evaluation of drug-drug interactions. Also, rapid anatomical and physiological changes are observed in neonates and infants which could complicate the dosing regimens [195]. Earlier reported increased mortality using chloramphenicol and sulphonamides indicate the importance of appropriate dose administration [167]. PBPK models could close the gap and assist in dose optimisation strategies in paediatric patients.

Additionally, PBPK models could be applied to simulate and predict drug distribution in other special population with specific anatomical and physiological characteristics such as elderly, pregnant women and patients with cirrhosis or other comorbidities. The application of computational pharmacokinetic models can support a

more detailed understanding of factors influencing drug distribution in different sub-population of patients facilitating a tailored dose optimisation approach. [111, 196].

Regulatory authorities such as FDA and European Medicines Agency (EMA) have introduced new regulations where pharmacokinetic modelling is identified as a valuable tool to reduce the number of clinical subjects in paediatric clinical studies [197, 198]. Thus, PBPK modelling could be an effective tool which could help reduce the cost and time in dose optimisation and also assist in detailed understanding of drug pharmacokinetics, bridging the gap between *in vitro* and *in vivo* data.

CHAPTER 4

Simulation of rilpivirine and cabotegravir long-acting administration in paediatric and adolescent patients

Contents

4.1. Introduction

Adherence to HIV therapy is one of the major issues hindering treatment effectiveness. Currently available formulations necessitate lifelong, daily dosing and poor adherence has been attributed to numerous factors including pill fatigue, side effects and a range of social conditions associated with affected populations [121]. Problems can be particularly exacerbated in specific sub-populations of patients such as paediatric patients, where drug administration is additionally influenced by the caregiver, the family or the social surroundings, which may further complicate this problem [199].

LAI formulations have the potential of improving the adherence issue related to oral formulation, reducing the amount of API used for therapy and consequently the cost of therapy. The use of LAI formulation in paediatric patients has been already hypothesised in different disease areas and sustained therapeutic concentration of APIs have been obtained for LAI antipsychotics in children [200].

Two LAI ARV formulations have been recently developed and several other are currently under investigation [36]. Rilpivirine, due to its long half-life and potency, has been selected for monthly LA strategies [87]. Recently a novel HIV integrase inhibitor, cabotegravir, was developed by ViiV Healthcare. It has an extended half-life that potentially allows it to be administered as a LAI once every three months through an IM injection [36]. A combination of cabotegravir and rilpivirine LAI formulation is currently in a clinical trial to assess its safety and efficacy in adults [201].

The identification of safe and effective dosing strategies for paediatric patients is complicated by numerous factors. Differences in anatomical and physiological characteristics of children and adolescents compared to adults have a relevant effect on

ADME processes and are not correctly captured through allometric scaling approach [164]. Additionally, logistic and ethical challenges in designing dose finding/optimisation studies in children limits the number of clinical studies [179].

PBPK modelling represents a feasible option to optimise doses prior to clinical trials in paediatric patients thus minimising the time and cost invested in optimising doses. It is a bottom up approach which integrate *in vitro* data such as apparent permeability using Caco-2 cells, intrinsic clearance, protein binding in a mathematical description of ADME to extrapolate to *in vivo* pharmacokinetics [50]. The aim of this study was to simulate pharmacokinetics and inform optimal doses of LA IM formulations of cabotegravir and rilpivirine in children and adolescents through PBPK modelling.

4.2. Methods

Children between the ages 3-18 years were categorised into weight groups suggested by WHO, and 100 virtual individuals were generated in each weight category. For the development of the PBPK approach, instant and uniform distribution of drugs in tissues, no reabsorption of the drug from the large intestine and a blood-flow limited model were assumed. The PBPK model was constructed using Simbiology® v.4.3.1, a product of Matlab® v.8.2 (MathWorks, Natick, MA, USA 2013). Cabotegravir and rilpivirine LA IM pharmacokinetics were assessed and validated in adult PBPK models and later optimised for different weight categories of children and adolescents.

4.2.1. Anatomy

Adult PBPK model was defined by key characteristics such as age, and weight of the individual. These defining characteristic values were further used for the computation of organs, tissue volumes and blood flow rates through allometric equations as described by Bosgra et al. [129]. The anatomy and physiology of children and adolescents was obtained from various literature sources and has been validated against available clinical data prior to dose optimisation (Chapter 3). To improve the confidence of the constructed paediatric PBPK model, it was also validated against intravenous lorazepam and intramuscular ceforanide as reference drugs (Chapter 3).

4.2.2. Simulation of ADME processes

Drug diffusion from the IM compartment obey first-order rate kinetics and the equation was obtained from Tegenge et al.[124]. Release rate of cabotegravir was obtained from literature [202] and for rilpivirine, it was derived using 48-week clinical data from LATTE-2 study [36].

The intrinsic clearance values derived from *in vitro* data have been obtained from the literature [203] and extrapolated to systemic clearance [204]. The analysis of drug distribution to different organs and tissues was performed using previously published equations [120].

4.2.3. Model validation

The physicochemical properties of cabotegravir and rilpivirine used in the model are represented in Table 4.1. The validation of the drug properties against clinical data was conducted in 100 virtual adults for 800 mg quarterly dose of cabotegravir (from weeks 12-28) and for a subsequent monthly dose of 900 mg rilpivirine (after the initial dose of 1200 mg) [36]. The release rate of rilpivirine was identified from the clinical data using the PBPK model [36]. The release rate was also validated against the LATTE-2 pharmacokinetic curve of cabotegravir and rilpivirine. Cabotegravir release rate was observed to be same, however there was a decrease in the release rate of rilpivirine from 0.0009 to 0.0005 h^{-1}, since it was a reformulation of the previously published rilpivirine nanoformulation [87, 205].

4.2.4. Dose prediction

After the validation of the physicochemical parameters, the physiology and the anatomy has been modified to describe the children and adolescents using appropriate allometric equations obtained from the literature [129, 176, 179, 181-183, 206]. Following IM injection, dose optimisation in paediatric patients was conducted such that at least 95 out of the 100 virtual individuals had a mean C_{trough} over the cut-off limits for the required duration. Similar to LATTE-2 study, 10 mg PO C_{trough} (1.35 µg/ml) value was used as the minimum cut-off value for cabotegravir dose predictions and 25 mg PO (70 ng/ml) C_{trough} was used as the average concentration (C_{av}) for rilpivirine

[205]. An oral dosing regimen for 4 weeks (steady-state) followed by a loading dose and eleven maintenance doses for a 4-weekly IM administration of rilpivirine and cabotegravir were simulated, for a total period of 52 weeks.

4.2.5. Sensitivity analysis

Differential sensitivity analysis was performed as previously described in chapter 2, section 2.2.10 [135]. Analysis was performed for the loading dose and the first maintenance dose of cabotegravir and rilpivirine LA IM formulation in adults. Drug plasma concentration was analysed against six parameters – blood-to-plasma ratio, cardiac output, clearance, liver weight, protein binding, and release rate by varying 20 % from its mean value. For each parameter, the simulations were performed for100 runs while keeping the rest of the parameters constant.

Table 4.1 Physicochemical properties, *in vitro* and population pharmacokinetic data of ARVs

	Cabotegravir	**Rilpivirine**
Molecular weight	427	366
log $P_{o:w}$	1.04 [207]	4.32 [208]
Protein binding	99.30 % [123]	99.70 % [208]
pK_a	10.04 [207]	3.26 [208]
R	0.441 [209]	0.67 [208]
CYP3A4 CL_{int}	-	2.04[208]
UGT1A1 CL_{int}	4.5 [203]	-
UGT1A9 CL_{int}	2.2 [203]	-
Release rate (h^{-1})	0.00045 [202]	0.0009 [36]

log $P_{o:w}$ – Partition coefficient between octanol and water; pKa – logarithmic value of the dissociation constant; R – blood-to-plasma drug ratio; CL_{int} – intrinsic clearance; CYP – cytochrome P450 (µl/min/pmol); UGT - uridine diphosphate glucuronosyl-transferase (µl/min/mg).

Table 4.2 Validation of antiretrovirals at steady state: Clinical [36] vs. simulated pharmacokinetic data and the percent difference between them.

Drug	Dose (mg)	AUC			C_{max}			C_{trough}		
		Clinical	Predicted	Δ	Clinical	Predicted	Δ	Clinical	Predicted	Δ
Cabotegravir	800 mg quarterly	4467 (52)	5166 (23)	-13.5%	3.3 (59)	3.5 (21)	-5.7%	1.1 (140)	1.2 (24)	-8.3%
Rilpivirine	900 mg monthly	74,420 (35)	84,270 (44)	-11.7%	168 (37)	157 (42)	7.0%	79.1 (44)	72.1 (45)	9.7%

Values are represented as Geometric mean (% CV – coefficient of variation expressed as a percentage), AUC – area under the concentration-time curve, C_{max} – maximum plasma concentration, C_{trough} – trough plasma concentration, cabotegravir pharmacokinetics are represented as μg/ml for C_{max} and C_{trough} and μg × h/ml for AUC at day 84, rilpivirine pharmacokinetics are represented as ng/ml for C_{max} and C_{trough} and ng × h/ml for AUC at day 28. Δ - percentage difference between mean clinical and predicted value

4.3. Results

The PBPK model was initially validated against clinical data for both cabotegravir and rilpivirine to ensure that the selected drug properties were appropriate. The pharmacokinetic parameters mean simulated C_{max}, C_{trough} and AUC were compared against available clinical data for LAI formulations for both these drugs (cabotegravir – second IM dose of 800 mg and rilpivirine – 900 mg after the initial dose of 1200 mg) (shown in Table 4.2 and Figure 4.1). To increase the accuracy of the simulations, the PBPK model was considered validated if the mean value was within 0.5-fold from the clinical value instead of the conventional 2-fold limit [152].

The formulation characteristics were maintained equal for the simulations in paediatric and adolescent patients assuming a similar release rate of the drugs from the formulations, hypothesising the use of the same formulations in paediatric and adolescent patients. IM doses were optimised to have a pharmacokinetic profile over the 10 mg PO C_{trough} for cabotegravir over the duration of treatment and an average concentration over the C_{trough} of 25 mg PO rilpivirine for the first 12 IM doses (Figure 4.2). For rilpivirine, it was also ensured that the concentrations are always above $PAIC_{90}$ value subsequent to the loading dose. Summary of predicted doses for both cabotegravir and rilpivirine for different weight categories are shown in Table 4.3.

a)

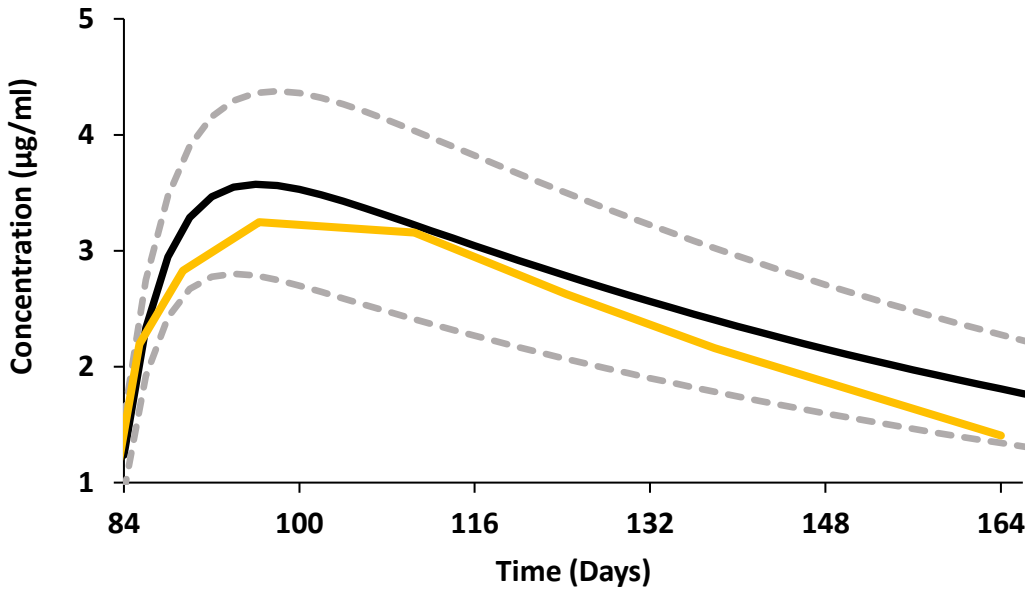
5
4
3
2
1
Concentration (µg/ml)
84
100
116
132
148
164
Time (Days)

b)

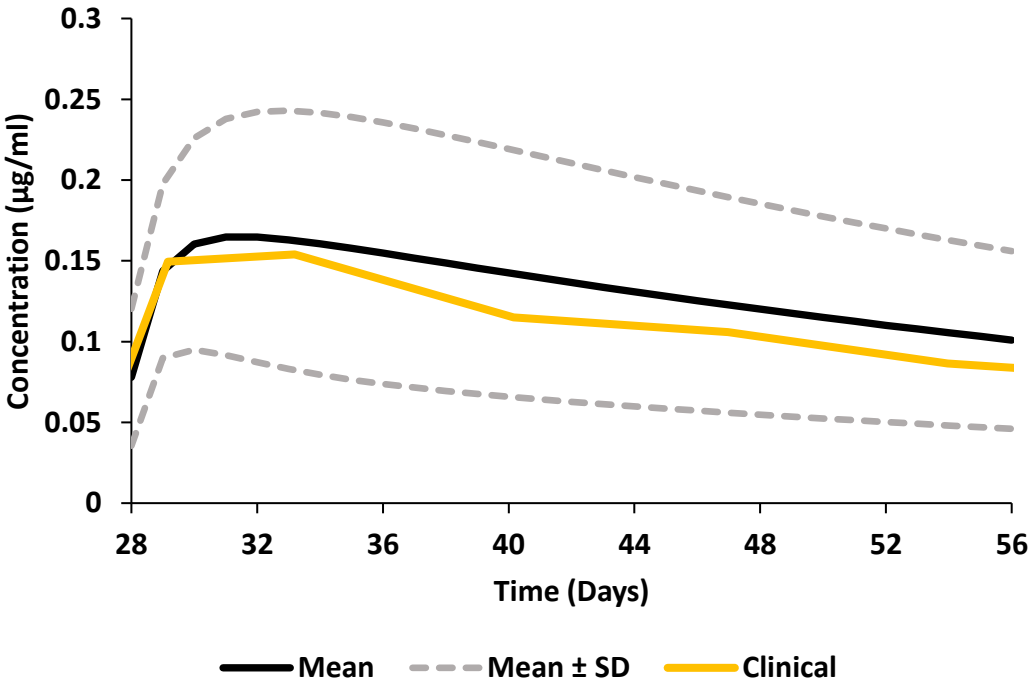
0.3
0.25
0.2
0.15
0.1
0.05
0
Concentration (µg/ml)
28
32
36
40
44
48
52
56
Time (Days)
Mean
Mean ± SD
Clinical

c)

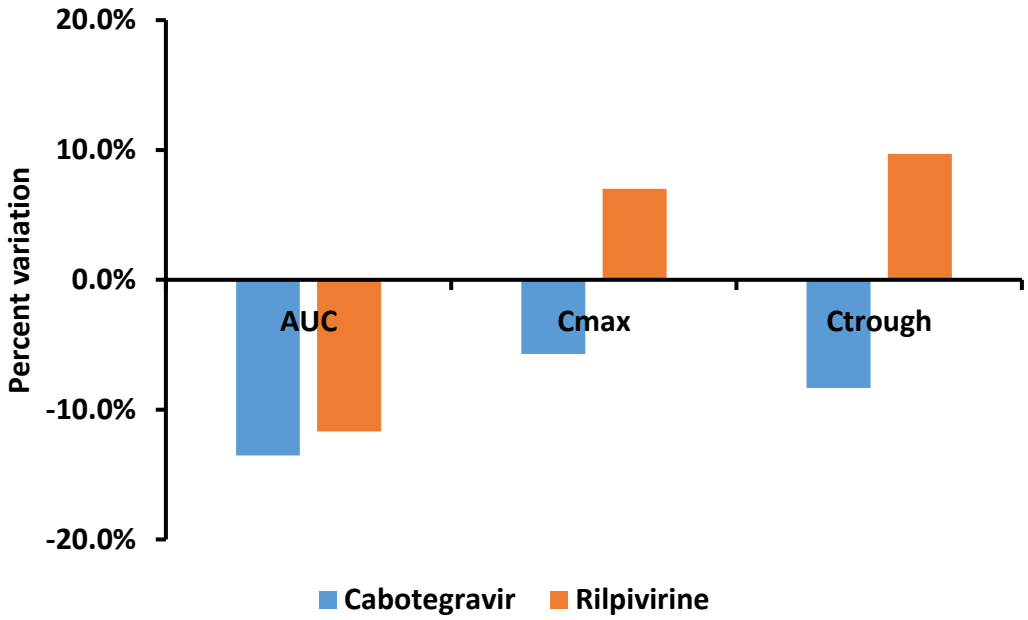

Figure 4.1 Validation of the PBPK model against clinical data for the second IM administration. a) Cabotegravir (800 mg followed by 800 mg quarterly) b) Rilpivirine (1200 mg followed by 900 mg monthly) [36] c) Percentage variation of the mean simulated pharmacokinetics from the mean clinical data

4.3.1. Cabotegravir

The validation for 800 mg of IM cabotegravir resulted in a mean predicted AUC, C_{max} and C_{trough} that were at +15.6 %, +6.1 % and +9.1 % compared to clinical value respectively [36]. A target concentration of 1.35 µg/ml (10 mg PO C_{trough}) was chosen from the literature [36]. The doses for the different weight groups were informed such that at least 95 out of the 100 virtual individuals has a C_{trough} value over the target concentration for a duration of 48 weeks. The monthly oral dose administered for a period of 4 weeks was 10 mg for weights ranging between 14-50 kg and 20 mg for weights between 50-70 kg. For IM cabotegravir, the loading dose ranged between 200-600 mg and maintenance doses between 100-250 mg (Figure 4.3) for the simulated plasma C_{trough} to stay over the 10 mg PO C_{trough} as described in Table 4.3.

4.3.2. Rilpivirine

The simulated mean AUC, C_{max} and C_{trough} values were +13.2 %, -6.5 % and -8.8 %, compared to the clinical data [36]. After the validation of rilpivirine PBPK model, the first order kinetic release rate was identified to be 0.0009 h^{-1}. The validation was then performed to find the optimal release rate for rilpivirine pharmacokinetics from LATTE-2 study. Due to reformulation of rilpivirine nanoformulation, the optimal release rate was observed to be 0.0005 h^{-1} (Figure 4.2). The optimal doses were informed for different weight categories such that the average drug C_{trough} plasma concentrations of 48 weeks stay over 70 ng/ml (25 mg PO C_{trough}) [205]. Fixed oral dose of 25 mg was administered for 4 weeks prior to IM doses. The loading dose ranged from 250 – 550 mg and the maintenance doses from 200 – 500 mg across weight groups

from 15-70 kg individuals (Figure 4.3). The optimal doses ensured plasma concentrations over the $PAIC_{90}$ value and average IM concentrations over 25 mg PO C_{trough} for at least 95 out of 100 individuals.

a)

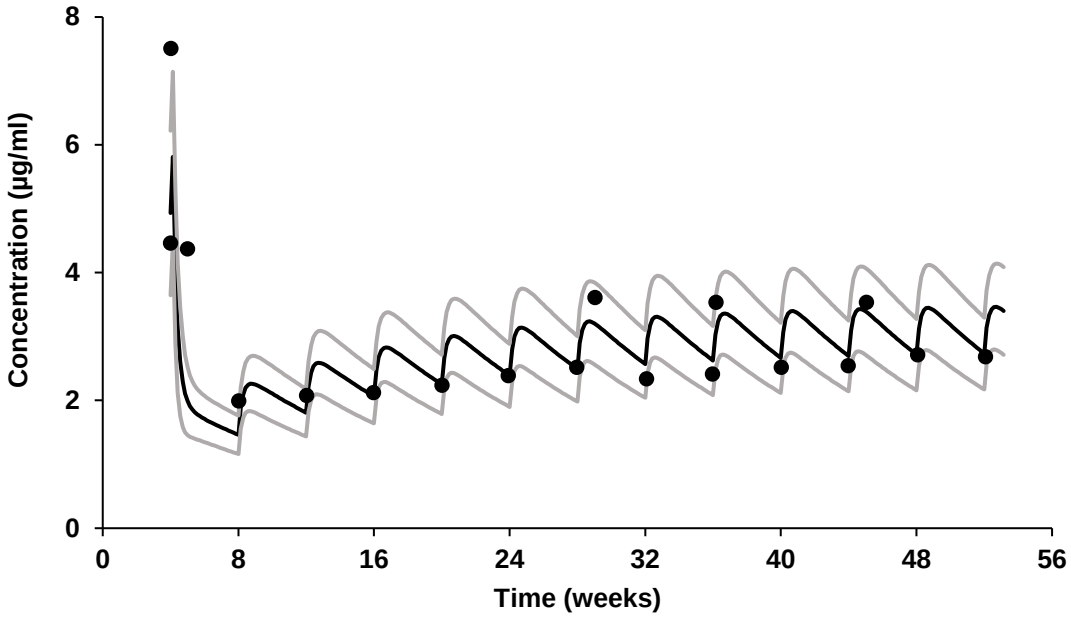

b)

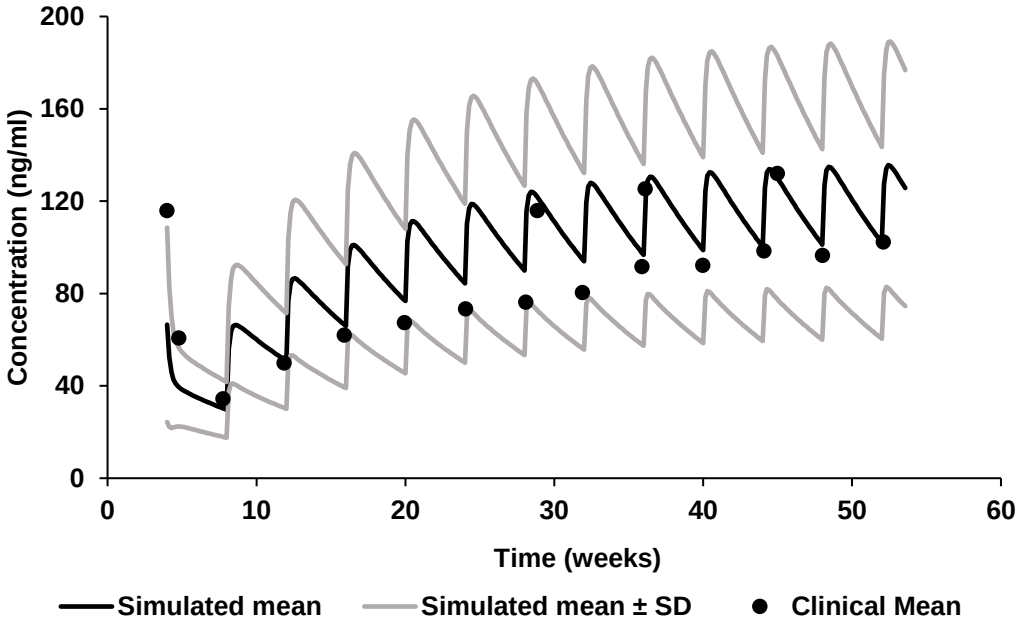

Figure 4.2 Validation of the PBPK model against clinical data from 48-week LATTE-2 study. a) Cabotegravir b) Rilpivirine [205]

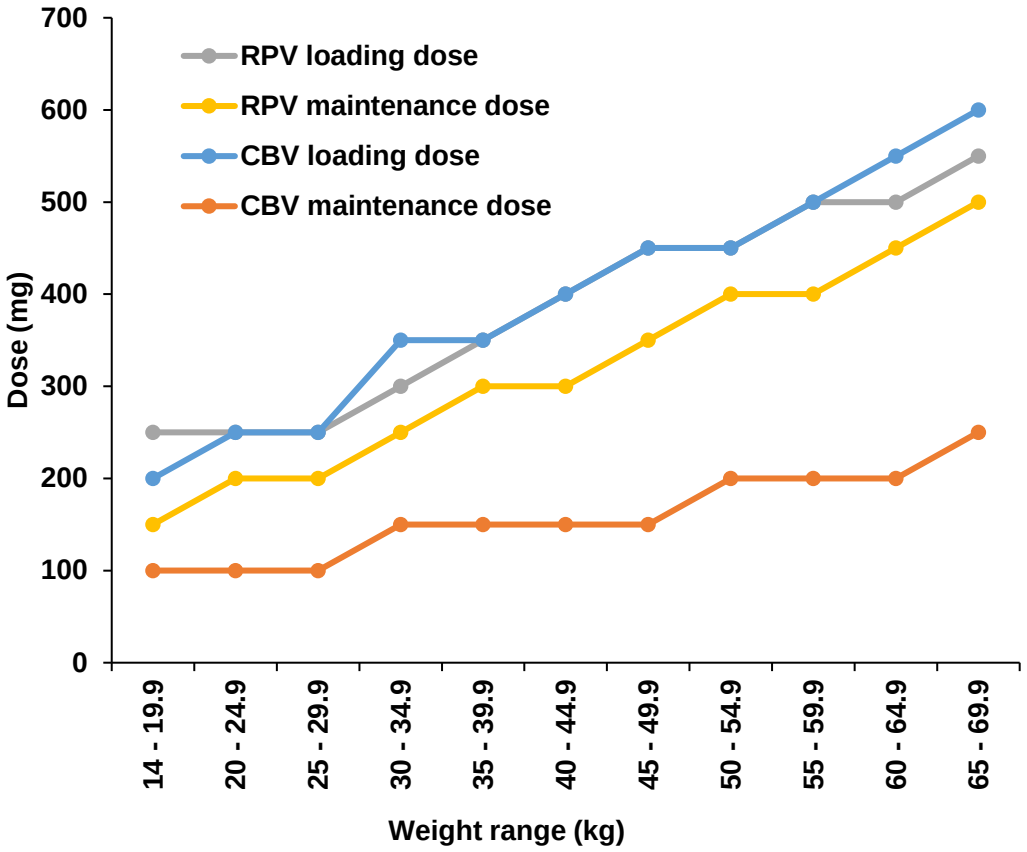

Figure 4.3 Dose prediction of loading and maintenance doses of cabotegravir and rilpivirine for various weight categories of children and adolescents

4.3.3. Sensitivity Analysis

Figure 4.4 shows the mean differential sensitivity analysis plot of 100 runs for six chosen parameters with respect to time. The analysis was performed for two successive (loading and maintenance) monthly IM doses of cabotegravir and rilpivirine in adults.

For cabotegravir, the analysis indicated that the plasma concentration is sensitive to only two of the six factors and higher influence was observed in the first days following administration. Cardiac output and systemic clearance of drug had higher sensitivity towards the variation in plasma concentrations. Protein binding, release rate, liver weight and blood-to-plasma ratio were negligibly sensitive. This indicates that

physiological factors and the UGT content in the liver had higher potential to influence the simulated pharmacokinetics. Sensitivity against cardiac output was negative for most of the duration indicating an increased effect against plasma concentration even when the value changes by ± 20% from the mean. Sensitivity against systemic clearance had a similar trend to cardiac output but with lower intensity. During the initial days after the administration of maintenance dose, both these factors showed positive relationship against plasma concentration indicating lower effect.

Extent of sensitivity observed for rilpivirine formulation was lower compared to cabotegravir. Change in plasma concentration was not sensitive when cardiac output, liver weight and release rate varied ± 20 % from the mean. Blood-to-plasma ratio had a higher positive effect immediately after dosing implying lower influence on plasma concentration. Blood-to-plasma ratio and systemic clearance showed positive relationship over the entire dosing period indicating decreased effect against plasma concentration. Protein binding fluctuated between positive and negative, however the variation is minimal signifying minimal or no effect on plasma concentration.

a)

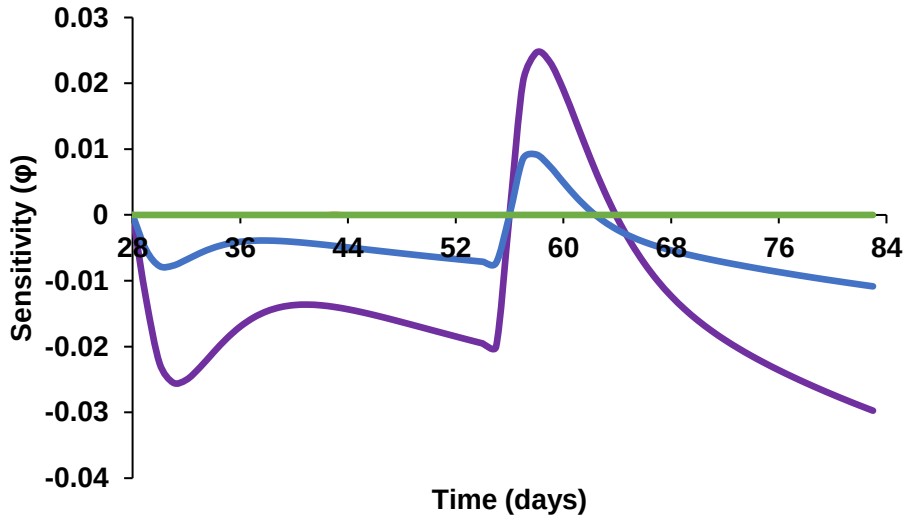

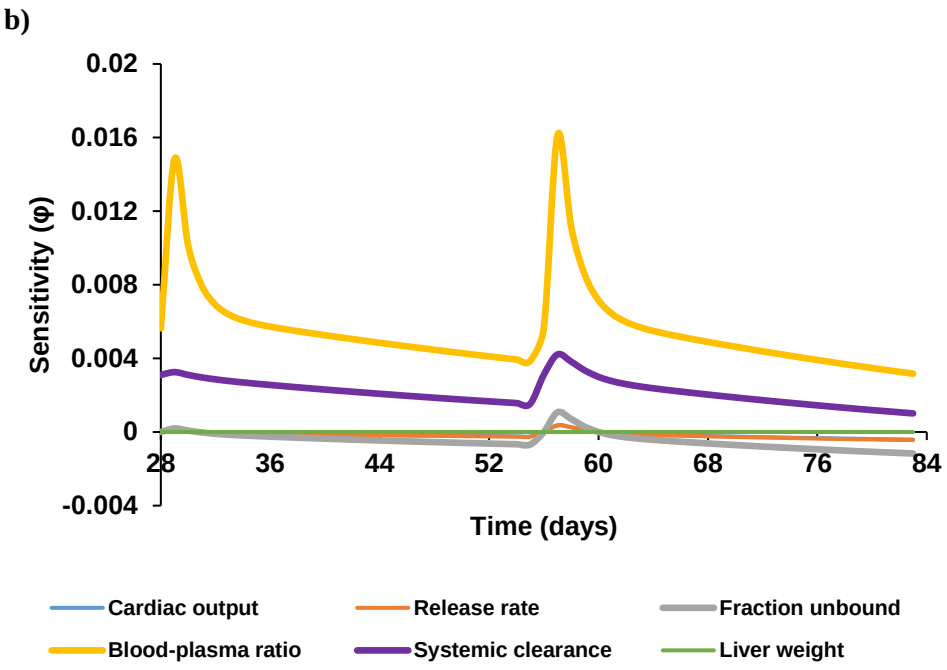

Figure 4.4 Differential sensitivity analysis of the key parameters in the PBPK model. a) Cabotegravir, b) Rilpivirine

Table 4.3 Prediction of the dose (in mg) for loading and maintenance intramuscular injections of cabotegravir and rilpivirine for different weight categories.

	Rilpivirine			Cabotegravir		
Weight (kg)	**Daily oral dose**	**Loading dose**	**Maintenance dose**	**Daily oral dose**	**Loading dose**	**Maintenance dose**
14 - 19.9	25	250	150	10	200	100
20 - 24.9	25	250	200	10	250	100
25 - 29.9	25	250	200	10	250	100
30 - 34.9	25	300	250	10	350	150
35 - 39.9	25	350	300	10	350	150
40 - 44.9	25	400	300	10	400	150
45 - 49.9	25	450	350	10	450	150
50 - 54.9	25	450	400	20	450	200
55 - 59.9	25	500	400	20	500	200
60 - 64.9	25	500	450	20	550	200
65 - 69.9	25	550	500	20	600	250
Target concentration (ng/ml)	70 (25 mg PO C_{trough}) [205]			1370 (10 mg PO C_{trough}) [205]		

4.4. Discussion

Optimal treatment adherence is essential to sustain an effective inhibition of the viral replication and prevent development of resistance to ARVs. Although oral formulations support therapeutic concentrations, sub-optimal-adherence in patients who are receiving drugs daily for treatment and prevention has been described [82, 210-213]. Alternative administration could further support higher adherence by reducing the frequency of administration and improving pill fatigue. More specifically, formulations allowing a monthly or quarterly administration could support higher adherence levels, thus decreasing the risk of drug resistance. ARVs with high potency and favourable pharmacokinetics are essential for the development of these strategies. The recent development of LA formulations such as cabotegravir and rilpivirine constitute a remarkable step towards addressing this pivotal issue, providing innovative pharmacological tools [36]. Dose optimisation in special populations of patients such as children and adolescents is a challenge due to their unique physiological and anatomical characteristics compared to adults. . The present study aimed to identify dosing strategies of cabotegravir and rilpivirine using PBPK modelling.

Various PBPK models have been developed for adults and recently this modelling technique has also been used for paediatric and adolescent patients [194, 214]. Drug distribution can be simulated in this special population of patients through the integration of age-related anatomical and physiological changes into the mathematical PBPK framework. PBPK modelling has been recently used for the prediction of midazolam and theophylline in neonates, infants and children [179]. In two other studies,

relationship between adult and paediatric clearance rate was established using cytochrome P450 ontogeny for six compounds and then simulations were performed for five different drugs at different age groups [192, 215]. An oseltamivir PBPK model was used to predict pharmacokinetics in neonates and infants with influenza [193] and a disease specific model was also recently developed in children with and without liver cirrhosis [216].

Both cabotegravir and rilpivirine are characterised by long-half lives and physicochemical properties that are compatible with nanoformulations for LAI, representing attractive options for continuous therapy [36, 123]. Using physiochemical properties and *in vitro* data, the pharmacokinetics of cabotegravir and rilpivirine in adults was validated against clinical data conducted in adults. The model validation was conducted at the second dose of the LA ARVs to have a mathematical representation of the pharmacokinetics at steady-state. Low accuracy and precision was observed in ÉCLAIR study where the simulated C_{trough} value of cabotegravir was 1.35 µg/ml compared to the observed value which was less than 0.66 µg/ml (4*$PAIC_{90}$) [217]. Hence, stringent guidelines were applied for the validation process where ± 50 % deviation from the mean clinical values was considered acceptable instead of the conventional 2-fold deviation [152]. The pharmacokinetic parameters – AUC, C_{max} and C_{trough} simulated through the PBPK approach were in agreement with the clinical data and therefore our PBPK model was considered robust for predicting the LA IM doses in paediatric and adolescent patients. In the simulation of LA pharmacokinetics in children, the release rates of the LA formulations were maintained equal to the validation in

adults, to ease the bridging of the formulations for paediatric use. Although the physiology of the muscular tissues is different between adults and children, this could potentially support the use of the existing formulations in paediatric clinical studies with no further reformulation [218]. However additional studies are required since there is a possibility that smaller doses with less injection volume could decrease total surface area and strain in the muscle, thereby altering the pharmacokinetic profile. The doses were optimised such that the cabotegravir and rilpivirine concentrations were over the assumed cut-off limits (described in methods section) for the duration of the dose. Although $PAIC_{90/95}$ values indicate a cut-off limit to suppress the virus *in vitro*, this does not translate in effective therapeutic activity *in vivo* [154]. Therefore, the dose optimisation was also conducted considering LATTE-2 study cut-off values.

Two different cut-offs – $PAIC_{90/95}$ and MEC were chosen such that different doses could be prescribed either for PrEP or therapy. The required dose was proportional to the weight of the individual, which indicates an increase in volume of distribution. Required dose of cabotegravir tripled as the weight increased from 15 to 70 kg compared to rilpivirine which required just over double the dose. This indicates that doses cannot be linearly extrapolated based on weight and a deeper understanding of important mechanistic processes influencing the pharmacokinetics in children and adolescents is required. The loading doses are higher compared to the maintenance doses as the extra dose is essential to maintain drug plasma concentrations over the $C_{trough}/PAIC_{90}$ values.

LAI formulations improve the problems faced with low adherence of ART in children. Focus on the clinical evaluation of the paediatric dose in patients should also be

given priority as most of the prescribed drugs are scaled from adult doses. Chloramphenicol dose scaling from adults in neonates and infants reached toxic levels which led to higher mortality rate, an example where the developmental pharmacology of paediatric patients was ignored [219]. Mortality rate was higher in neonates affected with kernicterus who were administered penicillin/sulfisoxazole than with oxytetracycline in an another case [220]. In both these cases, an immature glucuronidation system led to the accumulation of drug, resulting in high plasma concentrations and conclusively demonstrating that the physiological processes of the child cannot always be accounted for by scaling adult doses [167, 220].

Although the informed doses for children could represent an initial guideline for drug safety and efficacy studies, a few processes have not been mathematically described in the model regarding the anatomy and physiology of paediatric patients and associated complex biological processes due to unavailability of data [124]. Low clinical C_{max} (Figure 4.1) compared to the simulated pharmacokinetic curve could be due to the fraction of drug distributed through the lymphatics. Absence of information on drug transporters at the depot site for these drugs could alter the absorption, distribution and metabolic processes which could not be captured in the PBPK model. Recent investigation with paliperidone LAI micro suspension revealed formation of a granuloma due to macrophage accumulation surrounding the site of injection. This phenomenon further controlled drug release from the depot and evidence also showed drug uptake and release from macrophages [79]. The extent of the occurrence of this phenomenon and the size of the depot could alter the release rates and thereby drug

pharmacokinetics which was not accounted for in this study. Physiological and metabolic variation of muscle composition in children compared to adults was not accounted during the dose optimisation process [218]. The potential adverse effects considering the differences in the anatomy and physiology of children compared to adults, prolonged exposure and inability to discontinue therapy once administered are important factors to be assessed before drug administration [121].

CHAPTER 5

In vitro experimental design to assess the drug release from long-acting formulations

Contents

5.1. Introduction

Nanotechnology has advanced a lot in the past decade paving a way for designing novel formulations with prolonged drug release. Recent advances in polymer science greatly aided in design of controlled release formulations with particle sizes ranging between nano- and micrometres[221]. Polymer content assists fine-tuning drug release from the formulation to suit physiological conditions and simultaneously meet pharmacological requirements [221]. Several articles have been published based on micro- and nanoformulations consisting of water-soluble, biodegradable polymers such as chitosan, poly (lactic-co-glycolic acid) etc. that not only encapsulate the drug and control its release from the particles but are also biodegradable and biocompatible [222, 223].

Formulation design to support LA release can be complicated by the lack of experimental approaches to characterise drug release from the site of injection. Drug release can be quantified in preclinical species but this approach has numerous shortcomings such as physiological and anatomical differences between the selected species and humans, as well as high costs [87, 224, 225]. *In vitro* methods could represent a cost-effective and faster strategy to assess drug release and therefore support a rational selection of lead candidates [226].

To date, the United States Pharmacopeia (USP) does not identify a standard procedure to evaluate LA IM or SC formulations *in vitro*. Although *in vitro* release methods such as basket (USP apparatus 1), paddle (USP apparatus 2), paddle over disk (USP apparatus 5), cylinder (USP apparatus 6) and reciprocating disk (USP apparatus 7) exist, they are specifically recommended for oral and transdermal formulations based on the use of large volumes of media. USP apparatus 3 is not suitable for small particulate formulations less than 420 µm, characterised by media evaporation for

longer duration experiments which could lead to wide variability in sampling and might not maintain sink conditions for sparingly solubilized drugs [227]. Drawbacks of USP apparatus 4 includes a stationary compartment for the formulation, leading to aggregation of the micro- or nanoformulations and usually has a high flow rate (≥ 2 ml/min) [228]. Therefore, there is a pivotal need to design a standard *in vitro* system to effectively assess the release profile of LA formulations.

Experimental *in vitro* methods have been preliminarily developed for the investigation of oil-based formulations. A rotating dialysis cell method was used to access release of flupentixol, bupivacaine and naproxen LA formulations based on fractionated coconut oil [229, 230], lidocaine and testosterone in castor oil [231]. A bulk equilibrium reverse dialysis bag technique was applied for the quantification of drug release for oil-in-water emulsions using phenylazoaniline and benzocaine as model drugs, mimicking the *in vivo* environment [232]. However, all these reported *in vitro* methods do not compare drug release against any *in vivo* or clinical data. Although these studies were focusing on oil-based formulations, water-based formulations have wider clinical applications due to their good tolerability at the injection site compared to oily formulations [233].

Lately, few *in vitro* methods have been used to evaluate the drug release from water-based LAI formulations. Microspheres made of poly-D, L-lactide containing indomethacin were compared across four *in vitro* dissolution apparatuses – USP 2 dissolution apparatus, rotating bottle, shaker incubator and modified flow-through cell [234]. Large molecules such as lysozymes encapsulated in PLGA microspheres, gelatin microspheres containing oligonucleotides and DNA-fragments were analysed using flow-through cell method that could differentiate the drug release pattern between various formulations [235, 236].

The aim of this chapter was to evaluate three different types of *in vitro* release rate experiments, namely microdialysis using rapid equilibrium dialysis membranes, flow-through cell dialysis and sample-and-separate methods. These *in vitro* methods were evaluated using commercially available LAI formulations of Depo-provera (medroxyprogesterone acetate), Risperdal consta (Risperidone), Xeplion (Paliperidone palmitate), Zypadhera (Olanzapine pamoate) and a test formulation of rilpivirine. The obtained *in vitro* release rates were then correlated against PBPK release rates to identify the predictive capability of these *in vitro* methods.

5.2. Materials and Methods

5.2.1. Materials used

Bovine serum albumin (Sigma, UK), γ-globulin (Sigma, UK), Depo-provera® 150 mg/ml medroxyprogesterone acetate (Pfizer Limited, UK), Xeplion® 100 mg/ml paliperidone (Janssen, UK), Zypadhera® 150 mg/ml olanzapine (Elli Lilly, UK), Risperdal Consta® 25 mg/ml risperidone (Janssen, UK), 300 mg/ml rilpivirine (Janssen, UK), phosphate buffer saline (Life Technologies, UK), isopropyl alcohol (Fisher Scientific, UK), docusate sodium (Sigma, UK), methanol (Sigma, UK), acetic acid (Fisher Scientific, UK), acetone (Sigma, UK), Float A Lyzer® G2 dialysis tubes 100 KDa MWCO (Spectrum Laboratories, UK), 0.3 ml and 1.8 ml high performance liquid chromatography (HPLC) vials (Thermo Scientific, UK), rapid equilibrium dialysis (RED) tubes 8 KDa MWCO (Thermo Scientific, UK), Fetal Bovine Serum (FBS) (Life Technologies, UK), Phosphate Buffered Saline (PBS) tablets (Sigma, UK).

5.2.2. Equipment used

Classic series New Brunswick Scientific Incubator (NJ, USA), Stuart scientific rotator drive STR4 (Chelmsford, UK), Scientific Industries Vortex Genie 2 (NY, USA), Thermo Electron Corporation IEC MicroCL 17R centrifuge (MA, USA), Dionex HPLC machine (Dionex, Germering, Germany), Fortis 3 µm C18 chromatographic column (Cheshire, UK), Jouan RC 10.10 rota evaporator (Nantes, France), Minitab Statistics package (Coventry, UK).

5.2.3. Static release experiments

Simulated interstitial fluid (SIF) was prepared by dissolving 3.5 g bovine serum albumin and 0.2 g γ-globulin in 100 ml distilled water [237]. The drug formulation

prior to use was dispersed by shaking the provided container according to the instructions provided by the product label. The average pore size of the dialysis tubes is less than ~2 nm (8000 Da) which prevents the transfer of intact nanoparticles. In the RED dialysis tubes, the maximum volume that could be accommodated is 500 µl and 1 ml in the donor and acceptor compartments respectively. Hence, 200 µl of the drug formulation along with 300 µl of SIF was added to the donor compartment and 1 ml SIF was added to the acceptor compartment (Figure 5.1). 0.6 ml SIF in acceptor compartment was replaced with fresh SIF at 0.5, 1, 2, 3, 4, 5 and 6 h from the onset of the experiment. During sample collection times, the contents of the donor compartment were agitated using a pipette to prevent sedimentation of the suspension. The whole setup was covered using parafilm to prevent eater evaporation. The collected samples were extracted (described in section 5.2.6) and analysed in HPLC (described in section 5.2.7).

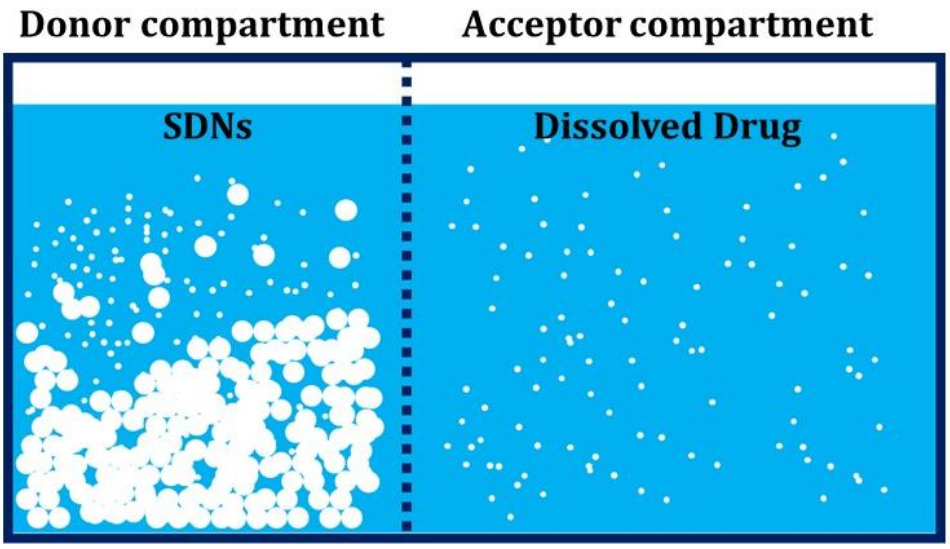

Figure 5.1 Rapid equilibrium dialysis system with drug particles in the donor compartment and the solubilised/diffused drug in the acceptor compartment

5.2.4. Sample-and-separate method

A sample-and-separate method obtained from Shen et al. has been used for release rate assessment [238]. A 200 µl aliquot of formulation was dispersed into 250 ml of PBS. The experiment was conducted aseptically to avoid bacterial growth in the medium. This apparatus was rotated at 100 rpm in a water bath at 37 °C. 1 ml samples were taken at regular time points daily for 30 days. The collected samples were centrifuged at 2100 x g for 3 minutes and 0.9 ml of supernatant fraction was collected. The remaining was reconstituted using 0.9 ml fresh PBS and was added back to the apparatus to maintain a constant volume. The collected samples were filtered through 0.22 µm filters prior to HPLC analysis. Medroxyprogesterone and rilpivirine were not filtered since the drug was retained in the filter. The sample collection and replacement of PBS were done under sterile conditions to avoid bacterial growth in the container. 200 µl of the collected samples were transferred to HPLC vials and analysed by a HPLC (described in section 5.2.7).

5.2.5. Dynamic release experiments

Dialysis tubes were soaked according to manufacturer's instructions in 10 % isopropyl alcohol (IPA) for 10 minutes to remove the glycerine coating from the dry dialysis membrane. The dialysis device was rinsed and soaked in distilled water for a further 20 minutes to wash off the IPA and the glycerine residue.

Key parameters such as composition of the media, volume in the donor compartment and flow rate were optimised using Taguchi's design of experiments to obtain maximum drug release from the dialysis tubes. The optimised parameters are mentioned here - the donor compartment was made up to the correct dilution using phosphate buffer saline (PBS) as 200 µl drug and 3.8 ml PBS. Drug/PBS solution was

deposited into the float-a-lyzer dialysis tube, and this apparatus was placed in a falcon tube with an inlet and outlet. The lid of the falcon tube was sealed with a glue gun and the falcon tube was securely strapped to the rotator plate and placed in an incubator at 37 °C.

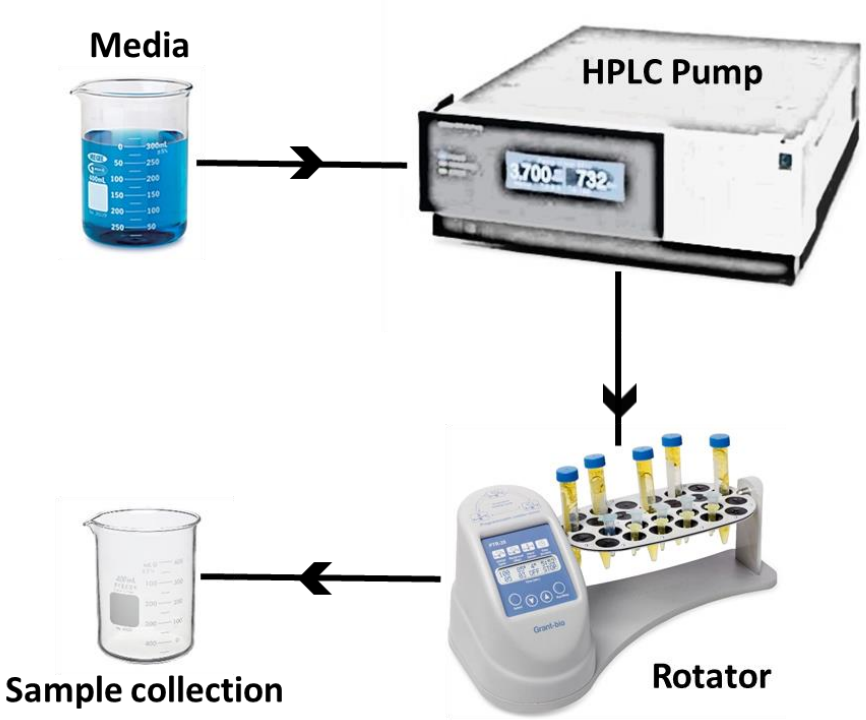

Figure 5.2 The apparatus used for dynamic release experiments. The media was pumped using the HPLC at a constant flow rate into the acceptor compartment of the falcon tube and the sample was collected from the outlet of the tube into a beaker.

The rotator was programmed such that it would rotate from -90° to +90° to and fro to avoid tangling of the pipes connecting the falcon tubes. Vibration of 1° for 1 sec was also set in the rotator for every rotation to induce additional agitation. 800 ml of 50 % FBS/50 % PBS solution was prepared and was pumped into the acceptor compartment with the help of a HPLC pump at a flow rate of 0.5 ml/min (Figure 5.2). This whole apparatus was placed in an incubator chamber maintained at an ambient temperature of 37 °C. The experiment was conducted for 24 h and the sample was collected into another beaker from the outlet of the falcon tube. The collected media

at 24 h was extracted (described in section 5.2.6) and analysed by HPLC (described in section 5.2.7).

5.2.6. Sample extraction

A 200 µl aliquot of the samples was transferred to new eppendorfs and mixed with 1 ml 100 % acetone (for medroxyprogesterone acetate and rilpivirine) or 99.9 % acetonitrile and 0.1 % acetic acid (for olanzapine, paliperidone and risperidone). These samples were placed in a rotator for 60 min to allow the transfer of dissolved drug from the aqueous phase to the organic phase. Following this, samples were centrifuged at 13,300 rpm for a further 30 min to precipitate the plasma proteins. The supernatant fractions were transferred to glass vials and left to dry overnight at room temperature in a rotary evaporator under vacuum. The following day, 200 µl of the appropriate reconstitution liquid (described in section 5.2.7) was added to the dry residue, which was then transferred to 300 µl vials for HPLC analysis.

5.2.7. HPLC analysis protocol

In order to analyse samples obtained from dialysis experiments, it was necessary to produce a standard curve using known concentrations of drug; standards from 39 to 20,000 ng/ml were used. This calibration curve was then used to calculate the drug amount in the unknown samples. A Dionex HPLC with UV detection was used for analysis, injection volume was set at 100 µl and a Fortis C_{18} column (3 µm, 4.6 x 100 mm) with a Fortis C_{18} Guard (3 µm, 4 x 10 mm) at room temperature was used for chromatographic separation in this process.

5.2.7.1. Medroxyprogesterone acetate

The mobile phase A consisted of 60: 40 water: methanol with 3 mM docusate sodium, 10 ml acetic acid and perchloric acid to adjust the pH to 3 in a one litre solution and 100 % methanol was used as mobile phase B. The gradient started with 50 % B at 0 min; 50 % B at 0.2 min; 90 % B at 0.5 min; 90 % B at 6.0 min, 50 % B at 6.1 min and the run time was set to 8 min. Flow rate was set at 0.8 ml/min and 254 nm was used as the wavelength to detect medroxyprogesterone acetate. The extracted samples were reconstituted with mobile phase A. The retention time observed was 5.24 min.

5.2.7.2. Olanzapine

Mobile phase A comprised 95: 5 10 mM potassium phosphate: acetonitrile and orthophosphoric acid was used to adjust the pH to 4. Mobile phase B consisted of 90: 10 acetonitrile: water. The flow rate of the mobile phase was set to 1 ml/min and the run time was 8 min. The gradient employed was 10 % B at 0 min, 10 % B at 0.5 min, 80 % B at 4 min, 80 % B at 6 min, 10 % B at 6.1 min. The UV detection wavelength was 257 nm. 80: 20 mobile phase A: acetonitrile was used as the reconstitution solvent for the analyte and the retention time was observed to be 4.56 min.

5.2.7.3. Paliperidone

Mobile phase A consisted of 95: 5 5 mM ammonium formate: acetonitrile and formic acid to adjust the pH to 4 and 90: 10 acetonitrile: water as mobile phase B. The flow rate was 1 ml/min and the composition of the mobile phase was varied as follows: 0 min: 10 % B, 0.5 min: 10 % B, 4 min: 95 % B, 6 min: 95 % B, 6.1 min: 10 % B and 8 min: 10 % B. The run time was set to 8 min and the retention time of the analyte was observed to be approximately 4.82 min. The reconstitution solvent used

to analyse the samples consisted of 80 % mobile phase A and 20 % acetonitrile. The detection wavelength used was 257 nm.

5.2.7.4. Risperidone

Mobile phase A was 95: 5 5 mM ammonium formate: acetonitrile and formic acid to adjust the pH to 4 was used as and 90 % acetonitrile with water was used as mobile phase B. The gradient started with 0 min: 20 % B, 0.2 min: 20 % B, 3 min: 100 % B, 6 min: 100 % B, 6.1 min: 20 % B, 8 min: 20 % B. 260 nm was used as the wavelength to detect risperidone. The extracted samples were reconstituted with 80 % mobile phase A and 20 % acetonitrile. The retention time observed was 5.67 min.

5.2.7.5. Rilpivirine

Mobile phase A comprised 95:5 10 mM potassium phosphate: acetonitrile and orthophosphoric acid was used to adjust the pH to 4. Mobile phase B consisted of 90:10 acetonitrile: water. The flow rate of the mobile phase was set to 1 ml/min and the run time was 8 min. The gradient employed was 0 min: 10 % B, 0.5 min: 10 % B, 4 min: 80 % B, 6 min: 80 % B, 6.1 min: 10 % B, 8 min: 10 % B. The UV detection wavelength was 257 nm. 80:20 mobile phase A: acetonitrile was used as the reconstitution solvent for the analyte and the retention time was observed to be 5.09 min.

Table 5.1 Physicochemical properties and drug specific parameters of drugs

	log $P_{o:w}$	**Solubility in H_2O (g/L)**	**Fraction unbound**	**Mean particle size (nm)**
Medroxyprogesterone acetate	3.5 [239]	0.0221 [239]	0.1 [239]	2,500 [240]
Olanzapine	3.39 [241]	0.094 [241]	0.07 [241]	7400 [242]
Paliperidone	1.76 [243]	0.03 [243]	0.26 [243]	1090 [79]
Rilpivirine	4.32 [244]	0.0116 [244]	0.003 [139]	200 [87]
Risperidone	3.27 [245]	0.0028 [245]	0.12 [245]	57,900 [246]

5.3. Results

5.3.1. Static release experiments

The cumulative drug release obtained during the sample analysis with the HPLC in 6 h are presented in Figure 5.3. Rilpivirine did not show any detectable amount of drug in the acceptor compartment. The slope obtained from the best fit line is considered as the *in vitro* release rate in h^{-1}. The regression value for all the four formulations is >0.90 indicating a linear, steady drug release into the acceptor compartment. Except for medroxyprogesterone acetate, it can be observed that the extent of release at 0.5 h is lower than the best fit line implying that the formulation takes some time to release the drug in a new environment. An additional sample was collected at 24 h (data not shown) but the drug release was limited indicating the saturation of SIF in the acceptor compartment after a few hours.

a)

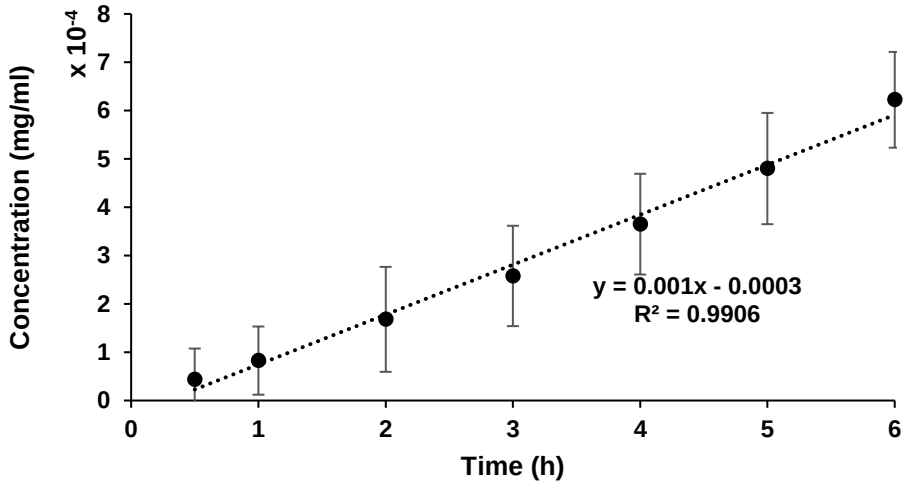

b)

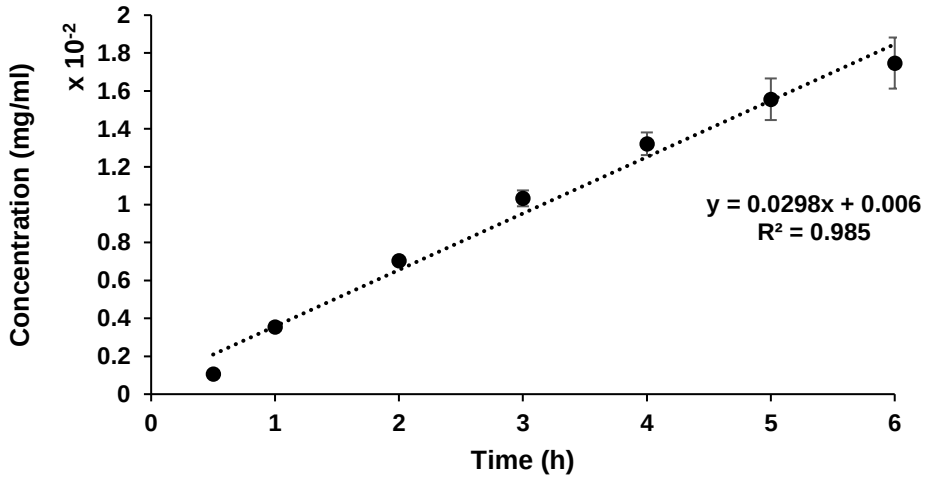

c)

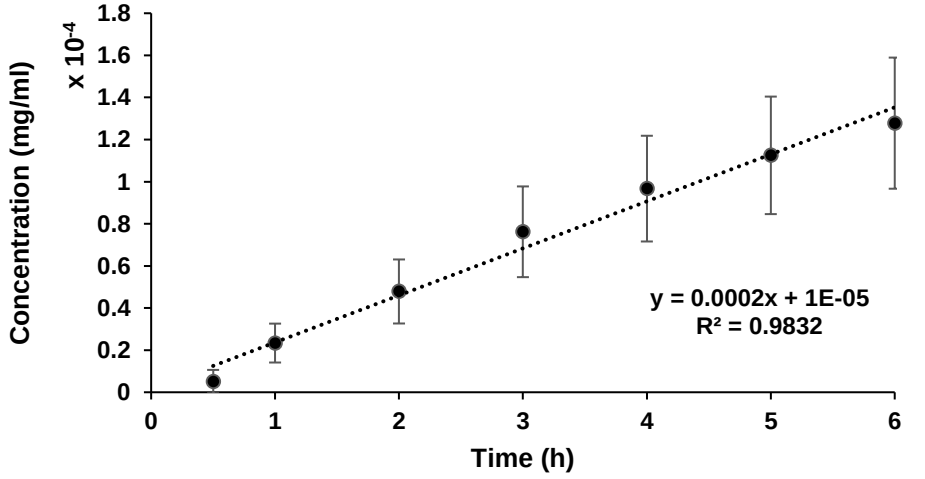

d)

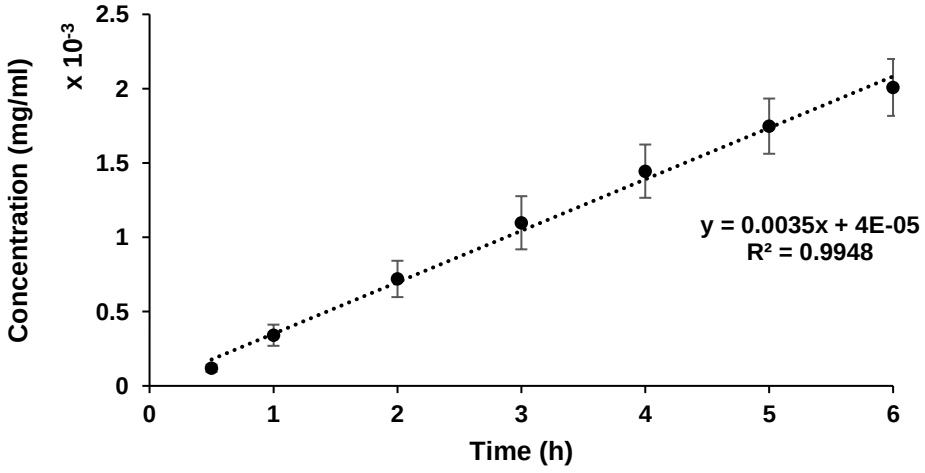

Figure 5.3 Summary of the cumulative drug release (n=3) from rapid equilibrium dialysis tubes for a) Medroxyprogesterone, b) Olanzapine, c) Paliperidone and d) Risperidone.

5.3.2. Sample-and-separate method

The cumulative formulation release trend of the drugs in PBS over a period of 30 days is shown in Figure 5.4. The variation in the percentage of the drug released over time from the formulation is minimal from day 1 to day 30 for all the drugs except risperidone.

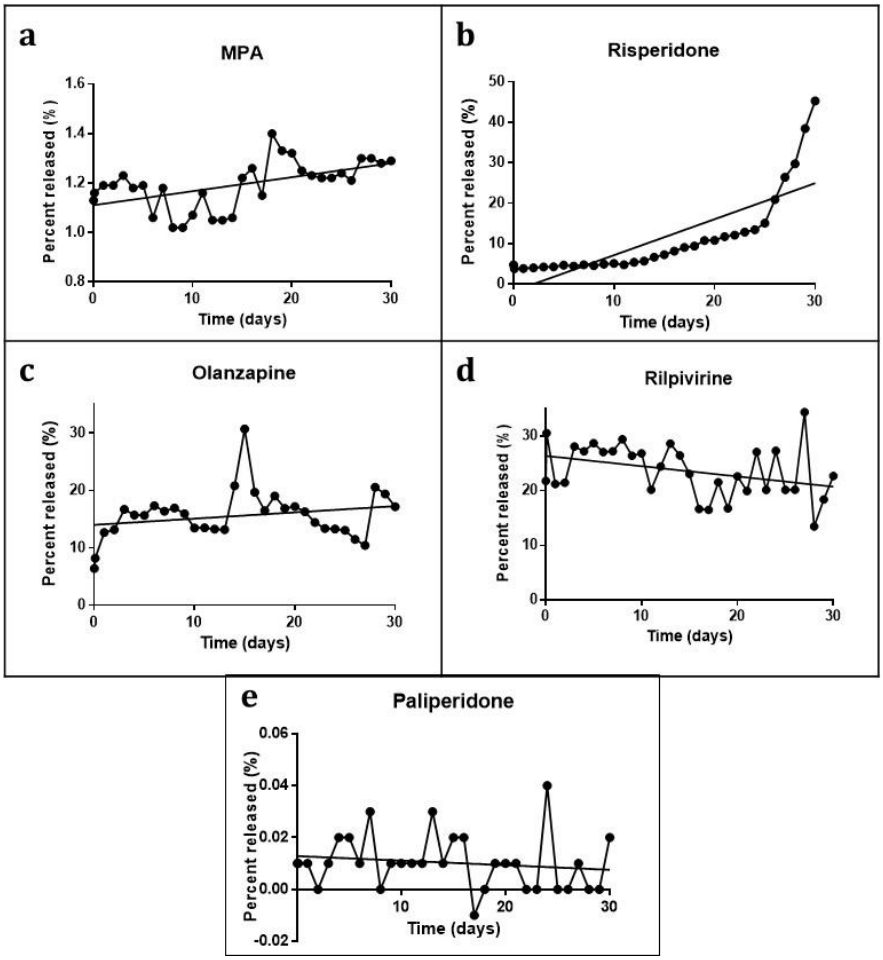

Figure 5.4 Percentage of drug released from the total formulation against time in days is shown for the five drugs. a) Medroxyprogesterone, b) Risperidone, c) Olanzapine, d) Rilpivirine and e) Paliperidone

Table 5.2 compares the observed vs. expected release from the formulation. Rilpivirine and risperidone are the only two among the five assessed drugs to have an observed percent release, over a period of 30 days, close to the expected release by a

factor of two (as shown in Table 2). This could be due to limited solubility of drugs in PBS. The percentage release is far off from the expected value implying that this *in vitro* method to evaluate drug release is not suitable for long-acting micro- or nanoformulations.

Table 5.2 Summary of the percentage of drug released *in vitro* using sample and separate method and the expected release in 30 days

Formulation	*In vitro* release for 30 days (%)	Expected release for 30 days (%)
Medroxyprogesterone acetate	1.28	~ 45
Olanzapine	17.3	> 90
Paliperidone	0.02	> 90
Rilpivirine	21.5	~ 35
Risperidone	46.2	~ 100

5.3.3. Dynamic release experiments

Medroxyprogesterone acetate was used to optimise the parameters for the dynamic release experiments initially. Taguchi's design of experiments was used with two values for each of the three parameters (Table 5.3). Maximum release was observed with 4 ml in the donor compartment (comprising 200 µl drug and 3.8 ml PBS), flow rate of 30 ml/h through the falcon tube and 50 % FBS in PBS as the composition of media circulated through the tube for 24 h (Table 5.6, Figure 5.5). Drug release with 50 % FBS in PBS has more release of medroxyprogesterone compared to 10 % FBS. High flow rate (6 vs 30 ml/h) and higher volume in the donor compartment (1 vs 4 ml) increased the overall drug amount released. To confirm the selection of optimum parameters, ANOVA analysis (Table 5.4) and signal-to-noise ratios (Table 5.5) were performed in Minitab.

Table 5.3 Summary of the parameter values and the amount of medroxyprogesterone released over time using Taguchi's design of experiments

Volume in donor Compartment (ml)†	Flow rate (ml/h)	% FBS in PBS	*In vitro* release per day (µg)
1	6	10	0.000001
1	6	50	0.005668
1	30	10	0.027212
1	30	50	0.038025
4	6	10	0.013714
4	6	50	0.048315
4	30	10	0.037924
4	30	50	0.084854

† Donor compartment consists of 200 µL medroxyprogesterone acetate and 0.8 ml or 3.8 ml phosphate buffered saline

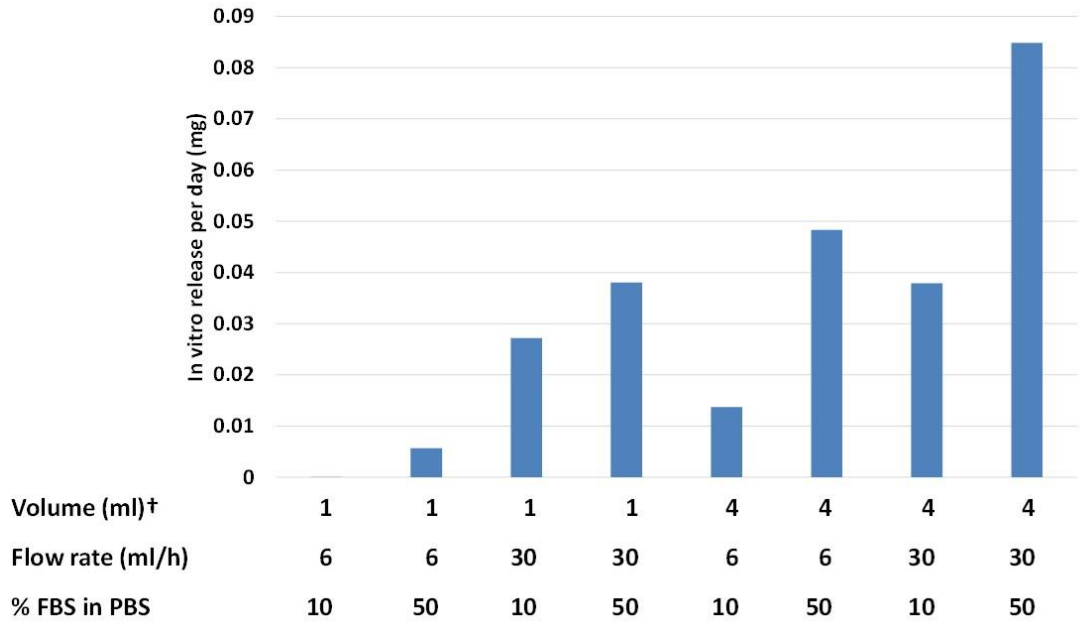

Figure 5.5 Release of medroxyprogesterone after 24 h using different release conditions; † Donor compartment consists of 200 µL medroxyprogesterone acetate and 0.8 ml or 3.8 ml phosphate buffered saline

Table 5.4 One-way ANOVA analysis for the eight experiments conducted using Taguchi's design of experiments for medroxyprogesterone. The P-value of each factor when compared with the release is also shown

	Release vs. Volume		Release vs. Flow rate		Release vs. % FBS	
	1 ml	4 ml	6 ml/h	30 ml/h	10 %	50 %
Arithmetic Mean	0.01775	0.0462	0.0169	0.047	0.01974	0.0442
Standard Deviation	0.01787	0.0296	0.0216	0.0257	0.01642	0.0326
95 % CI	(-0.01214, 0.04764)	(0.0163, 0.0761)	(-0.0121, 0.0460)	(0.0179, 0.0761)	(-0.01186, 0.05133)	(0.0126, 0.0758)
P-value	0.151		0.124		0.229	

Table 5.5 Response table for signal-to-noise ratios for the three parameters assessed for optimisation process. The lower the value, the optimum the level

No.	A - Volume in donor Compartment (ml)	B - Flow rate (ml/h)	C - % FBS in PBS
1	-46.16	-47.13	-44.25
2	-28.36	-27.39	-30.27
Delta	17.8	19.74	13.98
Rank	2	1	3

Table 5.6 Summary of the parameters considered to have major effect on the drug diffusion through the dialysis membrane

No.	A - Volume in donor Compartment (ml)	B - Flow rate (ml/h)	C - % FBS in PBS
1	1	6	10
2	4	30	50

Following the optimisation process, these parameters were used for the dynamic release experiments to conduct release experiments for the rest of the drugs. The summary of the results are shown in Table 5.7.

Table 5.7 Summary of *in vitro* release values in 24 h obtained from dynamic release experiments

Formulation	*In vitro* release in 24 h (mg)	% of initial dose released	% expected drug release
Medroxyprogesterone acetate	0.425	1.4	~1.5
Olanzapine	17.06	56.9	~3.0
Paliperidone	18.43	92.2	~3.0
Rilpivirine	0.05	0.1	~1.17
Risperidone	0.431	17.2	~3.3

The comparison of expected vs. observed percentage of drug amount released over 24 h is shown in Table 5.7. This indicates a suitable method for medroxyprogesterone acetate. However, for olanzapine, paliperidone and rilpivirine the observed release is >11 times than the expected release and <5 times for risperidone.

5.4. Discussion

A standardised *in vitro* test to evaluate drug release from LA formulations has not been validated till date. Currently, the majority of the studies to inform the selection of formulations are directly performed *in vivo* primarily in rats, rabbits, dogs and monkeys prior to human clinical trials. This strategy has several limitations, is complex, expensive, laborious, often not reproducible, and results in the sacrifice of many laboratory animals during development. Consequently, the design of a validated and reproducible experimental assay would provide an essential tool to identify optimal candidates prior to *in vivo* studies [205].

Various LAI antipsychotics and contraceptives are already used clinically [248]. These commercially available formulations were used as reference drugs to evaluate three *in vitro* methods to characterise the drug release from conditions mimicking the physiological depot environment. Evaluation of release rate by reducing the overall complexity involved in the design and cost was the primary rationale behind shortlisting these three experimental setups. Microdialysis which utilizes low amount of media, was the first choice for performing *in vitro* experiments. RED tubes attain equilibrium between donor and acceptor compartments quickly and a short experimental duration is sufficient to identify the initial release pattern. Figure 5.1 indicate a linear correlation between time and amount of drug released into the acceptor compartment. After the 6 h time point, an additional sample was collected at 24 h (data not shown) and the drug amount accumulated was way below expected indicating saturation of drug due to low drug solubility in the limited water content present in acceptor compartment. There were a few cases where media in the acceptor compartment dried up due to evaporation of water in both compartments when the experiment was conducted for a prolonged period of time. Drugs that bind to the filter membrane or the

container made of polymer cannot be analysed using this method. Although these experiments do not represent ideal physiological conditions, they could be used as a short duration high throughput screening option for rapidly evaluating potential LAI formulations.

The sample and separate method was adapted from Shen et al. and performed without the aid of dialysis tubes [238]. This method was used to evaluate drug release from formulations into the medium without any barrier. Since this experiment was performed at 37 ºC in PBS for 30 days, the sample collection was conducted under aseptic conditions to avoid any microbial contamination. Figure 5.4 shows significant increase in drug release for risperidone especially in the last 5 days compared to other drugs which indicate excipient degradation of the microparticles. There was no substantial change in percentage of drug released (< 5 %) for rest of the formulations on the last day compared to the release on the first day. Solubility in PBS could be the limiting factor for the amount of drug released. Aggregation of micro- or nanoparticles could affect the drug release profiles. When using small volumes of media, loss of drug during filtration could be a problem. Also drugs that bind to the filter cannot be assessed using this method. This method may be suitable for larger particle sizes and also drugs soluble in PBS.

The flow-through cell dialysis technique utilises large amounts of media pumped using a HPLC pump through a falcon tube containing the formulation packed in a dialysis bag. SIF was replaced with a cheaper alternative – FBS and PBS. Taguchi's design of experiments assisted in the identification of factors influencing drug release rates *i.e.* volume in donor compartment, flow rate through falcon tube and composition of media in order to achieve maximum drug release. Blood flow through the IM

depot was identified as 29 ml/h and therefore flow rate was set at 0.5 ml/min to simulate this [124]. Four millilitres of fluid was assumed to be present at the site of injection including maximum injection volume (2 ml) and interstitial fluid surrounding it. Higher protein content (10 % vs 50 %) in the media improved drug release across the dialysis membrane. Table 5.3 indicates that these parameters are the limiting factors that control drug release from formulation. The flow-through cell method tackles media saturation and evaporation observed in microdialysis experiments however it is 18 h longer utilising large media volumes compared to the static release experiment. Also, clogging of HPLC tubing with proteins from the media could result in large variation across samples.

Various factors affect the drug release from the encapsulated particles. Few of them include drug protein binding, solubility in the used media, effect of the excipients in the media, amount of media, type of agitation, mean particle size, log P and the duration of the experiment. From this study it would be difficult to identify the individual impact of each of these factors since a simultaneous effect of all the above mentioned factors would be observed during the experiments. Due to these factors, it would be difficult to compare experimental methods since two or more factors are varied across the performed experiments. Secondly, comparison across different drug formulations using a single method would be inconclusive since different drug physicochemical properties and formulation characteristics come into play. However, from the dynamic dialysis release experiment conducted using medroxyprogesterone (Table 5.3), there is a clear-cut influence of drug release due to an increase in the total volume present in the donor compartment, flow rate and the percentage of FBS in PBS. This indicates that drug release is facilitated with more volume of media in contact with drug formulation and increased protein content.

In summary, this chapter indicates that microdialysis and flow-through cell dialysis techniques could have potential for evaluating drug release profiles *in vitro* with lower particle sizes. The sample and separate method is suitable for particle sizes greater than 100 µm in diameter. Evaluation using *in vitro* techniques limits the ability to simulate physiological conditions but could provide initial release profiles. Release rate is also affected due to various physiochemical factors such as octanol-water partition coefficient, solubility, protein binding, particle size etc. Additional formulations with particle sizes ranging between nano-micro ranges should be evaluated in order to obtain a robust understanding of the effect of these factors on influencing release rate.

CHAPTER 6

In vitro - in vivo extrapolation of intramuscular release rate

Contents

6.1. Introduction

IVIVE is a bottom-up technique that utilises *in vitro* experimental data to predict the behaviour of drugs *in vivo*. This approach identifies a mathematical correlation between data generated using experimental *in vitro* methods and animal or human *in vivo* data. IVIVE can also be integrated in a comprehensive evaluation of factors influencing pharmacokinetics, combining drug physicochemical data such as logP, pKa etc., drug specific parameters such as intrinsic clearance, Papp etc., and human anatomical and physiological parameters such as organ weights and volumes, cardiac output, blood flow rates etc. to simulate the pharmacokinetics in humans through compartmental models [249].

IVIVE can support generation of data without the need of performing complex experiments in pre-clinical species or humans. Consequently, results obtained from preliminary *in vivo* experiments could be confirmed rather than being explored using IVIVE reducing the time and effort during optimisation. Although IVIVE has been applied successfully in drug discovery, it is characterised by limitations. IVIVE considers only the median value to describe a valuable correlation which defines the risk of poor prediction for data with extreme values. Variation among different races and ethnicities may not be considered which leads to biased results when several population types are being analysed. Limited data used for IVIVE could lead to biased results and could be applicable only to patients with similar characteristics [232, 250, 251].

Numerous IVIVE models have been published in recent years to extrapolate ADME processes [57, 133, 252, 253]. The correlation of *in vitro* apparent permeability and intrinsic clearance to effective permeability and human intestinal first-pass metabolism was characterised using a broad range of compounds [57]. The fraction unbound in microsomes was demonstrated to correlate with various drug specific

characteristics such as plasma protein binding, blood-to-plasma ratio, acidic phospholipid and neutral lipid content and drug ionisation in plasma and erythrocytes [252]. Competitive inhibition and time-dependent CYP3A4 inactivation was predicted using enzyme inactivation, synthesis and degradation rate constants and inhibitor concentrations in the liver [253]. Tissue-to-plasma drug distribution and volume of distribution were predicted based on parameters such as logP, pKa, plasma protein binding, blood-to-plasma ratios and tissue composition (volume of neutral lipids, phospholipids and water) [133].

The mechanistic backbone of PBPK models is the combination of IVIVE equations and a mathematical description of physiological and anatomical factors of virtual individuals. *In vitro* data such as passive permeability, the role of transporters, and intrinsic clearance, which describe the ADME processes are integrated into PBPK models to inform simulation of drug pharmacokinetics in virtual individuals [249]. Currently, LAI formulations are evaluated in preclinical species (such as rats, dogs, rhesus macaques) prior to studies in humans [121]. Experimental *in vitro* methods that characterise the release rate of LAI formulations prior to preclinical studies could present a useful tool to identify valuable lead candidates.

The aim of this chapter was to conduct an IVIVE by correlating *in vitro* experimental release rates obtained in Chapter 5 and PBPK predicted release rate for LAI formulations with the objective of extrapolating *in vitro* to *in vivo* release rate for future novel formulations.

6.2. Methods

Previously published PBPK models, validated for IM LAI formulations were used to derive the IM release rate from the marketed formulations (Chapter 2). PBPK models for medroxyprogesterone acetate, paliperidone palmitate, olanzapine pamoate and risperidone were developed using available physicochemical and experimental data from the literature (Table 6.1). Equations used in the construction of the PBPK model are described in the methods section of Chapter 2 (section 2.2).

The dosing regimen for each therapeutic agent was simulated according to available clinical studies. Medroxyprogesterone was validated for a single 150 mg LAI formulation for 12 weeks. Pharmacokinetic plasma concentration-time curve and available C_{max} value were used as reference [254]. Olanzapine reaches steady-state after 2-3 months, hence the fourth 4-weekly 300 mg injection was validated against the clinical pharmacokinetic curve and the pharmacokinetic parameters C_{max}, AUC and C_{av} (average concentration over the duration of the injection) were used to optimise the release rate [255]. Paliperidone is initially administered through the deltoid muscle, so the pharmacokinetic parameters C_{max}, AUC and C_{av} for the 4^{th} deltoid injection were used for the optimisation process [256]. Risperidone is a prodrug and converts to its major active metabolite – paliperidone. Available pharmacokinetic data in literature constitutes combined data of both risperidone and paliperidone. Hence the PBPK model was designed to accommodate the combination of both drugs and its pharmacokinetic data was validated using the published clinical data. Patients with a pre-administered oral dose of 2 mg OD for 4 weeks continued administration of 2 mg OD for further 3 weeks and 1 mg OD on the 4^{th} and 5^{th} week. Additionally, a biweekly IM LAI injection of 25 mg starting on day 8 and ending on day 64 was

administered. An oral dose of risperidone was not administered on the day of the injection. The optimisation was conducted using the pharmacokinetic curve of 25 mg IM LAI administered on day 36 [257].

Table 6.1 Physicochemical parameters of long-acting formulations used for the validation of the PBPK model

	MPA	Olanzapine	Paliperidone	Risperidone
Molecular weight	344	312	426	410
log $P_{o:w}$	3.5 [239]	3.39 [241]	1.76 [243]	2.63 [245]
Protein binding	90 % [239]	93 % [241]	74 % [243]	90 % [245]
pKa	12.7 [239]	14.17 [241]	13.74 [243]	8.76 [245]
R	†0.86	†2.7	0.8 [258]	0.67 [189]
PSA (Å^2)	54.37 [239]	30.87 [241]	82.17 [243]	61.94 [245]
HBD	1 [239]	1 [241]	1 [243]	0 [245]
Clearance (L/h)	38 ± 7.6 [259]	-	1.53 ± 0.255 [258]	-
Renal clearance (L/h)	-	-	3.19 ± 0.637 [258]	-
Clint2D6	-	-	-	25.2 [260]
Clint3A4	-	-	-	10.45 [260]
Cl_{app}	-	85 ±17 [241]	-	-

R – blood-to-plasma ratio, PSA – polar surface area, HBD – hydrogen bond donors, Clint2D6, 3A4 – intrinsic clearance (µl/min/mg of microsomal protein), Cl_{app} – apparent clearance (L/h), † predicted using correlation using molecular descriptors from Paixao et al. 2009 [189]

The pharmacokinetic curve of the clinical formulation was digitalised using an open source software – PlotDigitizer (v.2.6.8, Soundforge.net). The data obtained from this tool was exported into Simbiology (MATLAB v.2013b) and used as a reference to simulate the pharmacokinetics by varying the release rate. A range of release rates were simulated using the PBPK model. Plasma concentration of an average individual was correlated using digitalised clinical data points against PBPK predicted

data and release rate with the best coefficient of determination (R^2) was selected. The simulated pharmacokinetics obtained using the release rate with the highest R^2 was additionally compared against clinical data and the mean predicted pharmacokinetic parameters AUC, C_{max}, C_{trough} and C_{av} values deviated less than ± 100 % from the reported mean clinical values.

In vitro release rates obtained from experimental data for static and dynamic release experiments (reported in section 5.3) and derived release rate from clinical data obtained using PBPK models were correlated. A linear correlation was established from the experimental and PBPK data. The regression equation obtained from the correlation is reported in the results section (section 6.3).

6.3. Results

6.3.1. Quantification of release rate through PBPK modelling

Linear regression was performed for the pharmacokinetic curve of the clinical data points obtained from the literature against simulated data points by varying the release rates in the PBPK model. The rest of the physicochemical and drug specific parameters were kept constant in order to identify the optimal release rate. Various release rates and the regressions obtained for simulated pharmacokinetics against clinical data is shown in Figure 6.1. The optimal release rates with the best R^2 is shown in Table 6.2.

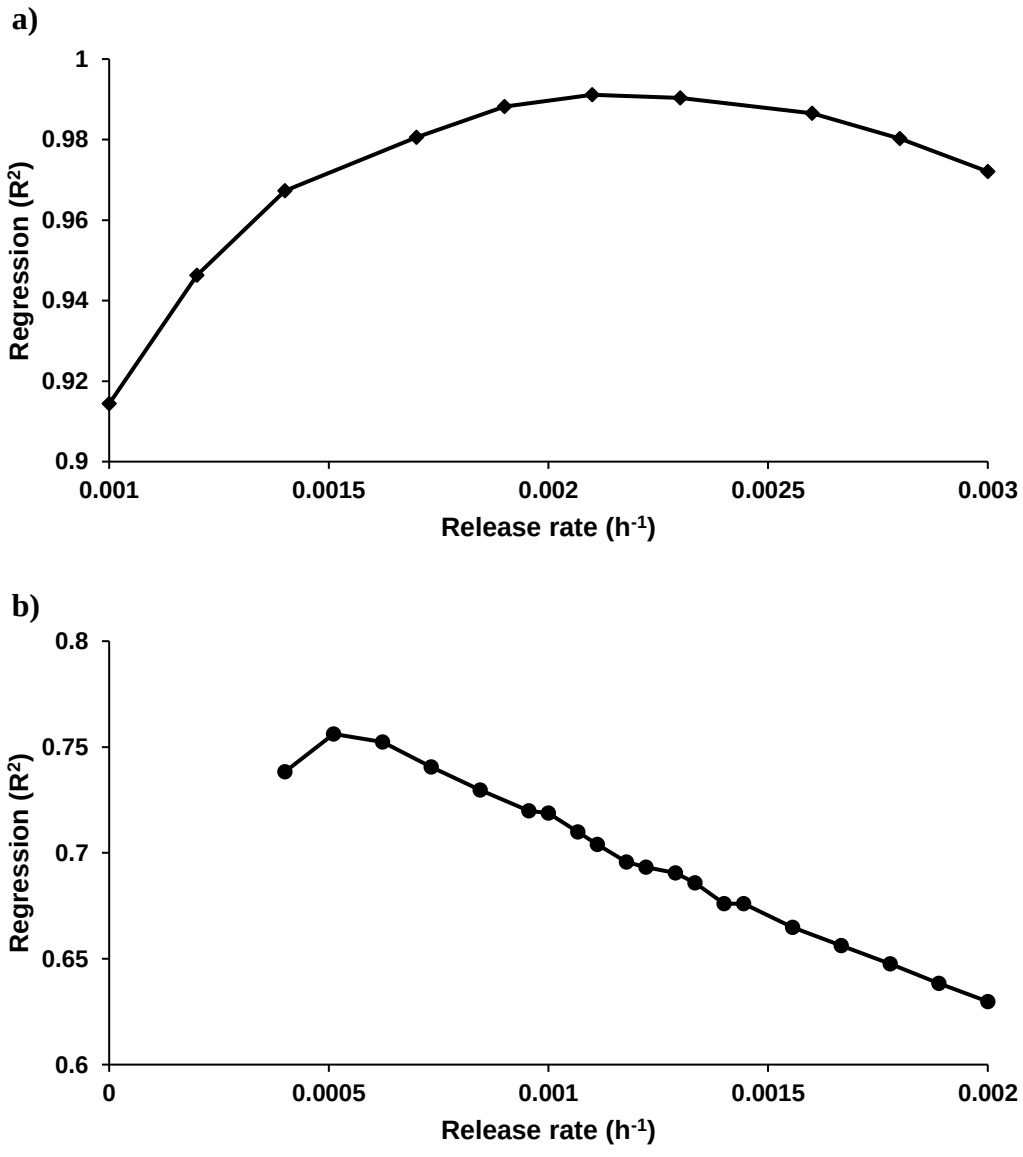

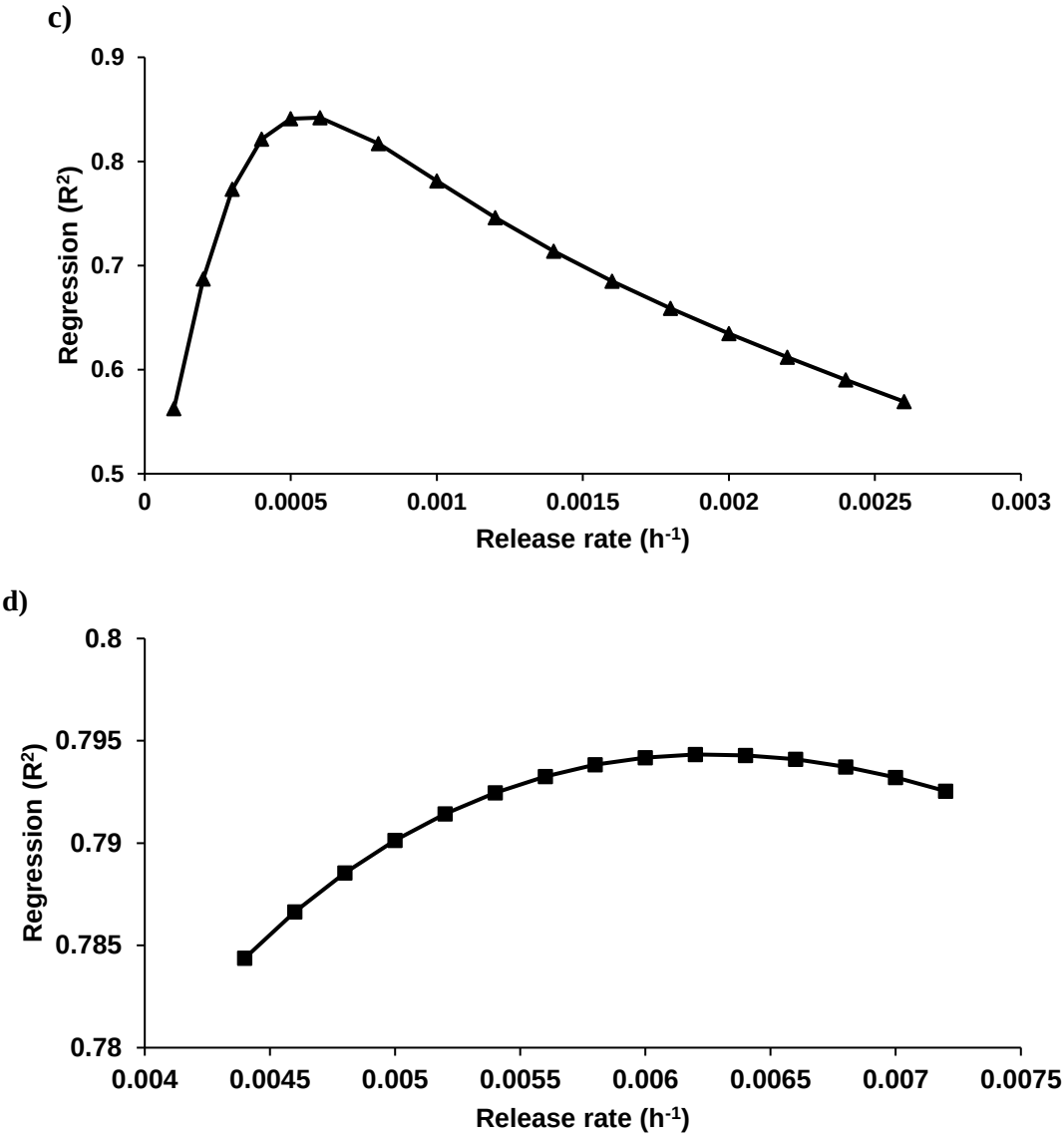

Figure 6.1 Release rate vs. regression value across various release rates for the four LAIs. a) Medroxyprogesterone acetate, b) olanzapine, c) paliperidone d) active moiety of risperidone

Table 6.2 Best coefficient of determination and the corresponding release rate for the four drugs

	PBPK release rate (h^{-1})	Correlation coefficient
Medroxyprogesterone	0.0021	0.9911
Olanzapine	0.00051	0.7561
Paliperidone	0.0006	0.8420
Risperidone	0.0062	0.7943

Pharmacokinetic validation of simulated data against clinical data for the four compounds is shown in Table 6.3a,b and the validation of predicted vs. clinical pharmacokinetic curve is shown in Figure 6.2. PBPK modelling of medroxyprogesterone returned an optimal release rate of 0.0021 h^{-1} for a single 150 mg IM dose administered for 12 weeks. The simulated C_{max} had a deviation of -10.8 % from the mean clinical value [254]. For olanzapine, a release rate of 0.00051 h^{-1} was observed for a 300 mg IM 4-weekly dose at steady state. PBPK simulated C_{max}, C_{av} and AUC had a deviation of -6.8 %, -1.4 % and +0.1 % respectively from the mean clinical value [255]. Paliperidone was validated against the 4th deltoid 100 mg IM injection where the simulated C_{max}, C_{av} and AUC deviated from the mean clinical value by -3.4 %, +2.4 % and +4.3 % [256]. The optimal release rate for paliperidone was observed to be 0.0006 h^{-1}. The third IM injection of 25 mg risperidone LAI was validated against the clinical data with an observed release rate of 0.0062 h^{-1}. The mean simulated C_{max}, C_{trough}, C_{av} and AUC were +66.5 %, -39.8 %, +30.4 % and +30.7 % from the mean clinical value.

a)

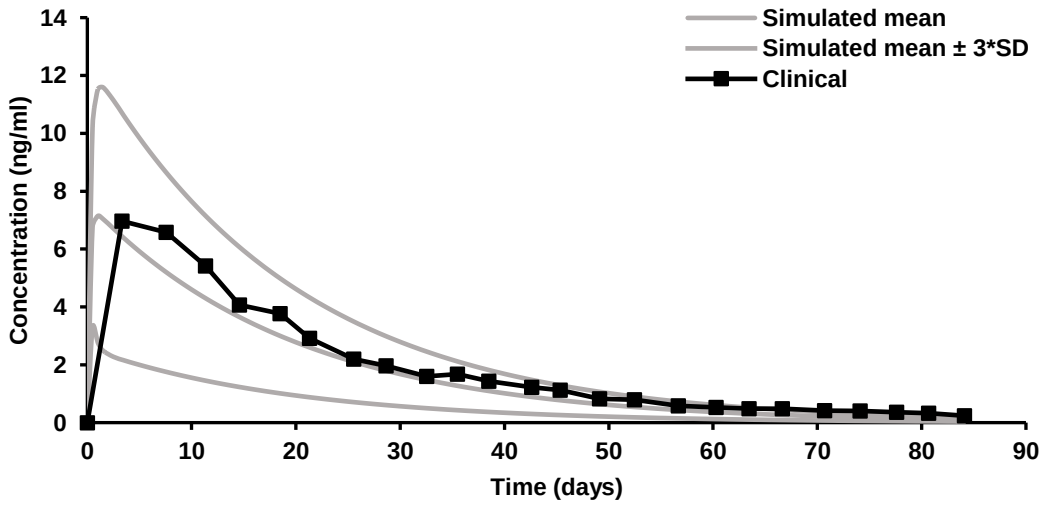

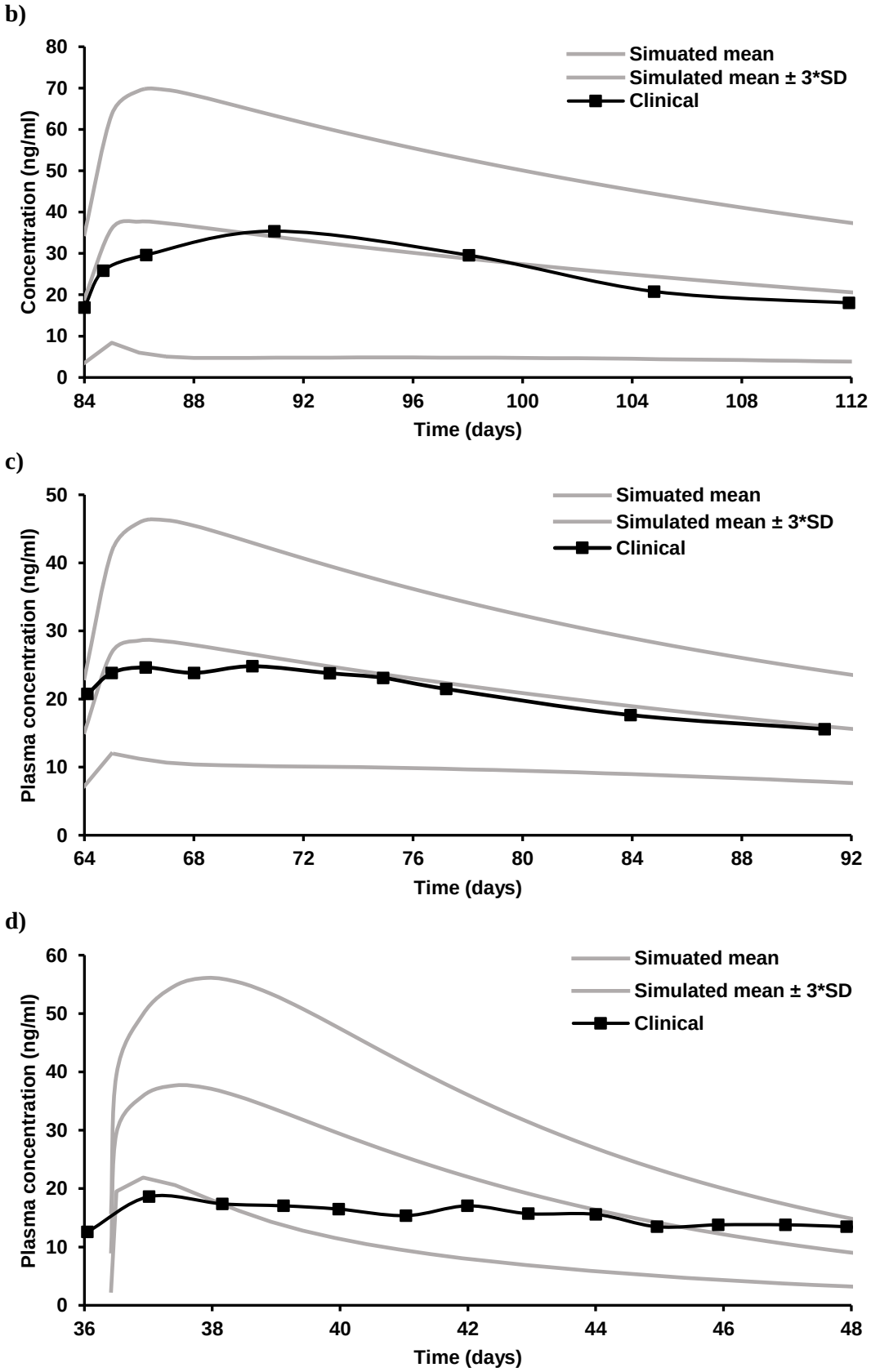

Figure 6.2 Comparison of simulated vs. clinical pharmacokinetic curve of a) medroxyprogesterone acetate, b) olanzapine, c) paliperidone and d) active moiety of risperidone

Table 6.3a Summary of simulated and clinical pharmacokinetics for commercially available LAI and the optimised release rates using the PBPK model

	Simulated				Clinical			
	C_{max}	**C_{trough}**	**AUC**	**C_{av}**	**C_{max}**	**C_{trough}**	**AUC**	**C_{av}**
Medroxyprogesterone	7.4 ± 1.6	0.11 ± 0.03	3661 ± 799	1.9 ± 0.4	8.3 ± 3.16 [254]	-	-	-
Olanzapine	36.9 ± 8.7	-	18914 ± 4251	27.7 ± 6.2	39.6 (45.2 %) [255]	-	18900 (44 %) [255]	28.1 (44 %) [255]
Paliperidone	28.4 ± 5.4	-	14704 ± 2474	21.6 ± 3.6	29.4 ± 14.4 [256]	-	14103 ± 5837 [256]	21.1 ± 8.8 [256]
Risperidone	37.8 ± 5.9	6.8 ± 1.5	6932 ± 1313	20.6 ± 3.9	22.7 ± 9.2 [257]	11.3 ± 4.5 [257]	5303 [257]	15.8 [257]

C_{max} - maximum plasma concentration expressed in ng/ml, C_{trough} – trough plasma concentration expressed in ng/ml, C_{av} – average plasma concentration in ng/ml, AUC – area under the curve expressed in ng x h/ml

Table 6.3b The percentage difference between the simulated and clinical pharmacokinetics

	% difference - simulated vs. clinical			
	C_{max}	C_{trough}	AUC	C_{av}
Medroxyprogesterone	-10.8	-	-	-
Olanzapine	-6.8	-	-52.8	-1.4
Paliperidone	-3.4	-	-66.6	2.4
Risperidone	66.5	-39.8	30.7	30.4

A summary of release rates obtained from *in vitro* experiments and optimised release rates using PBPK models is shown in Table 6.4. From Table 6.5 it can be observed that the ratio of static and dynamic release rates for all the four formulations was <0.2 indicating a higher release of drug in dynamic system which utilizes higher volume of media (6 ml vs 720 ml). However, the comparison of *in vitro* and PBPK release rates indicate a closer similarity to the static release than dynamic release with three data points having similar ratio in static compared to two with dynamic release experiments implying that there is a higher correlation with static release experimental method in identifying the PBPK release rate.

Table 6.4 Release rates (expressed as h^{-1}) obtained from *in vitro* and *in silico* methods

	Static release	Dynamic release	PBPK simulated
Medroxyprogesterone	0.0010	0.0177	0.0021
Olanzapine	0.0298	0.7100	0.00051
Paliperidone	0.0002	0.7670	0.0006
Risperidone	0.0035	0.0179	0.0062

Table 6.5 Comparison across *in vitro* and simulated release rates

	Static/Dynamic	Static/PBPK	Dynamic/PBPK
Medroxyprogesterone	0.05650	0.48	8.43
Olanzapine	0.04197	58.32	1389.43
Paliperidone	0.00026	0.33	1278.33
Risperidone	0.05650	0.56	2.89

6.3.2. IVIVE

IVIVE between static release experimental and simulated release rates is shown in Figure 6.3. The coefficient of determination obtained from the best fit line is 0.14 which is an unreliable correlation between *in vitro* and *in silico* release rate. A negative correlation between *in vitro* and PBPK release rate does not inform the correlation correctly. However, if the significant outlier ($P < 0.05$) value of olanzapine is removed, an agreeable correlation ($R^2 = 0.9993$), where the PBPK release rate is directly proportional to *in vitro* release rate was observed. The regression equation obtained from the correlation of *in vitro* and *in silico* release rate is as follows:

$$y = 1.6834x + 0.0003 \qquad (1)$$

where x is *in vitro* release rate and y is simulated release rate in h^{-1}.

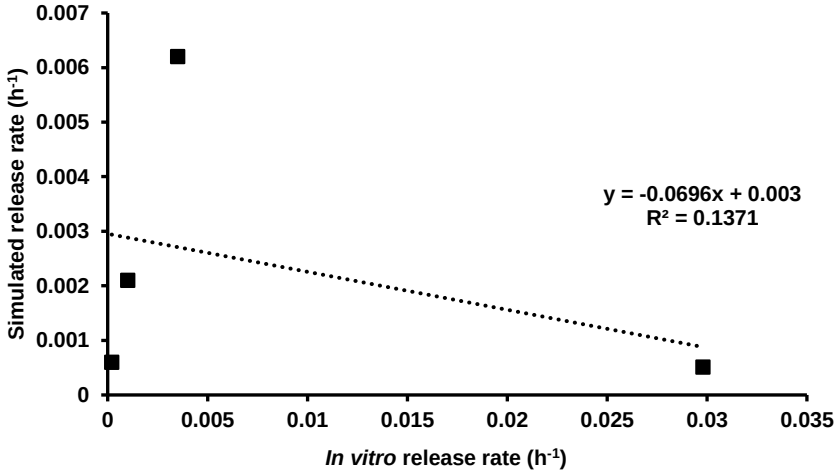

Figure 6.3 Correlation between *in vitro* static release experiments and *in silico* release from PBPK model

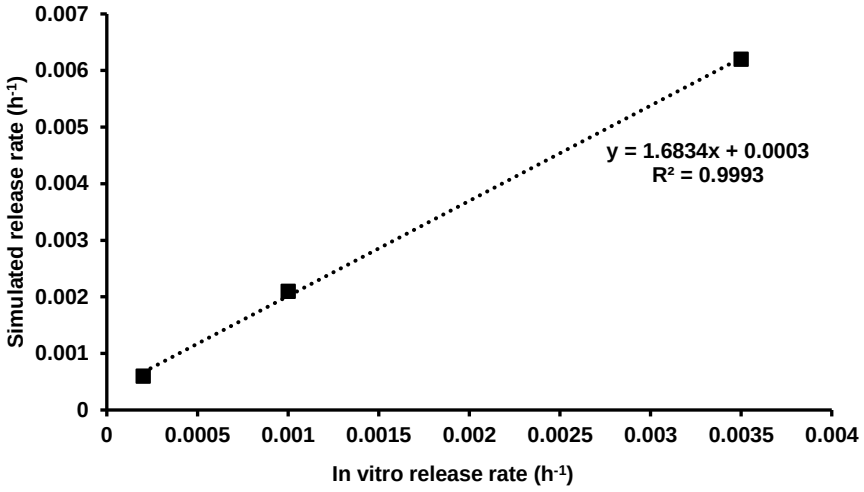

Figure 6.4 IVIVE of *in vitro* and *in silico* release rate with the exclusion of olanzapine

The correlation obtained using dynamic release experiments and *in silico* models has a regression value of 0.6024. The equation for IVIVE is as follows:

$$y = -0.005x + 0.0042 \qquad (2)$$

where x is the *in vitro* release rate and y is the *in silico* release rate

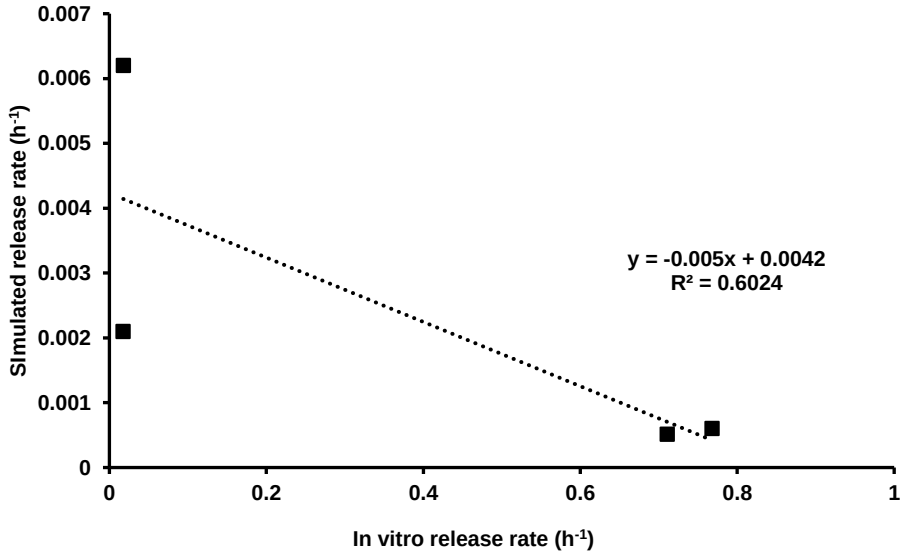

Figure 6.5 Correlation between *in vitro* dynamic release experiments and *in silico* release from PBPK model

The negative correlation indicates that the PBPK release rate or the *in vivo* human release rate decreases as the *in vitro* release rate increases. Theoretically, the *in vitro* and *in vivo* release rates are directly proportional since the *in vitro* experiments mimic the *in vivo* environment. This implies that the obtained correlation from dynamic release experiments contradicts the relation between *in vitro* and *in vivo* experiments. Hence the dynamic release experiments are inconclusive at this stage due to limited number of data points.

6.4. Discussion

IVIVE application of LAI formulations may accelerate the development of future drug formulations, supporting the extrapolation of *in vitro* data to predict *in vivo* results. IVIVE could help predict drug pharmacokinetics of various novel formulations in minimal time and assist in identifying the best LAI formulation through PBPK modelling. The current chapter focused on informing the mathematical correlation between *in vitro* and *in silico* release rates obtained using four commercially available formulations.

In this study, drug diffusion from the formulation into blood plasma was assumed to obey first-order kinetics. From Figure 6.2 and Table 6.3 it can be observed that PBPK simulated pharmacokinetic curve was similar to clinical curve and the pharmacokinetic parameters were ± 100 % from mean reported clinical values. The simulated C_{max} of risperidone active moiety was higher compared to the clinical curve, however the pharmacokinetic parameters were < ±100% from the clinical value, hence the model was assumed to have higher predictive value.

Comparison of static and dynamic release rates (Table 6.5) indicate that release rate across different methods is comparable (ratio > 0.04) for microformulations. Horizontal agitation of the static dialysis system could have led to sedimentation of formulation in the donor compartment restricting the total surface area in contact with media leading to slower release rate.

Static-to-PBPK release rate ratio is closer to one for three formulations except for olanzapine (Table 6.5). This phenomenon could be explained due to higher water solubility of olanzapine formulation compared to others. Water solubility is a key parameter in drug release for LAI. Solubility enhancers would be necessary for low

soluble compounds to achieve an increase in drug release and more stable micro- or nanoparticles are required to restrict drug release for highly soluble compounds. Restricted release was observed with paliperidone nanoformulation due to its smaller particle size and lower protein binding. Although physical parameters affect drug release widely across *in vitro* experiments, appropriate conditions are met *in vivo* to achieve necessary plasma concentrations.

Higher release rate (ratio >1) was obtained for all the formulations during dynamic release experiments compared to *in silico* release rate which could be explained due to the large amount of media used and greater extent of agitation during media circulation (Table 6.5). Higher surface area of nanoparticles could trigger greater drug release observed with the paliperidone formulation.

Exclusion of olanzapine led to a better regression and a positive correlation. This however reduces the number of formulations used for IVIVE to three (Figure 6.4). Dynamic release experiments returned a negative correlation which is counterintuitive. Various factors such as particle size, protein binding, drug solubility, surface area in contact, agitation, volume of media led to a wide variation in release rates. Particle size and total surface area of particles in contact are two interdependent parameters. Larger particle size leads to greater release for porous particles but as the particles become smaller the total surface area increases which further improves the overall drug release. Presence of proteins in the media favours drug release which could be observed from Table 5.3. Lack of agitation leads to accumulation of the formulation thus decreasing the overall surface area in contact with the media. Higher volume of media avoids saturation thereby favouring drug release from the formula-

tion (Table 5.3). The effect of these factors could be studied in detail with more number of formulations to obtain a better understanding of the relation between *in vitro* and *in vivo* release rate.

The evaluation of a small number of formulations could lead to inaccurate correlation thus giving biased IVIVE values for novel formulations. In other studies, large numbers of drugs have been evaluated to obtain a reliable IVIVE. For example, 25 CYP3A molecules were used to predict the intestinal first pass metabolism [57] and 29 drugs were used to predict the systemic clearance [261]. Since the number of clinically used water based LAI micro- and nanoformulations is very limited, future research will be essential to have a more comprehensive evaluation of this IVIVE approach. However, the presented data provides a platform into which other future agents can be included, as they are developed.

CHAPTER 7

General Discussion

HAART has improved life expectancy of HIV+ patients. However current therapeutic strategies do not eradicate the virus from the human body due to a variety of reasons - targeting CD4 T-cells that regulate immunity, existing therapies failing to eliminate HIV provirus, poor drug penetration in sanctuary sites and unexplored questions lying in the human genome to confront human endogenous retroviruses (HERVs) [50, 262]. Consequently, HIV patients are expected to continue HAART indefinitely and these regimens are currently administered as oral formulations, based on a daily dosage of multiple ARVs. Several ARVs have poor oral bioavailability, which results in a substantial portion of the dose unable to reach target sites that lead to increase in total daily drug intake to achieve therapeutic exposure thereby increase the total cost for therapy [73, 263]. Additionally, pill fatigue following chronic administration of oral formulations can result in suboptimal adherence, increasing the chance of developing resistance against prescribed therapy. Suboptimal adherence can not only lead to failure in treatment but also low protection rates in the case of PrEP. Reduced frequency of drug administration by prolonging treatment duration could help improve adherence. Recently LA formulations have been developed to support APIs extend the period of therapy through injectable SC or IM depot, thus effectively addressing the problem of oral suboptimal adherence. The IM or SC administration bypass the intestinal barrier and hepatic first-pass metabolism thus improving bioavailability, reducing the total dose and overall cost of therapy to achieve therapeutic exposures [88].

Currently, evaluation of IM formulations is directly performed *in vivo* in animals, since a validated experimental *in vitro* system has not been developed to characterise drug release pattern for LA formulations [86, 264]. A key challenge in the development of this type of experimental test is the evaluation of the predictive value for *in*

vivo pharmacokinetics. *In vitro* systems to predict pharmacokinetics of novel LA formulations represent an essential tool to inform the formulation's rational design with optimal exposure. The application of these experimental methods could reduce the cost and time of screening for large library of candidate formulations. The overall aim of this thesis was to develop experimental and computational methods to support the design of LA nanoformulations. A whole-body PBPK model has been applied to identify theoretical optimal doses and release rates of novel formulations in adults and paediatrics and experimental *in vitro* systems to characterise the formulation release rate were developed to extrapolate the pharmacokinetics in humans.

PBPK modelling as described in Chapter 1 is a predictive computational tool that assists in evaluating the pharmacokinetics through integration of physicochemical and ADME properties. Whole-body PBPK models integrate equations that describe anatomy and physiology of organisms (*i.e.* rat, mouse and human) and pharmacokinetic processes such as absorption, distribution, metabolism and elimination to simulate drug accumulation across various tissues and organs in the body.

An adult PBPK model was developed using Simbiology, a product of MATLAB. Version 2013b of the tool was used for designing the model due to its ease of use with the interactive user interface and low number of encountered errors during its operation. The PBPK model was constructed using various anthropometric equations available from literature describing weights and volumes of organs, blood flow-rates, drug distribution kinetics across tissues etc., described earlier in Chapter 2. The PBPK model was rigorously tested and anatomical and physiological values were cross checked with literature data before using it to determine drug pharmacokinetics. The PBPK model was further extended to include anatomy and physiology of children and adolescents. Since the growth pattern varies widely during development of paediatric

individuals, validation was performed at different age groups to ensure confidence in the generated virtual individuals (Chapter 3).

The majority of dose finding studies are conducted in healthy volunteers and often exposure in patients or individuals with specific physiological characteristics can vary significantly. Use of a whole-body PBPK model could assist the prediction of pharmacokinetics in subpopulations of patients or individuals who are not commonly included in clinical studies. Anatomical and physiological characteristics can vary widely across individuals, therefore a comprehensive description of correlation between anthropometric and anatomical factors have been included in the models, to provide a realistic anatomical description of the virtual patient. To further capture the potential predictability in patient populations, variability was added from the literature to each equation describing correlation between factors.

The developed PBPK models were validated against their oral counterparts and if available against IM formulations as well, prior to the prediction of optimal dose and release rates. Earlier published papers used a 2-fold range from the clinical mean as the acceptable validation range [152]. In the present study, a stringent validation range of 0.5-fold was used to improve the accuracy of predictions.

Currently, over 25 ARV drugs are marketed for HIV treatment but only a preferred few are used due to their advantages in effectively restricting the viral replications and mutations in infected individuals. To inform the design of LA nanoformulations for a weekly or a monthly administration, eight commonly used ARVs were selected. PBPK models were developed and validated against existing available clinical data for oral formulations in adult population for the chosen ARVs. To inform the first-order release rate kinetics of the nanoformulation, an additional IM compartment was

introduced in the PBPK model. Doses and release rates were optimised in Chapter 2 according to the mentioned cut-off values.

Ethical concerns hinder the dose optimisation studies in children and adolescents. Majority of doses are scaled down from adults and since evidence shows that anatomy and physiology of children varies widely from adults. Anthropometric equations were validated in Chapter 3 for various anatomical and physiological parameters by age to accommodate the age related changes in children and adolescents. WHO recommends use of different doses for children and adolescents across weight groups. To predict the optimal doses for different weight categories of paediatric individuals, in Chapter 4, validated PBPK models were used for existing adult LAI formulations of cabotegravir and rilpivirine.

The constructed PBPK models for adults and children could be used as a platform to evaluate the pharmacokinetics of new chemical entities. Using the provided data in this thesis, long-acting potential of ARVs was informed that could be used to inform appropriate design of formulations for their respective route of administration. The simulated data using the PBPK model could act as a reference for clinical studies of long-acting formulations in adults and children. Drugs such as tenofovir alafenamide, etravirine, rilpivirine are not prescribed in children less than 6 years [265]. The designed paediatric PBPK model could be applied to ARVs not evaluated in younger children yet, to inform appropriate doses of existing oral formulations.

Improved reliability on *in vitro* data ensures less dependency on clinical data to predict drug pharmacokinetics in humans for novel formulations. Preliminary screening of a formulation library during drug discovery and formulation phase could speed up the optimisation process. Three i*n vitro* experiments were conducted using four

different clinical LAI formulations. Appropriate release rates were identified for the four formulations in Chapter 5. PBPK models for the four formulations were developed and the optimal release rate were identified in Chapter 6. Mathematical expressions to compute IVIVE from the *in vitro* experiments and PBPK simulations were also described.

Although the reported PBPK models could inform the pharmacokinetics of the desired therapeutic agents, it has its disadvantages. The models are only as good as the data that is plugged in. They completely rely on the credibility of the *in vitro* data and one of the problems is the use of different *in vitro* methods to compute the same parameter. For example, caco-2 permeability could be evaluated using radioactive and non-radioactive methods [57, 266]. Also different experimental methods use different transepithelial electrical resistance (TEER) values to check the integrity of the monolayers [74, 266]. The effective permeability scaled from caco-2 permeability values was derived using just one type of experimental method. Using the same allometric equations for data derived from different experimental methods could reduce the reliability of the *in vitro* data. This necessitates the standardisation of methods that could generate reliable *in vitro* data by following the same experimental setup universally. Till date, transporter data could not be scaled up due to the poor understanding of the factors involved in the process [267]. Various processes such as metabolism, absorption and transporter activity occurring simultaneously complicates the independent understanding of each of these processes to derive correlations and are yet to be optimised [268, 269].

Limitations reported during dose optimisation studies using the PBPK model could be addressed in future studies. Transporter data refines the PBPK model by informing key processes involved in intestinal absorption, drug distribution across

tissues, clearance and elimination patterns. Introduction of lymphatic system in the PBPK model could improve the predictions of lipophilic drugs which inform kinetics between various lymphatic nodes and blood circulation system. Although drug distribution in various tissues is not of a particular interest in monitoring HIV virus, mathematical description of organ and tissue physiology could shed a light on penetration ability and pharmacodynamics of drugs that require targeted treatment. The experimental methods could not identify the independent effect of each of the drug physicochemical characteristics and various other parameters across release experiments. Further studies to identify the influence of each of these parameters on drug release could help derive a reliable mathematical correlation between *in vitro* and PBPK release rate.

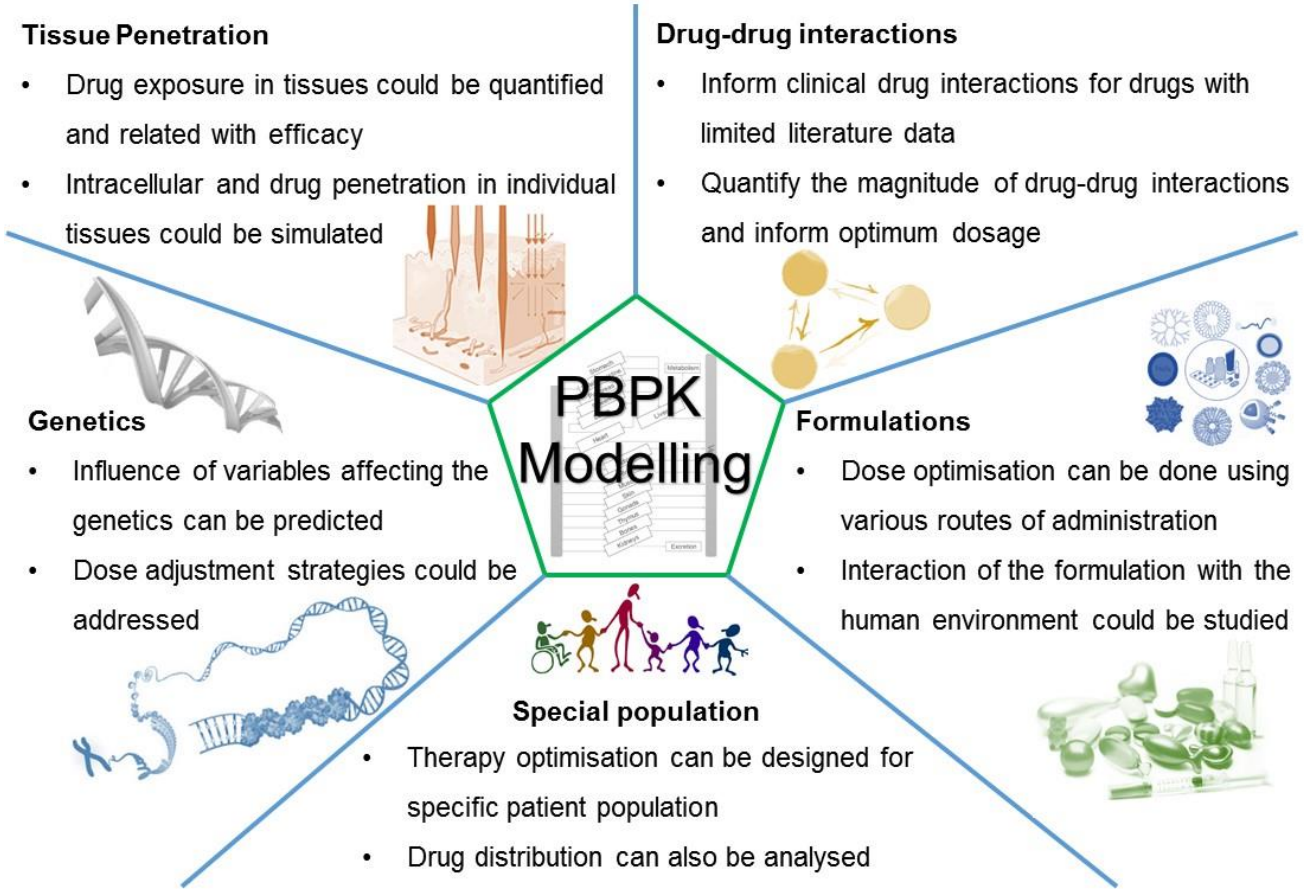

Figure 7.1 Summary of the various applications of a physiologically based pharmacokinetic model [111]

Optimisation of dose and release rates of novel formulations is only one of the many applications of PBPK modelling (Figure 7.1). In this thesis, dose evaluation was informed for healthy adult and paediatric individuals, however special populations such as elderly, pregnant women, organ impairments could also be evaluated through PBPK models. For example, drugs such as alfentanil, lidocaine, theophylline and levetiracetam were evaluated in different classes of liver cirrhosis patients [216]. Another study evaluated the disposition of midazolam in adults, elderly patients and compared against clinical data [270]. Genetic variation among individuals is normal and may contribute to the change in drug pharmacokinetics which has been evaluated in patients administered with efavirenz having low, medium and high systemic drug clearance depending on 516 GG, GT and TT polymorphisms [249]. Drug penetration in tissues is one of the most complicated tasks to analyse in humans. Identification of drug distribution across different organs and tissues could be evaluated using PBPK models to further improve the understanding of ADME processes. Curley et al. informed efavirenz drug penetration in CNS tissues using a PBPK model and validated against clinical data from rodents and humans [271]. Penetration of levofloxacin was identified and compared with *in vivo* rat data in various tissues such as heart, liver, kidney and spleen. Models were extrapolated using rat data to inform the pharmacokinetics and tissue distribution in humans [272]. Opportunistic infections such as tuberculosis, hepatitis reportedly infect HIV+ patients due to their weak immune system. Infected patients administer multiple dosing regimens to suppress these infections. Drug interactions might occur during administration of multiple regimens due to the same metabolising enzyme involved in drug metabolic clearance. PBPK models could compute the effect and extent of drug-drug interactions (DDIs) on plasma pharmacokinetics and assist in dose adjustments accordingly. DDIs between efavirenz,

CYP inducers and inhibitors such as montelukast, paclitaxel, pioglitazone and repaglinide were evaluated and appropriate dosing adjustments were recommended [273]. Extent of interaction between efavirenz and various antidepressants was reported in another study [114]. Numerous applications of a PBPK model could make it an innovative pharmacological tool to predict and inform pharmacokinetics in individuals potentially simplifying ART.

In summary, a PBPK model was developed both for adults and paediatric patients to inform the dose and release rate of LAI nanoformulations. Novel experimental methods were developed to inform the *in vitro* release rate of LA formulations. The developed i*n vitro* and *in silico* models could assist in informing the pharmacokinetics of novel formulations thus improving the problem of suboptimal adherence and reducing time in dose optimisation and cost of therapy.

Bibliography

1. Gallo, R.C. and L. Montagnier, *The Discovery of HIV as the Cause of AIDS.* New England Journal of Medicine, 2003. **349**(24): p. 2283-2285.
2. Faria, N.R., et al., *The early spread and epidemic ignition of HIV-1 in human populations.* Science, 2014. **346**(6205): p. 56-61.
3. UNAIDS, *How AIDS changed everything — MDG6: 15 years, 15 lessons of hope from the AIDS response.* 2015.
4. UNAIDS, *Facts about UNAIDS : an overview*. 1996.
5. Sharp, P.M. and B.H. Hahn, *Origins of HIV and the AIDS Pandemic.* Cold Spring Harbor Perspectives in Medicine:, 2011. **1**(1): p. a006841.
6. Desrosiers, R.C., *Prospects for an AIDS vaccine.* Nat Med, 2004. **10**(3): p. 221-223.
7. Pubmed. 2016 [cited 2016 20/01/2016]; Available from: http://www.ncbi.nlm.nih.gov/pubmed.
8. Jardine, J.G., et al., *Priming a broadly neutralizing antibody response to HIV-1 using a germline-targeting immunogen.* Science, 2015. **349**(6244): p. 156-161.
9. Sanders, R.W., et al., *HIV-1 neutralizing antibodies induced by native-like envelope trimers.* Science, 2015. **349**(6244).
10. Cohen, J., *AIDS pioneer finally brings AIDS vaccine to clinic.* Science, 2015.
11. Engelman, A. and P. Cherepanov, *The structural biology of HIV-1: mechanistic and therapeutic insights.* Nat Rev Micro, 2012. **10**(4): p. 279-290.
12. Walker, B.D. and X.G. Yu, *Unravelling the mechanisms of durable control of HIV-1.* Nat Rev Immunol, 2013. **13**(7): p. 487-498.
13. Wilen, C.B., J.C. Tilton, and R.W. Doms, *HIV: Cell Binding and Entry.* Cold Spring Harbor Perspectives in Medicine, 2012. **2**(8).
14. Bukrinsky, M.I., *HIV Life Cycle and Inherited Co-Receptors*, in *eLS*. 2001, John Wiley & Sons, Ltd.
15. Al-Jabri, A.A., *How does HIV-1 infect a susceptible human cell?: Current thinking.* Journal for scientific research. Medical sciences / Sultan Qaboos University, 2003. **5**(1-2): p. 31-44.
16. Gelderblom, H.R., M. Özel, and G. Pauli, *Morphogenesis and morphology of HIV structure-function relations.* Archives of Virology, 1989. **106**(1-2): p. 1-13.
17. Goff, S.P., *Host factors exploited by retroviruses.* Nat Rev Micro, 2007. **5**(4): p. 253-263.
18. Hu, W.-S. and S.H. Hughes, *HIV-1 Reverse Transcription.* Cold Spring Harbor Perspectives in Medicine, 2012. **2**(10): p. a006882.

19. Jayappa, K.D., Z. Ao, and X. Yao, *The HIV-1 passage from cytoplasm to nucleus: the process involving a complex exchange between the components of HIV-1 and cellular machinery to access nucleus and successful integration.* International Journal of Biochemistry and Molecular Biology, 2012. **3**(1): p. 70-85.
20. Hindmarsh, P. and J. Leis, *Retroviral DNA Integration.* Microbiology and Molecular Biology Reviews, 1999. **63**(4): p. 836-843.
21. Erb, P., et al., *Effect of antiretroviral therapy on viral load, CD4 cell count, and progression to acquired immunodeficiency syndrome in a community human immunodeficiency virus–infected cohort.* Archives of Internal Medicine, 2000. **160**(8): p. 1134-1140.
22. May, M.T., et al., *Impact on life expectancy of HIV-1 positive individuals of CD4(+) cell count and viral load response to antiretroviral therapy.* Aids, 2014. **28**(8): p. 1193-1202.
23. Briz, V., E. Poveda, and V. Soriano, *HIV entry inhibitors: mechanisms of action and resistance pathways.* Journal of Antimicrobial Chemotherapy, 2006. **57**(4): p. 619-627.
24. Moore, J.P. and R.W. Doms, *The entry of entry inhibitors: A fusion of science and medicine.* Proceedings of the National Academy of Sciences, 2003. **100**(19): p. 10598-10602.
25. Lieberman-Blum, S.S., H.B. Fung, and J.C. Bandres, *Maraviroc: A CCR5-receptor antagonist for the treatment of HIV-1 infection.* Clinical Therapeutics, 2008. **30**(7): p. 1228-1250.
26. Hardy, H. and P.R. Skolnik, *Enfuvirtide, a New Fusion Inhibitor for Therapy of Human Immunodeficiency Virus Infection.* Pharmacotherapy: The Journal of Human Pharmacology and Drug Therapy, 2004. **24**(2): p. 198-211.
27. Arts, E.J. and D.J. Hazuda, *HIV-1 Antiretroviral Drug Therapy.* Cold Spring Harbor Perspectives in Medicine, 2012. **2**(4): p. a007161.
28. Bazzoli, C., et al., *Intracellular Pharmacokinetics of Antiretroviral Drugs in HIV-Infected Patients, and their Correlation with Drug Action.* Clinical Pharmacokinetics, 2012. **49**(1): p. 17-45.
29. AIDSInfo. *FDA-Approved HIV Medicines*. 2016 20/01/2016]; Available from: https://aidsinfo.nih.gov/education-materials/fact-sheets/21/58/fda-approved-hiv-medicines.
30. Merluzzi, V.J., et al., *Inhibition of HIV-1 replication by a nonnucleoside reverse-transcriptase inhibitor.* Science, 1990. **250**(4986): p. 1411-1413.
31. Spence, R.A., et al., *Mechanism of inhibition of HIV-1 reverse-transcriptase by nonnucleoside inhibitors.* Science, 1995. **267**(5200): p. 988-993.

32. Feng, M., et al., *In Vitro Resistance Selection with Doravirine (MK-1439), a Novel Nonnucleoside Reverse Transcriptase Inhibitor with Distinct Mutation Development Pathways.* Antimicrobial Agents and Chemotherapy, 2015. **59**(1): p. 590-598.
33. Sluis-Cremer, N. and G. Tachedjian, *Mechanisms of inhibition of HIV replication by non-nucleoside reverse transcriptase inhibitors.* Virus Research, 2008. **134**(1–2): p. 147-156.
34. Richman, D.D., *HIV chemotherapy.* Nature, 2001. **410**(6831): p. 995-1001.
35. Cattaneo, D., et al., *Comparison of the In Vivo Pharmacokinetics and In Vitro Dissolution of Raltegravir in HIV Patients Receiving the Drug by Swallowing or by Chewing.* Antimicrobial Agents and Chemotherapy, 2012. **56**(12): p. 6132-6136.
36. Spreen, W., et al., *Pharmacokinetics, Safety, and Tolerability With Repeat Doses of GSK1265744 and Rilpivirine (TMC278) Long-Acting Nanosuspensions in Healthy Adults.* Jaids-Journal of Acquired Immune Deficiency Syndromes, 2014. **67**(5): p. 487-492.
37. Basavapathruni, A. and K.S. Anderson, *Reverse transcription of the HIV-1 pandemic.* Faseb Journal, 2007. **21**(14): p. 3795-3808.
38. Brechtl, J.R., et al., *The Use of Highly Active Antiretroviral Therapy (HAART) in Patients With Advanced HIV Infection.* Journal of Pain and Symptom Management. **21**(1): p. 41-51.
39. FDA, U.S. *FDA approves first drug for reducing the risk of sexually acquired HIV infection*. 2012; Available from: http://www.fda.gov/NewsEvents/Newsroom/PressAnnouncements/ucm312210.htm.
40. CDC. *Pre-Exposure Prophylaxis (PrEP)*. 2016 26/04/2016]; Available from: http://www.cdc.gov/hiv/risk/prep/index.html.
41. Abraham, B.K. and R. Gulick, *Next generation oral PrEP: Beyond tenofovir.* Current opinion in HIV and AIDS, 2012. **7**(6): p. 600-606.
42. Dolgin, E., *Long-acting HIV drugs advanced to overcome adherence challenge.* Nat Med, 2014. **20**(4): p. 323-324.
43. Alshammari, T.M., et al., *Comparison of different serum sample extraction methods and their suitability for mass spectrometry analysis.* Saudi Pharmaceutical Journal : SPJ, 2015. **23**(6): p. 689-697.
44. Pradeep K Vuppala, Dileep R Janagam, and P. Balabathula, *Importance of ADME and Bioanalysis in the Drug Discovery.* J Bioequiv Availab, 2013. **5**(4): p. e31.
45. Chiou, W.L., *The Rate and Extent of Oral Bioavailability versus the Rate and Extent of Oral Absorption: Clarification and Recommendation of Terminology.* Journal of Pharmacokinetics and Pharmacodynamics. **28**(1): p. 3-6.

46. Gerber, J.G., *Using Pharmacokinetics to Optimize Antiretroviral Drug-Drug Interactions in the Treatment of Human Immunodeficiency Virus Infection.* Clinical Infectious Diseases, 2000. **30**(Supplement 2): p. S123-S129.
47. Baheti, G., et al., *Plasma and Intracellular Population Pharmacokinetic Analysis of Tenofovir in HIV-1-Infected Patients.* Antimicrob. Agents Chemother., 2011. **55**(11): p. 5294-5299.
48. Wang, L.H., et al., *Pharmacokinetic and pharmacodynamic characteristics of emtricitabine support its once daily dosing for the treatment of HIV infection.* AIDS Res. Hum. Retroviruses, 2004. **20**(11): p. 1173-1182.
49. Duwal, S., C. Schütte, and M. von Kleist, *Pharmacokinetics and Pharmacodynamics of the Reverse Transcriptase Inhibitor Tenofovir and Prophylactic Efficacy against HIV-1 Infection.* PLoS ONE, 2012. **7**(7): p. e40382.
50. Siccardi, M., et al., *Physiologically based pharmacokinetic models for the optimization of antiretroviral therapy: recent progress and future perspective.* Future Virol. , 2013. **8**(9): p. 871-890.
51. Fletcher, C.V., et al., *Persistent HIV-1 replication is associated with lower antiretroviral drug concentrations in lymphatic tissues.* Proceedings of the National Academy of Sciences, 2014. **111**(6): p. 2307-2312.
52. Alomar, M.J., *Factors affecting the development of adverse drug reactions (Review article).* Saudi Pharmaceutical Journal : SPJ, 2014. **22**(2): p. 83-94.
53. Bangsberg, D.R., *Preventing HIV Antiretroviral Resistance through Better Monitoring of Treatment Adherence.* The Journal of Infectious Diseases, 2008. **197**(Supplement_3): p. S272-S278.
54. Moss, D.M., et al., *Predicting intestinal absorption of raltegravir using a population-based ADME simulation.* J Antimicrob Chemother, 2013. **68**: p. 1627-34.
55. Vermeir, M., et al., *Absorption, Metabolism, and Excretion of Darunavir, a New Protease Inhibitor, Administered Alone and with Low-Dose Ritonavir in Healthy Subjects.* Drug Metabolism and Disposition, 2009. **37**(4): p. 809-820.
56. Khojasteh, S., H. Wong, and C.C.A. Hop, *ADME Properties and Their Dependence on Physicochemical Properties,* in *Drug Metabolism and Pharmacokinetics Quick Guide*. 2011, Springer New York. p. 165-181.
57. Gertz, M., et al., *Prediction of Human Intestinal First-Pass Metabolism of 25 CYP3A Substrates from In Vitro Clearance and Permeability Data.* Drug Metab. Dispos., 2010. **38**(7): p. 1147-1158.
58. Laufer, R., et al., *Quantitative Prediction of Human Clearance Guiding the Development of Raltegravir (MK-0518, Isentress) and Related HIV Integrase Inhibitors.* Drug Metabolism and Disposition, 2009. **37**(4): p. 873-883.

59. Hay, M., et al., *Clinical development success rates for investigational drugs.* Nat Biotech, 2014. **32**(1): p. 40-51.
60. Shchukina, E.M. and D.G. Shchukin, *LbL coated microcapsules for delivering lipid-based drugs.* Advanced Drug Delivery Reviews, 2011. **63**(9): p. 837-846.
61. York, P., *Chemical Aspects of Drug Delivery Systems*, in *New Materials and Systems for Drug Delivery and Targeting*. 2007.
62. Lipinski, C.A., *Drug-like properties and the causes of poor solubility and poor permeability*. Journal of Pharmacological and Toxicological Methods, 2000. **44**(1): p. 235-249.
63. Parveen, S., R. Misra, and S.K. Sahoo, *Nanoparticles: a boon to drug delivery, therapeutics, diagnostics and imaging.* Nanomedicine: Nanotechnology, Biology and Medicine. **8**(2): p. 147-166.
64. Koo, O.M., I. Rubinstein, and H. Onyuksel, *Role of nanotechnology in targeted drug delivery and imaging: a concise review.* Nanomedicine: Nanotechnology, Biology and Medicine, 2005. **1**(3): p. 193-212.
65. Khadka, P., et al., *Pharmaceutical particle technologies: An approach to improve drug solubility, dissolution and bioavailability.* Asian Journal of Pharmaceutical Sciences, 2014. **9**(6): p. 304-316.
66. Zetner, D., L.P.H. Andersen, and J. Rosenberg, *Pharmacokinetics of Alternative Administration Routes of Melatonin: A Systematic Review.* Drug Res (Stuttg), 2016. **66**(04): p. 169-173.
67. Kaminsky, B.M., J.R. Bostwick, and S.K. Guthrie, *Alternate Routes of Administration of Antidepressant and Antipsychotic Medications.* Annals of Pharmacotherapy, 2015. **49**(7): p. 808-817.
68. Tiwari, G., et al., *Drug delivery systems: An updated review.* International Journal of Pharmaceutical Investigation, 2012. **2**(1): p. 2-11.
69. Lee, W.-H., et al., *Nano- and micro-based inhaled drug delivery systems for targeting alveolar macrophages.* Expert Opinion on Drug Delivery, 2015. **12**(6): p. 1009-1026.
70. Santos, J.L., et al., *Functionalization of poly(amidoamine) dendrimers with hydrophobic chains for improved gene delivery in mesenchymal stem cells.* Journal of Controlled Release, 2010. **144**(1): p. 55-64.
71. Nava, G., et al., *Formulation and in Vitro, ex Vivo and in Vivo Evaluation of Elastic Liposomes for Transdermal Delivery of Ketorolac Tromethamine.* Pharmaceutics, 2011. **3**(4): p. 954.
72. Nokhodchi, A., et al., *The Role of Oral Controlled Release Matrix Tablets in Drug Delivery Systems.* BioImpacts : BI, 2012. **2**(4): p. 175-187.

73. Gogtay, J.A. and G. Malhotra, *Reformulation of existing antiretroviral drugs.* Current Opinion in Hiv and Aids, 2013. **8**(6): p. 550-555.
74. McDonald, T.O., et al., *Antiretroviral Solid Drug Nanoparticles with Enhanced Oral Bioavailability: Production, Characterization, and In Vitro–In Vivo Correlation.* Advanced Healthcare Materials, 2014. **3**(3): p. 400-411.
75. Singh, G. and R.S. Pai, *Optimized self-nanoemulsifying drug delivery system of atazanavir with enhanced oral bioavailability: in vitro/in vivo characterization.* Expert Opinion on Drug Delivery, 2014. **11**(7): p. 1023-1032.
76. Sivin, I., *Risks and benefits, advantages and disadvantages of levonorgestrel-releasing contraceptive implants.* Drug Safety, 2003. **26**(5): p. 303-335.
77. Lu, H., et al., *Subcutaneous Angiotensin II Infusion using Osmotic Pumps Induces Aortic Aneurysms in Mice.* Journal of Visualized Experiments : JoVE, 2015(103): p. 53191.
78. Larsen, C., et al., *Role of in vitro release models in formulation development and quality control of parenteral depots.* Expert Opinion on Drug Delivery, 2009. **6**(12): p. 1283-1295.
79. Darville, N., et al., *Intramuscular Administration of Paliperidone Palmitate Extended-Release Injectable Microsuspension Induces a Subclinical Inflammatory Reaction Modulating the Pharmacokinetics in Rats*. Journal of Pharmaceutical Sciences, 2014. **103**(7): p. 2072-2087.
80. Zuidema, J., et al., *Release and absorption rates of intramuscularly and subcutaneously injected pharmaceuticals (II).* International Journal of Pharmaceutics, 1994. **105**(3): p. 189-207.
81. Heneine, W. and A. Kashuba, *HIV Prevention by Oral Preexposure Prophylaxis.* Cold Spring Harbor Perspectives in Medicine, 2012. **2**(3).
82. Chesney, M.A., *Factors Affecting Adherence to Antiretroviral Therapy.* Clinical Infectious Diseases, 2000. **30**(Supplement 2): p. S171-S176.
83. Hansana, V., et al., *Adherence to Antiretroviral Therapy (ART) among People Living With HIV (PLHIV): a cross-sectional survey to measure in Lao PDR.* BMC Public Health, 2013. **13**(1): p. 1-11.
84. Mitiku, H., T. Abdosh, and Z. Teklemariam, *Factors affecting adherence to antiretroviral treatment in harari national regional state, eastern ethiopia.* Isrn Aids, 2013. **2013**: p. 960954-960954.
85. Wasti, S.P., et al., *Factors Influencing Adherence to Antiretroviral Treatment in Nepal: A Mixed-Methods Study.* Plos One, 2012. **7**(5).

86. Baert, L., et al., *Development of a long-acting injectable formulation with nanoparticles of rilpivirine (TMC278) for HIV treatment.* European Journal of Pharmaceutics and Biopharmaceutics, 2009. **72**(3): p. 502-508.
87. van ′t Klooster, G., et al., *Pharmacokinetics and Disposition of Rilpivirine (TMC278) Nanosuspension as a Long-Acting Injectable Antiretroviral Formulation.* Antimicrob. Agents Chemother. , 2010. **54**(5): p. 2042-2050.
88. Dubey, R., *Controlled-release injectable microemulsions: recent advances and potential opportunities.* Expert Opinion on Drug Delivery, 2014. **11**(2): p. 159-173.
89. Aungst, B.J., *Absorption Enhancers: Applications and Advances.* The AAPS Journal, 2012. **14**(1): p. 10-18.
90. Pond, S.M. and T.N. Tozer, *First-Pass Elimination Basic Concepts and Clinical Consequences.* Clinical Pharmacokinetics, 2012. **9**(1): p. 1-25.
91. Richer, M. and S. Robert, *Fatal hepatotoxicity following oral-administration of amiodarone.* Annals of Pharmacotherapy, 1995. **29**(6): p. 582-586.
92. Kaplowitz, N., *Drug-Induced Liver Injury.* Clinical Infectious Diseases, 2004. **38**(Supplement 2): p. S44-S48.
93. Agid, O., G. Foussias, and G. Remington, *Long-acting injectable antipsychotics in the treatment of schizophrenia: their role in relapse prevention.* Expert Opinion on Pharmacotherapy, 2010. **11**(14): p. 2301-2317.
94. Sartorius, G., et al., *Factors influencing time course of pain after depot oil intramuscular injection of testosterone undecanoate.* Asian Journal of Andrology, 2010. **12**(2): p. 227-233.
95. Chou, Y.H., et al., *A Systemic Review and Experts' Consensus for Long-acting Injectable Antipsychotics in Bipolar Disorder.* Clinical Psychopharmacology and Neuroscience, 2015. **13**(2): p. 121-128.
96. Williams, R.O., et al., *Investigation of Excipient Type and Level on Drug Release from Controlled Release Tablets Containing HPMC.* Pharmaceutical Development and Technology, 2002. **7**(2): p. 181-193.
97. Lotfipour, F., et al., *The effect of hydrophilic and lipophilic polymers and fillers on the release rate of atenolol from HPMC matrices.* Il Farmaco, 2004. **59**(10): p. 819-825.
98. Sharma, N., P. Madan, and S. Lin, *Effect of process and formulation variables on the preparation of parenteral paclitaxel-loaded biodegradable polymeric nanoparticles: A co-surfactant study.* Asian Journal of Pharmaceutical Sciences, 2016. **11**(3): p. 404-416.
99. GlaxoSmithKline, *Summary of Product Characterisitics-Zinacef.* 1979. p. 1-30.

100. Bhagav, P., H. Upadhyay, and S. Chandran, *Brimonidine Tartrate–Eudragit Long-Acting Nanoparticles: Formulation, Optimization, In Vitro and In Vivo Evaluation.* AAPS PharmSciTech, 2011. **12**(4): p. 1087-1101.

101. Weng Larsen, S. and C. Larsen, *Critical Factors Influencing the In Vivo Performance of Long-acting Lipophilic Solutions—Impact on In Vitro Release Method Design.* The AAPS Journal, 2009. **11**(4): p. 762-770.

102. Liptrott, N.J., et al., *Flow cytometric analysis of the physical and protein-binding characteristics of solid drug nanoparticle suspensions.* Nanomedicine, 2014. **10**(9): p. 1407-1421.

103. Agur, Z. and S. Vuk-Pavlovic, *Mathematical Modeling in Immunotherapy of Cancer: Personalizing Clinical Trials.* Mol Ther, 2012. **20**(1): p. 1-2.

104. Dykstra, K., et al., *Reporting guidelines for population pharmacokinetic analyses.* Journal of Pharmacokinetics and Pharmacodynamics, 2015. **42**(3): p. 301-314.

105. Teorell, T., *Kinetics of distribution of substances administered to the body I The extravascular modes of administration.* Archives Internationales De Pharmacodynamie Et De Therapie, 1937. **57**: p. 205-225.

106. Huang, S.-M., et al., *The Utility of Modeling and Simulation in Drug Development and Regulatory Review.* Journal of Pharmaceutical Sciences, 2013. **102**(9): p. 2912-2923.

107. Barter, Z.E., et al., *Covariation of Human Microsomal Protein Per Gram of Liver with Age: Absence of Influence of Operator and Sample Storage May Justify Interlaboratory Data Pooling.* Drug Metab. Dispos., 2008. **36**(12): p. 2405-2409.

108. Siccardi, M., et al., *Use of a physiologically-based pharmacokinetic model to simulate artemether dose adjustment for overcoming the drug-drug interaction with efavirenz.* Silico Pharmacol. , 2013. **1**(1): p. 1-8.

109. Jones, H.M. and K. Rowland-Yeo, *Basic Concepts in Physiologically Based Pharmacokinetic Modeling in Drug Discovery and Development.* CPT: Pharmacometrics & Systems Pharmacology, 2013. **2**(8): p. 1-12.

110. Iga, K., *Use of Three-Compartment Physiologically Based Pharmacokinetic Modeling to Predict Hepatic Blood Levels of Fluvoxamine Relevant for Drug–Drug Interactions.* Journal of Pharmaceutical Sciences, 2015. **104**(4): p. 1478-1491.

111. Moss, D.M., et al., *Applications of physiologically based pharmacokinetic modeling for the optimization of anti-infective therapies.* Expert Opinion on Drug Metabolism & Toxicology, 2015. **11**(8): p. 1203-1217.

112. Westerhout, J., et al., *Physiologically Based Pharmacokinetic Modeling to Investigate Regional Brain Distribution Kinetics in Rats.* The AAPS Journal, 2012. **14**(3): p. 543-553.

113. Siccardi, M., et al., *Use of a physiologically-based pharmacokinetic model to simulate artemether dose adjustment for overcoming the drug-drug interaction with efavirenz.* In Silico Pharmacology, 2013. **1**(1): p. 4.

114. Siccardi, M., et al., *Prediction of drug-drug Interactions Between Various Antidepressants and Efavirenz or Boosted Protease Inhibitors Using a Physiologically Based Pharmacokinetic Modelling Approach.* Clinical Pharmacokinetics, 2013. **52**(7): p. 583-592.

115. Xu, C., et al., *CYP2B6 Pharmacogenetics–Based In Vitro–In Vivo Extrapolation of Efavirenz Clearance by Physiologically Based Pharmacokinetic Modeling.* Drug Metabolism and Disposition, 2013. **41**(12): p. 2004-2011.

116. Djebli, N., et al., *Physiologically Based Pharmacokinetic Modeling for Sequential Metabolism: Effect of CYP2C19 Genetic Polymorphism on Clopidogrel and Clopidogrel Active Metabolite Pharmacokinetics.* Drug Metabolism and Disposition, 2015. **43**(4): p. 510-522.

117. Peters, S.A., *Variability, Uncertainty, and Sensitivity Analysis*, in *Physiologically-Based Pharmacokinetic (PBPK) Modeling and Simulations*. 2012, John Wiley & Sons, Inc. p. 161-181.

118. Yu, L.X. and G.L. Amidon, *A compartmental absorption and transit model for estimating oral drug absorption.* Int. J. Pharm., 1999. **186**(2): p. 119-125.

119. Peters, S., *Evaluation of a Generic Physiologically Based Pharmacokinetic Model for Lineshape Analysis.* Clinical Pharmacokinetics, 2008. **47**(4): p. 261-275.

120. Rajoli, R.K.R., et al., *Physiologically Based Pharmacokinetic Modelling to Inform Development of Intramuscular Long-Acting Nanoformulations for HIV.* Clinical Pharmacokinetics, 2014. **54**(6): p. 639-650.

121. Spreen, W.R., D.A. Margolis, and J.C.J. Pottage, *Long-acting injectable antiretrovirals for HIV treatment and prevention.* Curr. Opin. HIV AIDS, 2013. **8**(6): p. 565-571.

122. Williams, J., et al., *Long-acting parenteral nanoformulated antiretroviral therapy: interest and attitudes of HIV-infected patients.* Nanomedicine (Lond). , 2013. **8**(11): p. 1807-1813.

123. Trezza, C., et al., *Formulation and pharmacology of long-acting cabotegravir.* Current Opinion in Hiv and Aids, 2015. **10**(4): p. 239-245.

124. Tegenge, M. and R. Mitkus, *A physiologically-based pharmacokinetic (PBPK) model of squalene-containing adjuvant in human vaccines.* J. Pharmacokinet. Pharmacodyn., 2013. **40**(5): p. 545-556.

125. Siccardi, M., et al., *Pharmacokinetic and Pharmacodynamic Analysis of Efavirenz Dose Reduction Using an In Vitro-In Vivo Extrapolation Model.* Clin Pharmacol Ther, 2012. **92**(4): p. 494-502.
126. de Roche, M., et al., *Efavirenz in an obese HIV-infected patient - a report and an in vitro-in vivo extrapolation model indicate risk of underdosing.* Antivir. Ther., 2012. **17**(7): p. 1381-1384.
127. Hyland, R., et al., *Maraviroc: in vitro assessment of drug–drug interaction potential.* British Journal of Clinical Pharmacology, 2008. **66**(4): p. 498-507.
128. Cancer, M.O. *Formula of Dubois and Dubois for Body Surface Area*. 2010 22/05/2017]; Available from: http://www.mymedal.org/index.php?n=OvarianCancer.020701.
129. Bosgra, S., et al., *An improved model to predict physiologically based model parameters and their inter-individual variability from anthropometry.* Crit. Rev. Toxicol., 2012. **42**(9): p. 751-767.
130. NSCEP, *Physiological Paramenter Values for PBPK Models*. 1994. p. 142.
131. Siccardi, M., et al., *Use of a physiologically-based pharmacokinetic model to simulate artemether dose adjustment for overcoming the drug-drug interaction with efavirenz.* Silico Pharmacol. , 2013. **1**(4).
132. Hubatsch, I., E.G.E. Ragnarsson, and P. Artursson, *Determination of drug permeability and prediction of drug absorption in Caco-2 monolayers.* Nat. Protocols, 2007. **2**(9): p. 2111-2119.
133. Poulin, P. and F.P. Theil, *Prediction of pharmacokinetics prior to in vivo studies. 1. Mechanism-based prediction of volume of distribution.* J Pharm Sci, 2002. **91**(1): p. 129-56.
134. Feng, J., et al., *The triple combination of tenofovir, emtricitabine and efavirenz shows synergistic anti-HIV-1 activity in vitro : a mechanism of action study*. Retrovirology, 2009. **6**(1): p. 1-16.
135. Hamby, D.M., *A review of techniques for parameter sensitivity analysis of environmental-models.* Environmental Monitoring and Assessment, 1994. **32**(2): p. 135-154.
136. ViiV Healthcare Pty Ltd, *Product Information - Tivicay*. 2014. p. 1-24.
137. Gilead Sciences, *Highlights of Prescribing Information - Emtriva*. 2013. p. 1-30.
138. Schöller-Gyüre, M., et al., *Clinical Pharmacokinetics and Pharmacodynamics of Etravirine.* Clin. Pharmacokinet., 2009. **48**(9): p. 561-574.
139. Center for Drug Evaluation and Research, *Application number: 202022Orig1s000. Clinical Pharmacology and Biopharmaceutics Review(s).* 2011.

140. Wajima, T. and R. Kubota, *Pharmacokinetic/pharmacodynamic Modeling and Long-term Simulation of Dolutegravir (DTG, S/GSK1349572) in Integrase Resistant Patients with a Simple Viral Dynamic Model*, in *20th Population Approach Group in Europe*. 2011: Athens, Greece.
141. Valade, E., et al., *Population Pharmacokinetics of Emtricitabine in HIV-1-Infected Adult Patients.* Antimicrob. Agents Chemother., 2014. **58**(4): p. 2256-2261.
142. Gilead Sciences, *Summary of Product Characteristics - VIREAD*. 2014. p. 1-183.
143. Colombo, S., et al., *Population Pharmacokinetics of Atazanavir in Patients with Human Immunodeficiency Virus Infection.* Antimicrob. Agents Chemother., 2006. **50**(11): p. 3801-3808.
144. Viiv Healthcare, *Highlights of Prescribing Information - Tivicay*. 2013. p. 1-37.
145. Kiser, J., et al., *The Effect of Lopinavir/Ritonavir on the Renal Clearance of Tenofovir in HIV-infected Patients.* Clin Pharmacol Ther, 2007. **83**(2).
146. Reese, M.J., et al., *In Vitro Investigations into the Roles of Drug Transporters and Metabolizing Enzymes in the Disposition and Drug Interactions of Dolutegravir, a HIV Integrase Inhibitor*. Drug Metabolism and Disposition, 2013. **41**(2): p. 353-361.
147. Yanakakis, L.J. and N.N. Bumpus, *Biotransformation of the Antiretroviral Drug Etravirine: Metabolite Identification, Reaction Phenotyping, and Characterization of Autoinduction of Cytochrome P450-Dependent Metabolism.* Drug Metab. Dispos., 2012. **40**(4): p. 803-814.
148. Villani, et al., *Pharmacokinetics of efavirenz (EFV) alone and in combination therapy with nelfinavir (NFV) in HIV-1 infected patients.* Br. J. Clin. Pharmacol. , 1999. **48**(5): p. 712-715.
149. Kakuda N T, et al., *Single- and multiple-dose pharmacokinetics of etravirine administered as two different formulations in HIV-1-infected patients.* Antivir Ther, 2008. **13**(5): p. 655-661.
150. Fayet Mello, A., et al., *Cell disposition of raltegravir and newer antiretrovirals in HIV-infected patients: high inter-individual variability in raltegravir cellular penetration.* Journal of Antimicrobial Chemotherapy, 2011. **66**(7): p. 1573-1581.
151. Bristol-Myers Squibb Company, *Highlights of Prescribing Information - Reyataz*. 2014.
152. Abduljalil, K., et al., *Deciding on Success Criteria for Predictability of Pharmacokinetic Parameters from In Vitro Studies: An Analysis Based on In Vivo Observations.* Drug Metab. Dispos. , 2014.
153. Azijn, H., et al., *TMC278, a Next-Generation Nonnucleoside Reverse Transcriptase Inhibitor (NNRTI), Active against Wild-Type and NNRTI-Resistant HIV-1*. Antimicrobial Agents and Chemotherapy, 2010. **54**(2): p. 718-727.

154. Acosta, E.P., et al., *Novel Method To Assess Antiretroviral Target Trough Concentrations Using In Vitro Susceptibility Data.* Antimicrob. Agents Chemother., 2012. **56**(11): p. 5938-5945.

155. Castellino, S., et al., *Metabolism, Excretion, and Mass Balance of the HIV-1 Integrase Inhibitor, Dolutegravir, in Humans.* Antimicrob. Agents Chemother., 2013. **57**: p. 3536-46.

156. Wilson, J.E., et al., *The 5'-triphosphates of the (-) and (+) enantiomers of cis-5-fluoro-1-[2-(hydroxymethyl)-1,3-oxathiolane-5-yl]cytosine equally inhibit human immunodeficiency virus type 1 reverse transcriptase.* Antimicrobial Agents and Chemotherapy, 1993. **37**(8): p. 1720-1722.

157. Yilmaz, A., et al., *Raltegravir Cerebrospinal Fluid Concentrations in HIV-1 Infection.* PLoS ONE, 2009. **4**(9): p. e6877.

158. Palleja S, et al., *In Vitro Anti-Hiv Efficacy Of The Chemokine Receptor 5 (CCR5) Antagonist TBR-652 In Combination With Four Other Classes Of Antiretroviral Agents* in *49th ICAAC*. 2009.

159. Soo Choi, H., et al., *Renal clearance of quantum dots.* Nat Biotech, 2007. **25**(10): p. 1165-1170.

160. Okwundu C I, Uthman O A, and Okoromah C AN, *Antiretroviral pre-exposure prophylaxis (PrEP) for preventing HIV in high-risk individuals, Issue 7,* in *Cochrane database Syst. Rev.* . 2012. p. 1-48.

161. Dolgin, E., *Long-acting HIV drugs advanced to overcome adherence challenge.* Nat. Med. , 2014. **20**(4): p. 323-324.

162. Jackson, A.G.A., et al., *A Compartmental Pharmacokinetic Evaluation of Long-Acting Rilpivirine in HIV-Negative Volunteers for Pre-Exposure Prophylaxis.* Clin Pharmacol Ther, 2014. **96**(3): p. 314-323.

163. Martin, P., et al., *Mediation of in Vitro Cytochrome P450 Activity by Common Pharmaceutical Excipients.* Mol. Pharm. , 2013. **10**(7): p. 2739-2748.

164. Leong, R., et al., *Regulatory Experience With Physiologically Based Pharmacokinetic Modeling for Pediatric Drug Trials.* Clinical Pharmacology & Therapeutics, 2012. **91**(5): p. 926-931.

165. Anderson, G.D. and A.M. Lynn, *Optimizing Pediatric Dosing: A Developmental Pharmacologic Approach.* Pharmacotherapy: The Journal of Human Pharmacology and Drug Therapy, 2009. **29**(6): p. 680-690.

166. Johnson, T.N., *The problems in scaling adult drug doses to children.* Arch Dis Child, 2008. **93**(3): p. 207-11.

167. Mahmood, I., *Dosing in Children: A Critical Review of the Pharmacokinetic Allometric Scaling and Modelling Approaches in Paediatric Drug Development and Clinical Settings.* Clinical Pharmacokinetics, 2014. **53**(4): p. 327-346.

168. Hines, R.N., *Ontogeny of human hepatic cytochromes P450.* Journal of Biochemical and Molecular Toxicology, 2007. **21**(4): p. 169-175.

169. Kuczmarski RJ, O.C., Guo SS, Grummer-Strawn LM, Flegal KM, Mei Z, Wei R, Curtin LR, Roche AF, Johnson CL., *2000 CDC Growth Charts for the United States: methods and development.* Vital Health Stat 11., 2002. **246**: p. 1-190.

170. Stephenson, T., *How children's responses to drugs differ from adults.* British Journal of Clinical Pharmacology, 2005. **59**(6): p. 670-673.

171. Khalil, F. and S. Läer, *Physiologically Based Pharmacokinetic Modeling: Methodology, Applications, and Limitations with a Focus on Its Role in Pediatric Drug Development.* Journal of Biomedicine and Biotechnology, 2011. **2011**: p. 907461.

172. Barrett, J.S., et al., *Physiologically Based Pharmacokinetic (PBPK) Modeling in Children.* Clinical Pharmacology & Therapeutics, 2012. **92**(1): p. 40-49.

173. Edginton, A.N., *Knowledge-driven approaches for the guidance of first-in-children dosing.* Pediatric Anesthesia, 2011. **21**(3): p. 206-213.

174. Chamberlain, J.M., et al., *Pharmacokinetics of Intravenous Lorazepam in Pediatric Patients with and without Status Epilepticus.* The Journal of Pediatrics, 2012. **160**(4): p. 667-672.e2.

175. Dajani, A.S., et al., *Pharmacokinetics of intramuscular ceforanide in infants, children, and adolescents.* Antimicrobial Agents and Chemotherapy, 1982. **21**(2): p. 282-287.

176. Centers for Disease Control and Prevention, *CDC growth charts: United States*, in *National Center for Health Statistics*. 2000.

177. Gehan, E.A. and S.L. George, *Estimation of human body surface area from height and weight.* Cancer Chemotherapy Reports Part 1, 1970. **54**(4): p. 225-&.

178. Valentin, J., *Annals of the ICRP: Basic Anatomical and Physiological Data for Use in Radiological Protection: Reference Values*. 2003, The International Commission on Radiological Protection.

179. Bjorkman, S., *Prediction of drug disposition in infants and children by means of physiologically based pharmacokinetic (PBPK) modelling: theophylline and midazolam as model drugs.* Br J Clin Pharmacol, 2005. **59**(6): p. 691-704.

180. Maharaj, A.R., J.S. Barrett, and A.N. Edginton, *A Workflow Example of PBPK Modeling to Support Pediatric Research and Development: Case Study with Lorazepam.* AAPS J, 2013. **15**(2): p. 455-64.

181. Price, P.S., et al., *Modeling Interindividual Variation in Physiological Factors Used in PBPK Models of Humans.* Critical Reviews in Toxicology, 2003. **33**(5): p. 469-503.

182. Haddad, S., C. Restieri, and K. Krishnan, *Characterization of age-related changes in body weight and organ weights from birth to adolescence in humans.* Journal of Toxicology and Environmental Health-Part A, 2001. **64**(6): p. 453-464.

183. Shankle, W.R., B.H. Landing, and J. Gregg, *Normal organ weights of infants and children: graphs of values by age, with confidence intervals.* Pediatric pathology / affiliated with the International Paediatric Pathology Association, 1983. **1**(4): p. 399-408.

184. McQueen, C.A., et al., *Comprehensive Toxicology, Volumes 1-14 (2nd Edition)*. Elsevier.

185. Ginsberg, G., et al., *Physiologically Based Pharmacokinetic (PBPK) Modeling of Caffeine and Theophylline in Neonates and Adults: Implications for Assessing Children's Risks from Environmental Agents.* Journal of Toxicology and Environmental Health, Part A, 2004. **67**(4): p. 297-329.

186. Williams, L.R., *Reference values for total blood volume and cardiac output in humans*. 1994.

187. DrugBank. *Lorazepam*. 2013 [cited 2016 13/5/2016]; Available from: http://www.drugbank.ca/drugs/DB00186.

188. DrugBank. *Ceforanide*. 2017 [cited 2017 06/03/2017]; Available from: https://www.drugbank.ca/drugs/DB00923.

189. Paixão, P., L.F. Gouveia, and J.A.G. Morais, *Prediction of drug distribution within blood.* European Journal of Pharmaceutical Sciences, 2009. **36**(4–5): p. 544-554.

190. de Wildt, S., et al., *Cytochrome P450 3A.* Clinical Pharmacokinetics, 1999. **37**(6): p. 485-505.

191. Ginsberg, G., et al., *Evaluation of Child/Adult Pharmacokinetic Differences from a Database Derived from the Therapeutic Drug Literature.* Toxicological Sciences, 2002. **66**(2): p. 185-200.

192. Edginton, A.N., W. Schmitt, and S. Willmann, *Development and Evaluation of a Generic Physiologically Based Pharmacokinetic Model for Children.* Clinical Pharmacokinetics, 2012. **45**(10): p. 1013-1034.

193. Parrott, N., et al., *Development of a Physiologically Based Model for Oseltamivir and Simulation of Pharmacokinetics in Neonates and Infants.* Clinical Pharmacokinetics, 2011. **50**(9): p. 613-623.

194. Maharaj, A.R., J.S. Barrett, and A.N. Edginton, *A Workflow Example of PBPK Modeling to Support Pediatric Research and Development: Case Study with Lorazepam.* The AAPS Journal, 2013. **15**(2): p. 455-464.

195. Johnson, T., A. Rostami-Hodjegan, and G. Tucker, *Prediction of the Clearance of Eleven Drugs and Associated Variability in Neonates, Infants and Children.* Clinical Pharmacokinetics, 2006. **45**(9): p. 931-956.

196. Siccardi, M., et al., *Intrapatient and Interpatient Pharmacokinetic Variability of Raltegravir in the Clinical Setting.* Therapeutic Drug Monitoring, 2012. **34**(2): p. 232-235.

197. Johnson, T.N., *Modelling approaches to dose estimation in children.* British Journal of Clinical Pharmacology, 2005. **59**(6): p. 663-669.

198. EMA. *2014 Activity report of the Modelling and simulation working group (MSWG)*. 2015 [cited 2016 27/07/2016]; Available from: http://www.ema.europa.eu/docs/en_GB/document_library/Report/2015/04/WC500185895.pdf.

199. Haberer, J. and C. Mellins, *Pediatric Adherence to HIV Antiretroviral Therapy.* Current HIV/AIDS reports, 2009. **6**(4): p. 194-200.

200. Owen S. Muir, A.A.-J., Padam Bhatia, MD, Sandeep Kapoor, John Kane, Christoph U. Correll, *Attitudes of Children and Adolescents and Their Caregivers Towards Long-Acting Injectable Antipsychotics in a Cohort of Youth Initiating Oral Antipsychotic Treatment*, in *60th Annual Meeting - American Academy of Child Adolescent Psychiatry*. 2013: Orlando, FL.

201. Healthcare, V. *A Phase IIb Study to Evaluate a Long-Acting Intramuscular Regimen for Maintenance of Virologic Suppression (Following Induction With an Oral Regimen of GSK1265744 and Abacavir/Lamivudine) in Human Immunodeficiency Virus Type 1 (HIV-1) Infected, Antiretroviral Therapy-Naive Adult Subjects*. 2014 04/02/2016 [cited 2016 15/03/2016]; Available from: https://clinicaltrials.gov/ct2/show/NCT02120352.

202. Ford, S.L., et al. *Population PK Approach to Predict Cabotegravir (CAB, GSK1265744) Long-Acting Injectable Doses for Phase 2b*. in *ICAAC*. 2014. Washington, DC.

203. Reese M, F.S., Bowers G, Humphreys J, Webster L, Gould E, Polli J, Generaux G, Johnson M, Clark P, Watson C, Lou Y, Piscitelli S. *In Vitro Drug Interaction Profile of the HIV Integrase Inhibitor, GSK1265744, and Demonstrated Lack of Clinical Interaction with Midazolam*. in *15th International Workshop on Clinical Pharmacology of HI V and Hepatitis Therapy*. 2014. Washington, DC.

204. Iwatsubo, T., et al., *Prediction of in vivo drug metabolism in the human liver from in vitro metabolism data.* Pharmacology & Therapeutics, 1997. **73**(2): p. 147-171.

205. David A. Margolis, D.P., Hans-Jurgen Stellbrink, Thomas Lutz, Jonathan B. Angel, Gary Richmond, Bonaventura Clotet, Felix Gutierrez, Louis Sloan, Sandy K. Griffith, Marty St Clair, David Dorey, Susan Ford, Joseph Mrus, Herta Crauwels, Kimberly Y. Smith, Peter E. Williams, William R. Spreen. *Cabotegravir + Rilpivirine as Long-Acting Maintenance Therapy: LATTE-2 Week 48 Results* in *International AIDS Conference*. 2016. Durban, South Africa.

206. McQueen, C.A., *Comprehensive Toxicology*. 2nd ed. Vol. 12. 2010. 1-358.

207. Chemaxon. *Chemicalize.org, Properties viewer*. 2016 [cited 2016 18/03/2016]; Available from: http://www.chemicalize.org/.

208. *Application number: 202022Orig1s000. Clinical Pharmacology and Biopharmaceutics Review(s).* 2011, Center for Drug Evaluation and Research.

209. A Culp, G.B., E Gould, S Ford, Y Lou, R Pan, D Margolis, S Piscitelli. *Metabolism, Excretion, and Mass Balance of the HIV Integrase Inhibitor, Cabotegravir (GSK1265744) in Humans*. in *ICAAC 2014 54th Interscience Conference on Antimicrobial Agents and Chemotherapy*. 2014. Washington, DC.

210. Wakibi, S.N., Z.W. Ng'ang'a, and G.G. Mbugua, *Factors associated with non-adherence to highly active antiretroviral therapy in Nairobi, Kenya.* AIDS Research and Therapy, 2011. **8**(1): p. 1-8.

211. Hansana, V., et al., *Adherence to Antiretroviral Therapy (ART) among People Living With HIV (PLHIV): a cross-sectional survey to measure in Lao PDR.* BMC Public Health, 2013. **13**(1): p. 1-11.

212. Simoni, J.M., et al., *Adherence to antiretroviral therapy for pediatric HIV infection: A qualitative systematic review with recommendations for research and clinical management.* Pediatrics, 2007. **119**(6): p. E1371-E1383.

213. Buchanan, A.L., et al., *Barriers to Medication Adherence in HIV-Infected Children and Youth Based on Self- and Caregiver Report.* Pediatrics, 2012. **129**(5): p. e1244-e1251.

214. Ginsberg, G., et al., *Physiologically based pharmacokinetic (PBPK) modeling of caffeine and theophylline in neonates and adults: Implications for assessing children's risks from environmental agents.* Journal of Toxicology and Environmental Health-Part a-Current Issues, 2004. **67**(4): p. 297-329.

215. Edginton, A.N., et al., *A Mechanistic Approach for the Scaling of Clearance in Children.* Clinical Pharmacokinetics, 2012. **45**(7): p. 683-704.

216. Edginton, A.N. and S. Willmann, *Physiology-Based Simulations of a Pathological Condition.* Clinical Pharmacokinetics, 2008. **47**(11): p. 743-752.

217. Martin Markowitz, I.F., Robert Grant, Kenneth H. Mayer, David A. Margolis, Krischan J. Hudson, Britt S. Stancil, Susan L. Ford, Alex R. Rinehart, William Spreen. *ÉCLAIR: Phase 2A Safety and PK Study of Cabotegravir LA in HIV-Uninfected Men*. in *Conference on Retroviruses and Opportunistic Infections*. 2016. Boston.

218. Dotan, R., et al., *Child—Adult Differences in Muscle Activation — A Review.* Pediatric exercise science, 2012. **24**(1): p. 2-21.

219. Weiss , C.F., A.J. Glazko , and J.K. Weston *Chloramphenicol in the Newborn Infant.* New England Journal of Medicine, 1960. **262**(16): p. 787-794.

220. Silverman, W.A., et al., *A Difference In Mortality Rate and Incidence of Kernicterus among Premature Infants Allotted to Two Prophylactic Antibacterial Regimens.* Pediatrics, 1956. **18**(4): p. 614.

221. Kamaly, N., et al., *Degradable Controlled-Release Polymers and Polymeric Nanoparticles: Mechanisms of Controlling Drug Release.* Chemical Reviews, 2016. **116**(4): p. 2602-2663.

222. Hua, X., et al., *Externally Controlled Triggered-Release of Drug from PLGA Micro and Nanoparticles.* PLoS ONE, 2014. **9**(12): p. e114271.

223. Agnihotri, S.A., N.N. Mallikarjuna, and T.M. Aminabhavi, *Recent advances on chitosan-based micro- and nanoparticles in drug delivery.* Journal of Controlled Release, 2004. **100**(1): p. 5-28.

224. Yehia, S.A., A.H. Elshafeey, and I. Elsayed, *Biodegradable donepezil lipospheres for depot injection: optimization and in-vivo evaluation.* Journal of Pharmacy and Pharmacology, 2012. **64**(10): p. 1425-1437.

225. Xie, X., et al., *In Vitro and In Vivo Evaluations of PLGA Microspheres Containing Nalmefene.* PLoS ONE, 2015. **10**(5): p. e0125953.

226. Polli, J.E., *In Vitro Studies are Sometimes Better than Conventional Human Pharmacokinetic In Vivo Studies in Assessing Bioequivalence of Immediate-Release Solid Oral Dosage Forms.* The AAPS Journal, 2008. **10**(2): p. 289-299.

227. Yu, L.X., J.T. Wang, and A.S. Hussain, *Evaluation of USP apparatus 3 for dissolution testing of immediate-release products.* AAPS PharmSci, 2002. **4**(1): p. 1-5.

228. C. Sree Lakshmi, A.V.B., *An Updated Review of Dissolution Apparatus for Conventional and Novel Dosage Forms.* International Journal of Pharma Research & Review, 2013. **2**(7): p. 42-53.

229. Schultz, K., et al., *Rotating dialysis cell as in vitro release method for oily parenteral depot solutions.* International Journal of Pharmaceutics, 1997. **157**(2): p. 163-169.

230. Larsen, D.B., et al., *In vivo release of bupivacaine from subcutaneously administered oily solution. Comparison with in vitro release.* Journal of Controlled Release, 2002. **81**(1–2): p. 145-154.
231. Larsen, D.B., K. Fredholt, and C. Larsen, *Addition of hydrogen bond donating excipients to oil solution: effect on in vitro drug release rate and viscosity*. European Journal of Pharmaceutical Sciences, 2001. **13**(4): p. 403-410.
232. Chidambaram, N. and D.J. Burgess, *A novel in vitro release method for submicron-sized dispersed systems*. AAPS PharmSci, 1999. **1**(3): p. 32-40.
233. Geerts, P., G. Martinez, and A. Schreiner, *Attitudes towards the administration of long-acting antipsychotics: a survey of physicians and nurses.* BMC Psychiatry, 2013. **13**(1): p. 1-13.
234. Conti, B., et al., *Testing of "In Vitro" Dissolution Behaviour of Microparticulate Drug Delivery Systems.* Drug Development and Industrial Pharmacy, 1995. **21**(10): p. 1223-1233.
235. Aubert-Pouessel, A., et al., *A novel in vitro delivery system for assessing the biological integrity of protein upon release from PLGA microspheres.* Pharmaceutical Research, 2002. **19**(7): p. 1046-1051.
236. Cortesi, R., et al., *Gelatin microspheres as a new approach for the controlled delivery of synthetic oligonucleotides and PCR-generated DNA fragments.* International Journal of Pharmaceutics, 1994. **105**(2): p. 181-186.
237. Zurovsky, Y., G. Mitchell, and J. Hattingh, *Composition and viscosity of interstitial fluid of rabbits.* Experimental Physiology, 1995. **80**(2): p. 203-207.
238. Shen, J., et al., *In vitro-in vivo correlation of parenteral risperidone polymeric microspheres.* Journal of Controlled Release, 2015. **218**: p. 2-12.
239. DrugBank. *Medroxyprogesterone*. 2013 [cited 2013 23/09/2013]; Available from: http://www.drugbank.ca/drugs/DB00603.
240. M K Ghorab, T.S.M., *Industrialization of medroxy progesterone acetate in prolonged parental suspension (part I).* International Journal of Pharmacy and Pharmaceutical Sciences, 2015. **7**(1): p. 364-369.
241. DrugBank. *Olanzpine*. 2016 [cited 2016 23/09/2016]; Available from: http://www.drugbank.ca/drugs/DB00334.
242. Paquette, S.M., et al., *Long-Acting Atypical Antipsychotics: Characterization of the Local Tissue Response.* Pharmaceutical Research, 2014. **31**(8): p. 2065-2077.
243. DrugBank. *Paliperidone*. 2016 [cited 2016 23/09/2016]; Available from: http://www.drugbank.ca/drugs/DB01267.
244. DrugBank. *Rilpivirine*. 2014 [cited 2014 20/02/2014]; Available from: http://www.drugbank.ca/drugs/DB08864.

245. DrugBank. *Risperidone*. 2016 [cited 2016 23/09/2016]; Available from: http://www.drugbank.ca/drugs/DB00734.

246. van Beers, M.M.C., et al., *Micro-Flow Imaging as a quantitative tool to assess size and agglomeration of PLGA microparticles.* European Journal of Pharmaceutics and Biopharmaceutics, 2017. **117**: p. 91-104.

247. Boffito, M., et al., *New Approaches to Antiretroviral Drug Delivery: Challenges and Opportunities Associated with the Use of Long-Acting Injectable Agents.* Drugs, 2014. **74**(1): p. 7-13.

248. Chou, Y.H., et al., *A Systemic Review and Experts' Consensus for Long-acting Injectable Antipsychot.* Clinical Psychopharmacology and Neuroscience, 2015. **13**(2): p. 121-128.

249. Siccardi, M., et al., *Pharmacokinetic and Pharmacodynamic Analysis of Efavirenz Dose Reduction Using an In Vitro–In Vivo Extrapolation Model.* Clinical Pharmacology & Therapeutics, 2012. **92**(4): p. 494-502.

250. Rostami-Hodjegan, A. and G.T. Tucker, *Simulation and prediction of in vivo drug metabolism in human populations from in vitro data.* Nat Rev Drug Discov, 2007. **6**(2): p. 140-148.

251. Jones HM, R.-Y.K., *Basic Concepts in Physiologically Based Pharmacokinetic Modeling in Drug Discovery and Development.* CPT: pharmacomet. syst. pharmacol., 2013. **2**: p. e63.

252. Poulin, P. and S. Haddad, *Microsome composition-based model as a mechanistic tool to predict nonspecific binding of drugs in liver microsomes.* Journal of Pharmaceutical Sciences, 2011. **100**(10): p. 4501-4517.

253. Fahmi, O.A., et al., *A Combined Model for Predicting CYP3A4 Clinical Net Drug-Drug Interaction Based on CYP3A4 Inhibition, Inactivation, and Induction Determined in Vitro.* Drug Metabolism and Disposition, 2008. **36**(8): p. 1698.

254. Fotherby, K., S. Koetsawang, and M. Mathrubutham, *Pharmacokinetic study of different doses of Depo Provera.* Contraception, 1980. **22**(5): p. 527-536.

255. Mitchell, M., et al., *Single- and Multiple-Dose Pharmacokinetic, Safety, and Tolerability Profiles of Olanzapine Long-Acting Injection: An Open-Label, Multicenter, Nonrandomized Study in Patients With Schizophrenia.* Clinical Therapeutics, 2013. **35**(12): p. 1890-1908.

256. Rossenu, S., et al., *Pharmacokinetic profile after multiple deltoid or gluteal intramuscular injections of paliperidone palmitate in patients with schizophrenia.* Clinical Pharmacology in Drug Development, 2014: p. n/a-n/a.

257. Eerdekens, M., et al., *Pharmacokinetics and tolerability of long-acting risperidone in schizophrenia.* Schizophrenia Research, 2004. **70**(1): p. 91-100.

258. Vermeir, M., et al., *Absorption, Metabolism, and Excretion of Paliperidone, a New Monoaminergic Antagonist, in Humans.* Drug Metabolism and Disposition, 2008. **36**(4): p. 769.

259. Medicines.org, *Depo-Provera 150mg/ml Injection Summary of product characteristics*. 2016.

260. Yasui-Furukori, N., et al., *Different Enantioselective 9-hydroxylation of Risperidone by the Two Human CYP2D6 and CYP3A4 Enzymes.* Drug Metabolism and Disposition, 2001. **29**(10): p. 1263-1268.

261. Obach, R.S., *Prediction of Human Clearance of Twenty-Nine Drugs from Hepatic Microsomal Intrinsic Clearance Data: An Examination of In Vitro Half-Life Approach and Nonspecific Binding to Microsomes.* Drug Metabolism and Disposition, 1999. **27**(11): p. 1350.

262. Zhang, J. and C. Crumpacker, *Eradication of HIV and Cure of AIDS, Now and How?* Frontiers in Immunology, 2013. **4**: p. 337.

263. Abel, S., D.J. Back, and M. Vourvahis, *Maraviroc: pharmacokinetics and drug interactions.* Antiviral Therapy, 2009. **14**(5): p. 607-618.

264. Gao, Y., et al., *In Vitro Release Kinetics of Antituberculosis Drugs from Nanoparticles Assessed Using a Modified Dissolution Apparatus.* BioMed Research International, 2013. **2013**: p. 9.

265. Panel on Antiretroviral Therapy and Medical Management of HIV-Infected Children, *Guidelines for the Use of Antiretroviral Agents in Pediatric HIV Infection*. 2017.

266. Moss, D.M., et al., *Rilpivirine Inhibits Drug Transporters ABCB1, SLC22A1, and SLC22A2 In Vitro.* Antimicrobial Agents and Chemotherapy, 2013. **57**(11): p. 5612-5618.

267. Zhuang, X. and C. Lu, *PBPK modeling and simulation in drug research and development.* Acta Pharmaceutica Sinica B, 2016. **6**(5): p. 430-440.

268. Wagner, C., et al., *Predicting the Effect of Cytochrome P450 Inhibitors on Substrate Drugs: Analysis of Physiologically Based Pharmacokinetic Modeling Submissions to the US Food and Drug Administration.* Clinical Pharmacokinetics, 2015. **54**(1): p. 117-127.

269. Peters, S.A., et al., *Predicting Drug Extraction in the Human Gut Wall: Assessing Contributions from Drug Metabolizing Enzymes and Transporter Proteins using Preclinical Models.* Clinical Pharmacokinetics, 2016. **55**(6): p. 673-696.

270. Björkman, S., et al., *Prediction of the disposition of midazolam in surgical patients by a physiologically based pharmacokinetic model.* Journal of Pharmaceutical Sciences, 2001. **90**(9): p. 1226-1241.

271. Curley, P., et al., *Efavirenz is predicted to accumulate in brain tissue: an in silico, in vitro and in vivo investigation.* Antimicrobial Agents and Chemotherapy, 2016.

272. Zhu, L., et al., *Prediction of the pharmacokinetics and tissue distribution of levofloxacin in humans based on an extrapolated PBPK model.* European Journal of Drug Metabolism and Pharmacokinetics, 2016. **41**(4): p. 395-402.

273. Marzolini, C., et al., *Physiologically Based Pharmacokinetic Modeling to Predict Drug–Drug Interactions with Efavirenz Involving Simultaneous Inducing and Inhibitory Effects on Cytochromes.* Clinical Pharmacokinetics, 2016: p. 1-12.